DESIGNING MOLECULAR SOLIDS WITH STRUCTURAL CONTROL AND TUNABLE PHYSICAL PROPERTIES USING CO-CRYSTALLIZATION TECHNIQUES

by

SHEELU PANIKKATTU

M.S., Kishinchand Chellaram College, 2008

AN ABSTRACT OF A DISSERTATION

submitted in partial fulfillment of the requirements for the degree

DOCTOR OF PHILOSOPHY

Department of Chemistry
College of Arts and Sciences

KANSAS STATE UNIVERSITY
Manhattan, Kansas

2013

Abstract

Physical properties of bulk solids are typically governed by the molecular arrangement of individual building blocks with respect to each other in the crystal lattice. Thus the ability to synthesize molecular crystals with pre-organized connectivities allows for the rational design of functional solids with desirable and tunable physical properties. A thorough understanding of the various intermolecular interactions that govern the solid-state architectures is an important pre-requisite for the rational design of molecular solids.

In order to understand the role of molecular geometric complementarity in the design of solid-state architectures, we explored the structural landscape of two isomeric pyridine based acceptors (**3N** and **4N**) with binding sites oriented along different directions, *i.e.* parallel and at angle of 60° respectively, with a series of even chain diacid (colinear binding sites) and odd chain diacid (binding sites oriented along 120°) using co-crystallization technique. The results obtained shows a striking correlation between the observed solid state architecture and geometric complementarity of interacting species. Combinations of **3N** with odd and **4N** with even chain diacid produced 1-D chains whereas **3N** with even and **4N** with odd chain diacid generated 0-D ring architectures.

In order to exploit the possibility of fine-tuning physical properties using co-crystallization techniques, solubility measurements were performed on **3N** and **4N** co-crystals with the diacids. The results show that the solubilities of **3N** and **4N** in the co-crystal form were very different from their solubility in the pure form. Also, there was a strong correlation observed between the solubility of the co-crystals and their corresponding co-formers, *i.e.* diacids.

To explore the dependence of crystal structure on a physical property such as melting point, we synthesized co-crystals of 3,3'-azopyridine and 4,4'-azopyridine with a series of even chain diacids. Structural consistency was obtained within the two groups of co-crystals. In both groups, 1-D chains were formed with the diacid as the primary building block. However, In the series of 3,3'-azopyridine co-crystals, the co-crystal with succinic acid showed a different solid-state packing arrangement (although the primary building block was same as others) compared to the others in the same series. This difference is also reflected as a deviation in the melting point, while the others in the series showed a perfect correlation between the structural

consistency and melting point behavior. It was also observed that the co-crystals of 4,4'-azopyridine displayed higher melting points than co-crystals of 3,3'-azopyridine which could be due to the differences in the overall packing of the crystal which is a combination of different intermolecular interactions that exist between molecules in the solid state.

Using bi-functional donors (with both hydrogen and halogen bond donors on same backbone), we investigated the relative strengths of hydrogen and halogen bond donors in the presence of two isomeric acceptors, 3,3'-azopyridine and 4,4'-azopyridine, which exhibit geometric bias in their binding-site orientation. Based on the crystal structures, we noticed a preferential binding of hydrogen bond donors with 3,3'-azopyridine and both hydrogen and halogen bond donors with 4,4'-azopyridine. This shows that the two types of donors are very comparable and their binding preference is governed by the geometric complementarity between the donor-acceptor pair.

Finally, we explored the scope of using co-crystallization for tuning the physical properties of two agrochemicals, cyprodinil and terbuthylazine. The crystal structures of the actives with a series of even chain diacids displayed structural consistency in the primary motifs within the two groups, while few differences were observed in the packing arrangement and secondary interactions. By forming co-crystals we were able to improve the solubility and melting point of cyprodinil, while ensuring that the hygroscopicity of the active was unaltered.

DESIGNING MOLECULAR SOLIDS WITH STRUCTURAL CONTROL AND TUNABLE PHYSICAL PROPERTIES USING CO-CRYSTALLIZATION TECHNIQUES

by

SHEELU PANIKKATTU

M.S., Kishinchand Chellaram College, 2008

A DISSERTATION

submitted in partial fulfillment of the requirements for the degree

DOCTOR OF PHILOSOPHY

Department of Chemistry
College of Arts and Sciences

KANSAS STATE UNIVERSITY
Manhattan, Kansas

2013

Approved by:

Major Professor
Dr. Christer Aakeröy

Copyright

Abstract

Physical properties of bulk solids are typically governed by the molecular arrangement of individual building blocks with respect to each other in the crystal lattice. Thus the ability to synthesize molecular crystals with pre-organized connectivities allows for the rational design of functional solids with desirable and tunable physical properties. A thorough understanding of the various intermolecular interactions that govern the solid-state architectures is an important pre-requisite for the rational design of molecular solids.

In order to understand the role of molecular geometric complementarity in the design of solid-state architectures, we explored the structural landscape of two isomeric pyridine based acceptors (**3N** and **4N**) with binding sites oriented along different directions, *i.e.* parallel and at angle of 60° respectively, with a series of even chain diacid (colinear binding sites) and odd chain diacid (binding sites oriented along 120°) using co-crystallization technique. The results obtained shows a striking correlation between the observed solid state architecture and geometric complementarity of interacting species. Combinations of **3N** with odd and **4N** with even chain diacid produced 1-D chains whereas **3N** with even and **4N** with odd chain diacid generated 0-D ring architectures.

In order to exploit the possibility of fine-tuning physical properties using co-crystallization techniques, solubility measurements were performed on **3N** and **4N** co-crystals with the diacids. The results show that the solubilities of **3N** and **4N** in the co-crystal form were very different from their solubility in the pure form. Also, there was a strong correlation observed between the solubility of the co-crystals and their corresponding co-formers, *i.e.* diacids.

To explore the dependence of crystal structure on a physical property such as melting point, we synthesized co-crystals of 3,3'-azopyridine and 4,4'-azopyridine with a series of even chain diacids. Structural consistency was obtained within the two groups of co-crystals. In both groups, 1-D chains were formed with the diacid as the primary building block. However, In the series of 3,3'-azopyridine co-crystals, the co-crystal with succinic acid showed a different solid-state packing arrangement (although the primary building block was same as others) compared to the others in the same series. This difference is also reflected as a deviation in the melting point, while the others in the series showed a perfect correlation between the structural

consistency and melting point behavior. It was also observed that the co-crystals of 4,4'-azopyridine displayed higher melting points than co-crystals of 3,3'-azopyridine which could be due to the differences in the overall packing of the crystal which is a combination of different intermolecular interactions that exist between molecules in the solid state.

Using bi-functional donors (with both hydrogen and halogen bond donors on same backbone), we investigated the relative strengths of hydrogen and halogen bond donors in the presence of two isomeric acceptors, 3,3'-azopyridine and 4,4'-azopyridine, which exhibit geometric bias in their binding-site orientation. Based on the crystal structures, we noticed a preferential binding of hydrogen bond donors with 3,3'-azopyridine and both hydrogen and halogen bond donors with 4,4'-azopyridine. This shows that the two types of donors are very comparable and their binding preference is governed by the geometric complementarity between the donor-acceptor pair.

Finally, we explored the scope of using co-crystallization for tuning the physical properties of two agrochemicals, cyprodinil and terbuthylazine. The crystal structures of the actives with a series of even chain diacids displayed structural consistency in the primary motifs within the two groups, while few differences were observed in the packing arrangement and secondary interactions. By forming co-crystals we were able to improve the solubility and melting point of cyprodinil, while ensuring that the hygroscopicity of the active was unaltered.

Table of Contents

List of Figures

List of Tables

Acknowledgements

I would like to express my deepest gratitude to my major advisor Christer Aakeröy for his endless support and encouragement over the last five years. Your constant persuasion and belief in me has made me a much more confident individual today. In you, I found an excellent advisor and a colleague who always made time to listen to the smallest of my problems and made me feel like I was never alone. You have taught me how to never give up when things fail, but use that as a stepping stone and always look at the brighter side of things. Every time I faltered, you were there to guide me and help me recover. I have learnt invaluable lessons about science and life from you and I will always hold on to them. Thanks for being such an awesome advisor.

I would like to thank my committee members, Professors Eric Maatta, Stefan Bossmann, Michael Kanost and Amit Charkrabarti for their invaluable time. Thank you for being on my committee and making adjustments for me only to ensure that my defense could take place as scheduled.

I wish to extend my special gratitude to Dr. John Desper for all the beautiful crystal structures you have solved. Without these structures, this dissertation would have been impossible.

I would like to extend my gratitude to the Department of Chemistry and Johnson Cancer Research Center at Kansas State University as well as Syngenta for funding my PhD research.

Thanks to Dr. Leila Maurmann for your invaluable help with the HPLC instrument. If it was not for your patience with me and the instrument, a major part of my work would have been incomplete. You were a great help and I have a much better understanding about the instrument now, than I had before.

Thanks to Ron Jackson for fixing things especially the HPLC parts, time and again without any hesitation. You always made yourself available to help and thanks to you things proceeded much smoothly and efficiently.

Thanks to Jim Hodgson and Tobe Eggers for finding a solution to any broken or faulty things and making them available at the earliest to ensure work is never interrupted.

Thank you to various office staff members for all their assistance at various points of my career at K-state.

Finally, thank you all the past and present members of the Aakeröy research group. You have been fun and a wonderful support throughout. We are indeed a rocking group!!!

Dedication

I would like to dedicate this dissertation to my little brother, the apple of my eye and the best ever god sent gift to me. Staying away from you was not the easiest thing to do. Thank you for being such a sweetheart and I wish you luck in pursuing your dreams.

This is especially dedicated to my parents for all the sacrifices they have made for me, for all the challenges that they have faced along the way, only to ensure that their daughter always gets the best. Thank you for helping me pursue my dream and giving me a chance to make you proud of your daughter.

Finally this dissertation is also a special dedication to all my dear friends, without whom my world is incomplete. If it was not for your constant support, encouragement and trust in me, it would not have been an easy journey for me. Thank you for being so caring, accommodating and making my five years away from home livable and enjoyable. You all have a special place in my heart.

Preface

Research carried out at Kansas State University, Department of Chemistry for this dissertation led to the following publications in scientific journals.

Aakeröy, C.B.; Panikkattu, S.; DeHaven, B.; Desper, J. "Establishing Supramolecular Control Over Solid-State Architectures: A Simple Mix And Match Strategy" *Cryst. Growth Des*., **2012**, 12, 2579–2587

Aakeröy, C.B.; Panikkattu, S.; Dehaven, B.; Desper, J. "Interdependence Of Structure And Physical Properties In Co-Crystals Of Azopyridine" *CrystEngComm,* **2013**,15, 463-470

Aakeröy, C. B.; Panikkattu, S.; Chopade, P. and Desper, J., "Competing Hydrogen And Halogen Bond Donors In Crystal Engineering" *CrystEngComm,* **2013,** 15, 3125-3136

Chapter-1 Introduction

1.1 Molecular chemistry vs supramolecular chemistry

Molecular chemistry is a science based on covalent bonds. In a typical chemical synthesis, reactants undergo modifications that involve covalent bond breaking and bond formation on the road towards the desired final product often along with, some undesirable byproducts. These reactions are often multi-step processes that frequently require high-temperature conditions, catalysts, solvents, isolation of intermediates and purification by chromatography. The concept of synthetic chemistry began with Wöhlers synthesis of urea in 1828[1], and since then, scientists have developed synthetic routes and techniques in order to synthesize large and complex natural products.[2]

Supramolecular chemistry is defined as '*the chemistry of molecular assemblies and of the intermolecular bond*', by Jean-Marie Lehn, who won the Nobel Prize in 1987 for his outstanding contributions to the field.[3] The origin of supramolecular chemistry can be traced back to the use of crown ethers and cryptands in binding of alkali metals.[4] Recently it has gained global importance due to its wide array of applications in sensing[5], anion recognition[6], catalysis[7], biomimetic materials[8], porous materials[9] and pharmaceutics.[10] Supramolecular chemistry is concerned with how molecules recognize and communicate with each other using non-covalent interactions such as hydrogen bonds, halogen bonds, van der Waals forces[11], Π-Π interactions[12] and metal coordination[13] (Table 1.1).[14] Thus, unlike molecular chemistry that relies on covalent bonds in forming new products, supramolecular chemistry relies on reversible and relatively weak interactions for constructing multi-component assemblies (Table 1.1 and Fig 1.1). In addition, supramolecular synthesis is a one-pot method with no intermediates to isolate or no purification needed unlike covalent synthesis.

Table 1.1 Estimated strengths of intermolecular interactions[14, 7, 8]

Type of interaction	Strength (kJ/mol)
Covalent	100-400
Hydrogen bond	10-65
Π-Π	0-50
Metal-ligand	0-400
Van der Waal	<5
Halogen bond	5-180

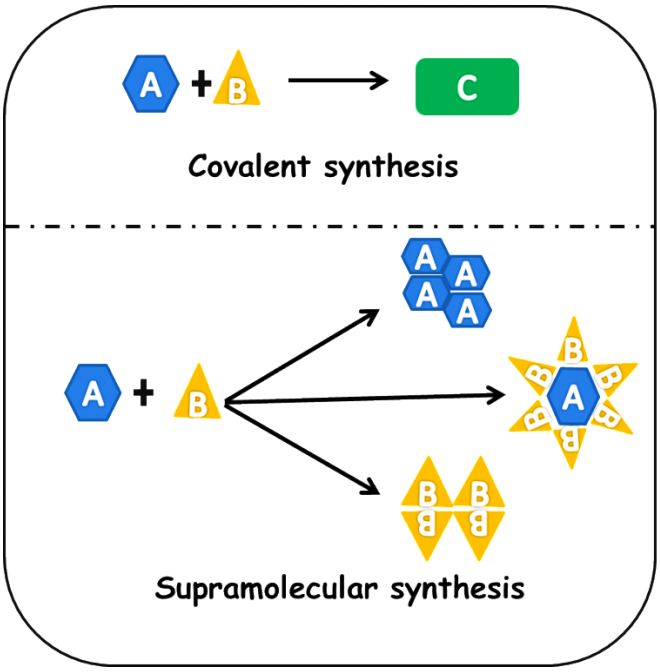

Figure 1.1 Covalent synthesis vs supramolecular synthesis

1.2 Crystal Engineering

The term crystal engineering was coined by Schmidt in 1971, with reference to photodimerization of cinnamic acid in the solid state.[15] Crystal engineering, a sub-section of supramolecular chemistry, is the rational design of molecular solids via intermolecular interactions to produce new functional solids with specific physical properties.[16]

1.2.1 Molecular Recognition

Molecular recognition is the key step towards building a multi-dimensional supramolecular framework.[17] Molecules can be deliberately made to interact with each other and self-assemble under a given set of conditions. Every molecule has a unique set of features associated with its molecular structure, *i.e.* shape, geometry, chemical surface etc. When molecules (host and guest) are made to communicate, they selectively interact with a partner that has complementing features and form a supermolecule (Fig 1.2). Molecular recognition is thus selective binding with a purpose.[18]

Figure 1.2 Molecular recognition

1.2.2 Co-crystallization vs recrystallization

Co-crystallization is a tool for probing intermolecular interactions between molecules.[19] In a co-crystal, two or more distinctly different molecular entities are brought in close proximity and made to communicate via non-covalent interactions within the same crystal lattice. This is done without making or breaking any covalent bonds. The end result is the formation of a heteromeric species (co-crystallization) over homomeric species (a result of recrystallization), Fig 1.3.

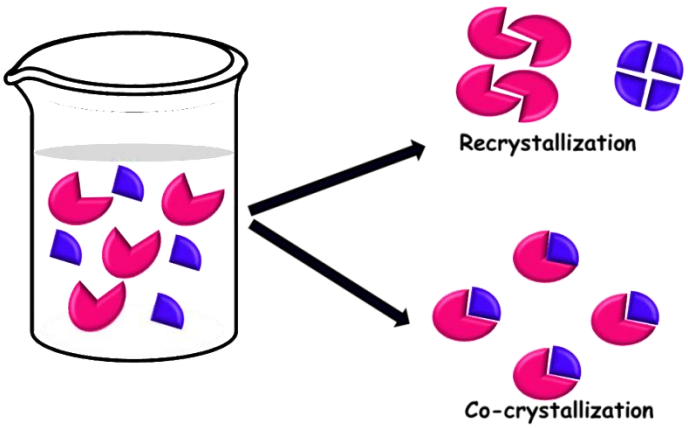

Figure 1.3 Schematic representation of co-crystallization and recrystallization processes

1.2.3 Intermolecular interactions

Molecular crystals are formed by periodic assembly of molecules connected via intermolecular interactions such as van der Waal interactions (sum of all attractive and repulsive interactions, dispersion interactions, close packing), hydrogen bonds (strong, moderate and weak) and halogen bonds.[20] A crystal structure is the result of many intermolecular interactions of varying strengths, angles and directionalities. Apart from stronger interactions such as hydrogen and halogen bonds numerous weaker interactions exists in the crystal structure that significantly influence the overall crystal packing. Thus the resulting crystal is a balance between all the numerous strong and weak non-bonded interactions that co-exist between molecules.

1.2.3.1 Hydrogen bond

The hydrogen bond is arguably the most widely used interaction for constructing supramolecular structures.[21] A hydrogen-bond donor has a hydrogen atom (with partial positive charge) attached to an electronegative atom (D). It interacts with a hydrogen bond acceptor (A) which is an electron-withdrawing atom (with partial negative charge) forming D-H...A hydrogen bonds (Fig 1.4). The best example of hydrogen bonding can be found in nature, *i.e.* DNA, the molecule of life. The base pairs in DNA are connected using hydrogen bonds which are very selective and specific (Fig 1.5).[22]

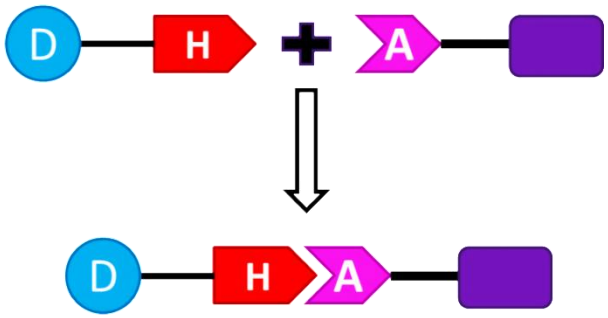

Figure 1.4 Schematic representation of a hydrogen bond

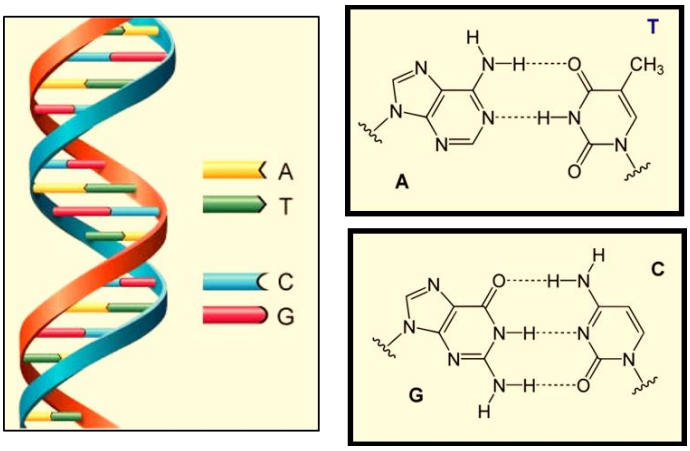

Figure 1.5 Representation of DNA (left) and hydrogen-bonded base pairs (right)[23]

Hydrogen bond interactions are electrostatic in nature and directional (D-H···A angles tends to close to linear). They can be strong (N-H···O, O-H···O, N-H···N) or weak (C-H···O, C-H···Π) depending on the electro negativities of the bonded atoms.[20] Since in the solid state the energy of hydrogen bonds cannot be measured directly, computational studies provide us with various hydrogen bond energies that are calculated using high theory levels of calculation.[24]

1.2.3.1.1 Methods for detecting hydrogen bondings

Often single crystal X-ray diffraction (SCXRD) is used to observe hydrogen-bonding interactions.[25] This requires good quality crystals of reasonable size for diffraction purposes. Since growing single crystals is not always easy, SCXRD cannot always be relied on as the sole option to detect hydrogen bonding. Other characterization techniques like NMR and IR spectroscopy can also be used to detect the presence of hydrogen bonds in a given system.

1.2.3.1.1.1 1H NMR studies

When a hydrogen atom interacts with an electronegative atom (acceptor), the hydrogen nuclues experiences a deshielding effect. This will result in a chemical shift of the nucleus towards higher frequencies, *i.e.* downfield shifted.[26] For example, when a tripodal urea scaffold binds a terephthalate anion via N-H···O^- hydrogen's between the urea N-H protons and the O^- of the carboxylate group, the interaction results in downfield shift of the N-H protons as seen in figure 1.6.[27]

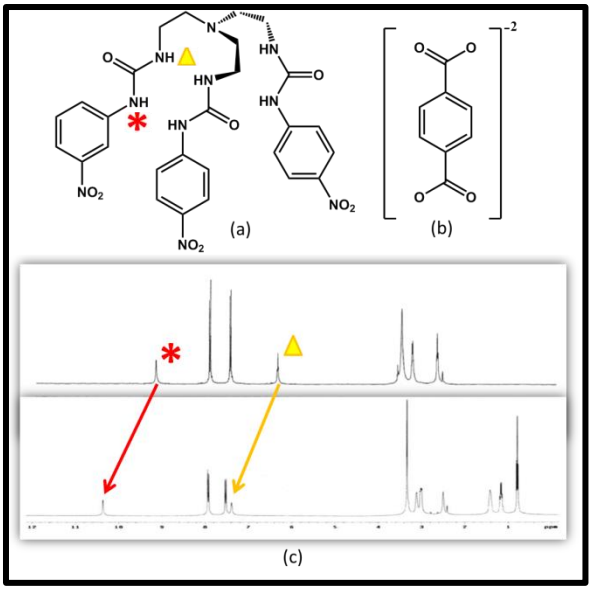

Figure 1.6 a) Tripodal host molecule b) terephthalate anion guest and c) NMR spectrum of (a+b) indicating the downfield shift in the two N-H protons due to N-H...O hydrogen bonding interactions with the guest molecule[27]

1.2.3.1.1.2 IR spectroscopy

IR spectroscopy is a very useful tool in the pharmaceutical industries to characterize different solid forms of the crystalline sample.[28] IR spectroscopy can also be used as a powerful tool to detect hydrogen-bond interactions in different systems.[29] A hydrogen bonded O-H···N interaction between a hydrogen bond donor and a heterocyclic nitrogen atom can be detected by the two broad stretches around 2450 and 1950 cm^{-1} region in the IR spectrum (Fig 1.7).[30]

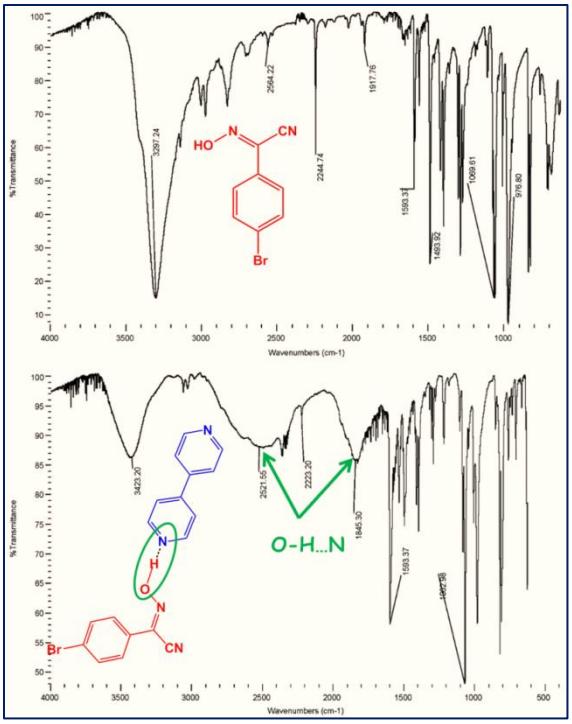

Figure 1.7 IR spectrum of an oxime hydrogen bond donor (above) and a hydrogen bond formed between donor and bipyridine acceptor (below)[30]

1.2.3.2 Halogen bonding

Halogen bonds are non-covalent interactions between a covalently bound halogen atom and a Lewis base.[31] In a covalently bonded halogen atom, *i.e.* C-X (X= F, Cl, Br or I) there exists a positive σ hole along the C-X bond axis farthest away from the carbon atom.[20] This positive σ hole can interact electrostatically with electron pairs on Lewis bases. The equatorial zone of the halogen atom is polarized negatively. A covalently bonded halogen atom can thus interact electrostatically with both electronegative and electropositive species depending on the direction of approach (Fig 1.8).

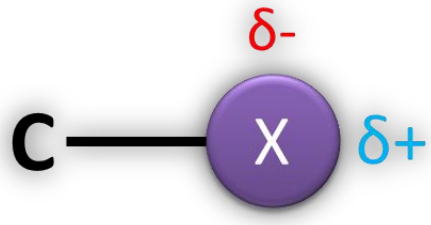

Figure 1.8 Region around covalently bonded halogen atom displaying positive and negative zone[20]

The strength of halogen bonding increases with an increase in the polarizability of the halogen atoms, i.e. F < Cl < Br < I, as can be seen from the MEP surface diagrams, when moving from F to I, the region of the positive σ hole increases (Fig 1.9).[32] Just like hydrogen bonds (D-H…A), halogen bonds (D-X…A where X= halogen) are directional and prefer linear interactions with acceptor sites.[33] Halogen bonds have a wide range of applications in liquid crystals[34], anion receptors[35] and biological systems[36].

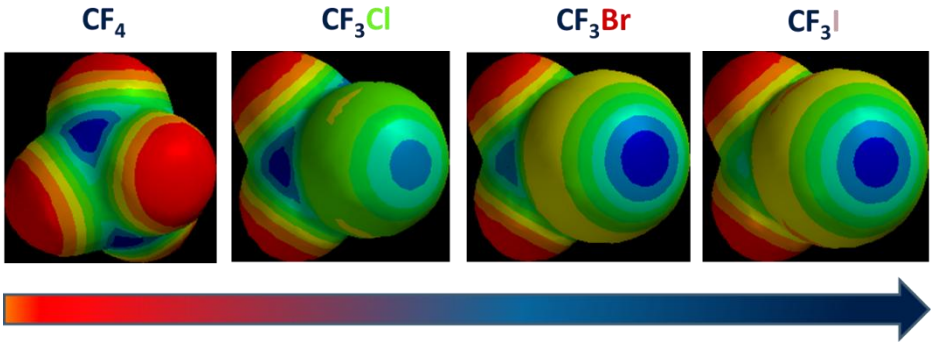

Figure 1.9 MEP surface diagram showing increasing hole

CF_4 < CF_3Cl < CF_3Br< CF_3I[32]

1.3 Potential applications of crystal engineering

1.3.1 The pharmaceutical sciences

Chemists and engineers in the pharma industry seek to deliver the active ingredients in crystalline form to ensure optimum delivery, stability and purity. Currently there are several forms in which the active pharmaceutical ingredients (API's) occur such as salts, hydrates/solvates, polymorphs and co-crystals (Fig 1.10).[37]

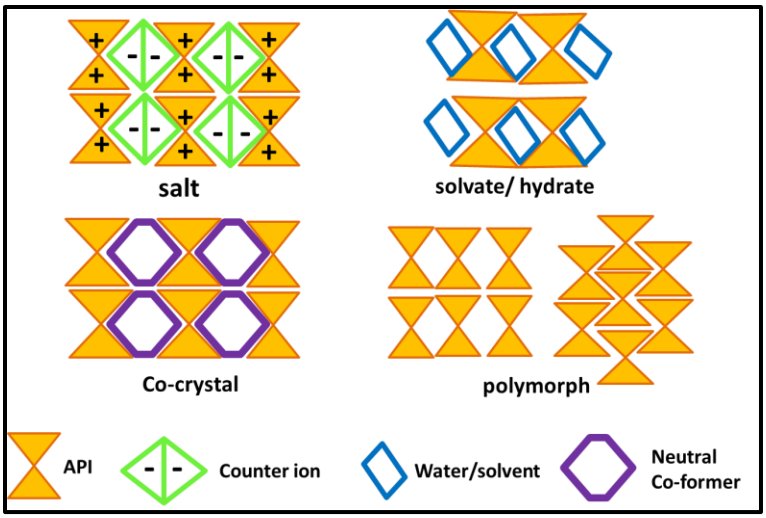

Figure 1.10 Schematic representation of the solid-state forms of API[37]

During drug development, there are many problems encountered at different stages (Fig 1.11).[38] Crystal engineering can be used to solve some of the problems related to the bioavailability, *i.e.* solubility of the API by formulating different solid forms (co-crystals) of the drug that may have improved physico-chemical properties than the API component itself.[39]

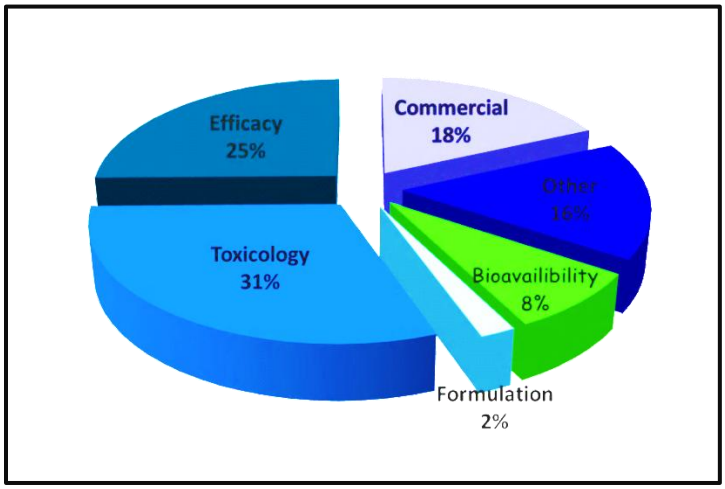

Figure 1.11 Reasons for failure of drug compounds[39]

1.3.2 The agrochemical sciences

The term "agrochemical" refers to a collection of chemicals used for agricultural purposes such as pesticides, insecticides, herbicides and fungicides.[40] Nearly 40% of the crop produced is inaccessible to humans due to loss by infestation (Fig 1.12).[41] Agrochemicals are

therefore used to protect crops from pests and thus help improve the quality and quantity of crop production.

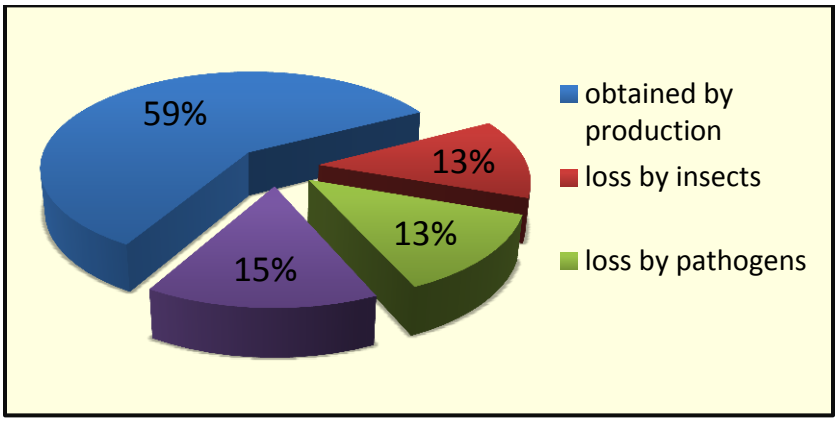

Figure 1.12 Pie chart representing crop production[41]

When used with caution, agrochemicals can promote better and increased crop production.[42] However, they also pose serious health and environmental risks due to the contamination of soil and water reserves.[42] The extent of environmental contamination is significantly influenced by the physical property of pesticides. Highly water soluble pesticides are likely to be run-off by running water and leached into the ground.[43]

Physical properties such as solubility, hygroscopicity, thermal stability, filterability and flowability are influenced by the solid forms of materials. These properties affect the overall usability and efficacy of a given agrochemical. Designing different solid forms can affect these physical properties and make them more suitable for a particular form of application. Recently, co-crystals have been tested as an efficient alternative form for solid-state modification of the active ingredient.[44] For example, 4-{[(6-chloropyrid-3-yl)methyl](2,2'-difluroethyl)amino}furan-2-(5H)-one is an active ingredient (AI) with insecticidal properties. Co-crystals of the AI with salicylic acid (1:1) has been synthesized which displays a higher melting point, 85 °C when compared to that of the active by itself (72-74 °C). Due to the increased thermal stability, the AI can be treated and handled at higher temperatures. The co-crystal also displays improved storage stability and solubility than the pure substance (Fig 1.13).[45]

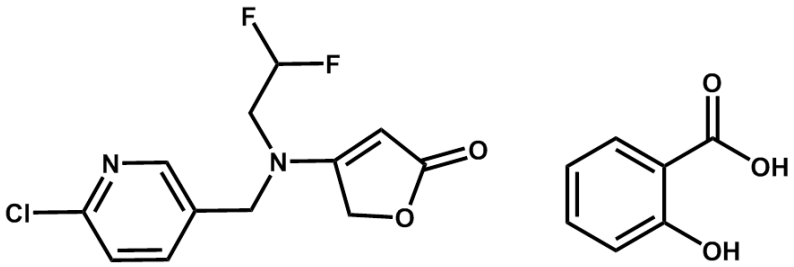

4-{[(6-chloropyrid-3-yl)methyl](2,2'-difluroethyl)amino}furan-2-(5H)-one

Salicylic acid

Figure 1.13 Structure of the insecticidal AI and co-former[45]

1.4 Goals of the thesis

An improved knowledge of intermolecular interactions is critical for the design of molecular solids with pre-programmed connectivities. Since the molecular solid-state arrangement defines physical properties of bulk solids, a control of their architecture and assembly can make way for a reliable prediction and alteration of their bulk properties in a desirable manner.

This dissertation will focus on five areas:

1. **Systematic study of intermolecular interactions and the resulting solid-state architectures in co-crystals of pyridine-amino pyridine based ligands**

The ligand of choice is a pyridine-amino/pyridine based molecule because these functionalities are found in a wide variety of pharmaceutically relevant compounds.[46] Systematically studying the binding preference of these functional groups in small molecules will provide us with an understanding of their behavior and binding pattern in larger and more complicated molecules. Two isomeric ligands will be synthesized and their interactions with a series of dicarboxylic acids will be studied using co-crystallization techniques. In addition, we will examine the extended architectures formed by different donor-acceptor combinations and elucidate structural trends.

2. **Using co-crystallizations to modulate physico-chemical properties of an API mimic**

In this section we will focus on altering the solubility of an API mimic in a systematic manner via co-crystallization with a series of FDA approved dicarboxylic acids. We will also

attempt to correlate the property of bulk solid with molecular properties (melting point and solubility) of its individual components. Finally, we will investigate the binding events of the co-crystals in aqueous solution environment using isothermal titration calorimetry.

3. Studying the interdependence of structure and physical property of molecular solids

Two isomeric azopyridine molecules will be synthesized and its resulting supramolecular structure with a series of even-dicarboxylic acids will be systematically analyzed. The solid-state arrangement and a physical property like thermal behavior will be examined to establish for possible structure-property interdependence.

4. Comparing hydrogen bond and halogen bond binding preferences as a function of geometric bias in the acceptor sites

Since hydrogen and halogen bonds have properties that parallel each other,[47] they are likely to be structurally competitive. In order to examine their competitiveness for an acceptor site, we will perform systematic co-crystallization experiments on a series of bi-functional donors (with both hydrogen and halogen bond donor on the same backbone) with two isomeric pyridine based acceptors. The study will establish the binding preference of the pyridine for hydrogen or halogen atom as a function of the geometric bias in the acceptor molecules.

5. Application of crystal engineering in tailoring physical properties of an agrochemical compounds using co-crystallization technology

We will use our knowledge of intermolecular interactions and co-crystallization to design new solid forms of an agrochemical pesticide (Cyprodinil and Terbuthylazine), investigate and modulate their physical properties as compared to the pesticide by itself.

---

1 Wöhler, F. H. *Ann. Phys.Chem*. **1828**, 12, 253.

2 Woodward, R. B.; Doering, W. E., *J. Am. Chem. Soc*. **1944**, 66, 849-849; Evans, D. A.; Wood, M. R.; Trotter, W. B.; Richardson, T. I.; Barrow, J. C.; Katz, J. L., *Angew. Chem. Int. Ed*.

1998, 37, 2700-2704; Wender, P. A.; Jesudason, C. D.; Nikahira, H.; Tamura, N.; Tebbe, A. L.;Ueno, Y., *J. Am. Chem. Soc*. **1997**, 119, 12976-12977; Kadota, I.; Takamura, H.; Sato, K.; Ohno, A.; Matsuda, K.; Yamamoto, Y. *J. Am. Chem. Soc.* **2003**, 125, 46

3 Jean- Marie Lehn, Nobel Lecture, December 8, **1987**.

4 Pedersen, C. J.; *J. Am. Chem. Soc.,* **1967**, 89, 7017–36; Dietrich B, Lehn J.M, and Sauvage J.P, *Tetrahedron Lett.,***1969**, 2885–2888.

5 Ludwig, R.; Dzung, N.T.K.; *Sensors,* **2002**, 2, 397-416; Grady, T.; Cadogan, A.; McKittrick, T.; Harris S.J.; Diamond, D.; McKervey, M.A. *Anal. Chem. Acta* **1996,** 336, 1-12; Zeng, X.S.; Sun, H.; Chen, L.X.; Leng, X.B.; Xu, F.B.; Li, Q.S.; He, X.W.; Zhang, Q.W.; *Org. Bio. Chem.* **2003**, 1, 1073-1079; Que, E. L. and Chang, C. J.; *Chem. Soc. Rev.,* **2010**, 39, 51-60

6 McDonald, K.P.; Hua, Y.; Lee, S.; and Flood, A. H.; *Chem. Commun.,* **2012**, 48, 5065-5075; Kang, O.; Llinares, J.M.; Day, V. W; Bowman, K. J.; *Chem. Soc. Rev.* **2010**, 39, 3980-4003.

7 Vriezema, D. M.; Comellas Aragonés, M.; Elemans, J. A. A. W.; Cornelissen, J. J. L. M.; Rowan, A. E.; Nolte, R. J. M; *Chem. Rev.* **2005**, 105, 1445-1489; Pemberton, B.C.; Barooah, N.; Srivatsava, D. K. and J. Sivaguru; *Chem. Commun.,* **2010**, 46, 225–227

8 Chung, W.J.; Oh, J. W.; Kwak, K.; Lee, B.Y, Meyer, J.; Wang, E.; Hexemer, A. and Lee, S. W.; *Nature,* **2011**, 478, 364-368; Zhang, S. G.; *Nature Biotechnology*, **2003,** 21, 1171–1178.

9 Rowsell, J. L. C.; Yaghi, O. M. *Microporous and Mesoporous Materials*, **2004**, 73, 3; Atwood, J. L.; Barbour, L. J.; Dalgarno, S. J.; Hardie, M. J.; Raston, C. L.; Webb, H. R. *J. Am. Chem. Soc.* **2004**, 126, 13170; Fujita, M.; Oguro, D.; Miyazawa, M.; Oka, H.; Yamaguchi, K.; Ogura, K. *Nature*, **1995**, 378; Karagiaridi, O.; Bury, W.; Sarjeant, A.A.; Stern, C.L; Farha, O.K.; Hupp, J. T.; *Chemical Science,* **2012**, 3, 3256-3260.

10 Good D. J; Rodrıguez-Hornedo N., **2010**. *Cryst Growth Des*., 10, 1028–1032; Gao Y, Zu H, Zhang J. **2011**. *J PharmPharmacol*., 63, 483–490;

11 Kitaigorodski, A. I. *Molecular Crystals and Molecules*, Academic press, New York, 1973.

12 Barooah, N.; Sarma, R. J.; Baruah, J. B. *CrystEngComm,* **2006**, 8, 608; Motohiro, N. *CrystEngComm*, **2004**, 6, 130.

13 Yoshizawa, M.; Miyagi, S.; Kawano, M.; Ishiguro, K.; Fujita, M. *J. Am. Chem. Soc*. **2004**, 126, 9172; Fox, O. D.; Drew, M. G. B.; Beer, P. D. *Angew. Chem., Int. Ed.* **2000**, 39, 135

14 Steed, J. W.; Atwood, J. L. *Supramolecular Chemistry*; Wiley &Sons: Chichester, **2000**, Freek J. M. Hoeben, E. W. Meijer, *Chemical Reviews*, **2005**, 105, 1491

15 Schmidt, G. M. *J. Pure Appl. Chem.* **1971**, 27, 647.

16 Seddon, K. R. and Zaworotko, M., *Crystal engineering: The design and application of functional solids,* Vol 539, **1999**; Desiraju, G. R., *Crystal Engineering: The design of Organic Solids,* Elsevier, **1989**;

17 Desiraju, G. R.; Krishnamohan, S. *Perspectives in Supramolecular Chemistry: The Crystal as a Supramolecular Entity*, Volume 2, John Wiley & Sons, Ltd. **2007**

18 Lehn, J.-M. *Supramolecular Chemistry*. Weinheim: Wiley-VCH, **1995**;

19 Aakeröy, C.B.; Salmon, D.J. *CrystEngComm*. **2005**, 7, 439

20 Desiraju, G, R.; Vittal, J. J.; Ramanan, A., *Crystal Engineering: A Textbook*, **2011**.

21 Lehn, J. M., *Science,* **2002**, 295, 2400

22 Jeffrey, G. A.; Saenger, W. *Hydrogen Bonding in Biological Structures*, Springer-Verlag, Berlin, Heidelberg, New York, **1991**

23 http://www.astrochem.org/sci/Nucleobases.php

24 S. Scheiner, *Hydrogen Bonding. A Theoretical Perspective*, Oxford University Press, Oxford, **1997**; A. K. Rapp, E. R. Bernstein, *J. Phys. Chem. A* **2000**, 104, 6117-6128; K. M, ller-Dethlefs, P. Hobza, *Chem. Rev***. 2000**, 100, 143-167; M. J. Calhorda, *Chem. Commun*. **2000**, 801-809.

25 Aakeröy, C.; Grommet, A.; Desper, J., *Pharmaceutics*, **2011**, 3, 601-614; Aakeröy, C.; Hurley, E.; Desper, J., *Cryst. Growth Des.,* **2012**, 12, 5806–5814

26 http://www.chemistry.ccsu.edu/glagovich/teaching/316/nmr/factors.html

27 Chutia, R.; Dey, S. K.; Das G., *Cryst. Growth Des.,* **2013**, 13, 883–892

28 Brittain, H. G., *Physical Characterization of Pharmaceutical Solids*, Marcel Dekker, New York, **1995**.

29 Bratož, S.; Hadži, D.; Sheppard, N.; *Spectrochim. Acta,* **1956,** 8, 249**–**261; Bellamy, L.J., *Advances in Infrared Group Frequencies,* Methuen &Co.: London, **1968**; Mukherjee, A.; Tothadi, S.; Chakraborty, S.; Ganguly, S.; Desiraju, G. R., *CrystEngComm,* **2013**, Accepted Manuscript

30 Aakeröy, C. B.; Salmon, D.J.; Smith, M. M.; Desper, J., *Cryst. Growth Des.* **2006**, 4, 1033-1042; Schultheiss, N.; Newman, A., *Cryst. Growth Des.,* **2009**, 2950-2967.

31 Metrangolo, P. and Resnati, G. *Halogen Bonding: Fundamentals and Applications, Structure and Bonding*, Springer, Berlin, **2007**

32 Clark, T.; Hennemann, M.; Murray, J.; Politzer, P., *J Mol Model*, **2007**, 13, 291–296

33 Legon, A. C. *Angew. Chem.* **1999**, 111, 2850; Legon, A. C. *Halogen Bonding Fundamentals and Applications*, Metrangolo, P.; Resnati, G. Springer, Berlin, **2008**, 17-64; Legon, A. C. *Angew. Chem. Int. Ed.* **1999**, 38, 2686

34 Nguyen, H. L.; Horton, P. N.; Hursthouse, M. B.; Legon, A. C.; Bruce, D. W. *J. Am. Chem. Soc.* **2004**, 126, 16.

35 Chudzinski, M. G.; McClary, A. C.; Taylor. M. S. *J. Am. Chem. Soc.,* **2011**, 133, 10559; Sarwar, M. G.; Dragisic, B.; Sagoo, S.; Taylor, M. S. *Angew. Chemie.* **2010**, 122, 1718

36 Auffinger, P.; Hays, F. A.; Westhof, E.; Shing, H. P., *Proc Nat Acad Sci,* **2004**, 101, 16789–16794

37 Almarsson, Ö.; Zaworotko, M.J. *Chem. Commun.* **2004**, 1889

38 Kola, I,; Landis, J. *Nature reviews*, **2004**, 3, 711

39 Vishweshwar, P.; McMahon, J. A.; Bis, J. A.; Zaworotko, M. J.; *J Pharm Sci,* **2006**; 95:499-516; Sarma, B.; Reddy, L. S.; Nangia, A.; *Cryst Growth Des*., **2008,** 8, 4546-4552

40 Encyclopedia of Agrochemicals, DOI: 10.1002/047126363X

41 http://ipipotash.org

42 Graham Matthews, 2006, Pesticides: Health, Safety and the Environment

43 http://www.agf.gov.bc.ca/pesticides/c_2.htm

44 Neil, G.; Forrest, J.; Rebecca, B., Aakeröy, C., Patent, WO2011128618; Nauha, E.; Kolehmainen, E.; Nissinen, M., *CrystEngComm,* **2011**, 13, 6531-6537; Nauha, E.; Nissinen, M., *Journal of Molecular Structure,* **2011**, 566‑569; Mereiter, K., *Acta Crystallogr Sect E*. **2011**, 67, 2321–2322

45 Weiss et al., United States Patent, #EP2010/066095

46 Lukevits, È. *Chemistry of Heterocyclic Compounds*, **1995**, 31, 639

Chapter-2 Establishing supramolecular control over solid-state architectures: A simple mix and match strategy

2.1 Introduction

Molecular self-assembly is at the core of supramolecular synthesis. The knowledge of supramolecular synthons[1] is a pre-requisite for the systematic design and assembly of molecular building blocks into predictable architectures. In crystal engineering[2], robust heteromeric synthons like the acid...pyridine,[3] acid...aminopyridine[4] and hydroxy...pyridine[5] are most commonly used to construct binary and ternary co-crystals via O-H···N hydrogen bonds[6], Figure 2.1.

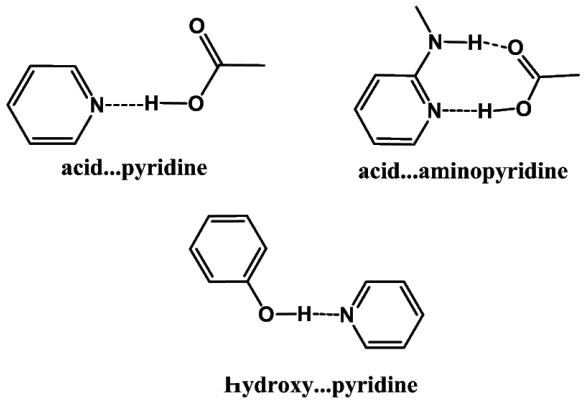

Figure 2.1 Examples of supramolecular heterosynthons

Hydrogen-bond interactions primarily depend on the chemical nature around the hydrogen atom, *i.e.* if it is part of an acid, hydroxy, oxime, amine *etc*, and on the electrostatic environment around it. The strength of a hydrogen bond typically ranges between 10–65 kJ/mol[7]. In supramolecular synthesis, the shape and dimensionality of the resulting assembly is governed by the geometric complementarity between the donor and acceptor units during the self-assembly process, Figure 2.2. A better understanding of the dependence of solid-state architecture on the geometric match between the building blocks can provide a path to more efficient design of reliable assemblies with controllable, pre-determined connectivities.

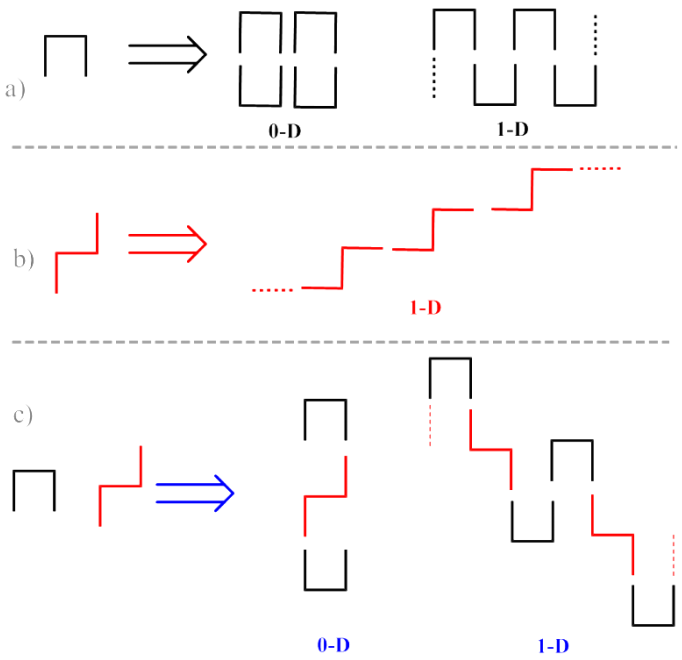

Figure 2.2 Examples of geometrically complementary building blocks forming assemblies of different dimensionalities

In this study we sought to explore the link between the molecular geometry of the individual building blocks and the resulting structural outcome. Reliable and robust acid-pyridine/acid-aminopyridine heterosynthons were used as the key interactions to lay a foundation for the construction of a supramolecular framework. We carried out systematic co-crystallization experiments between two ditopic pyridine based acceptors (N-(3-pyridin-2-yl) nicotinamide, **3N** and N-(4-pyridin-2-yl) isonicotninamide, **4N**) and a set of odd (malonic, glutaric, pimelic and azelaic) and even-chain (succinic, adipic,suberic and sebacic) di-carboxylic acid donors. The acceptors differ in the relative orientation of the two binding sites (Fig 2.3); **3N** has the binding sites positioned parallel with respect to each other, whereas in **4N** they are at an angle of approximately 60° with respect to each other. Among the donors, odd-chain diacids have their two donor sites positioned at an angle of approximately 120° while in even-chain diacids, they are almost co-linear (Fig 2.4).

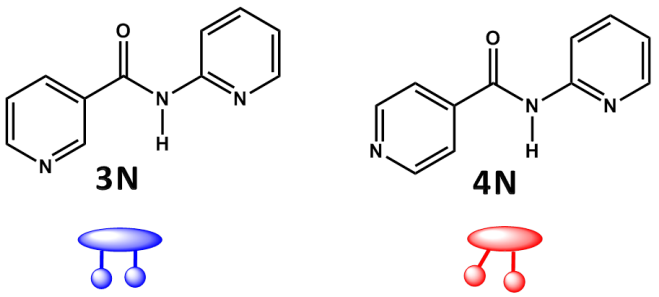

Figure 2.3 Binding site orientation in 3N and 4N

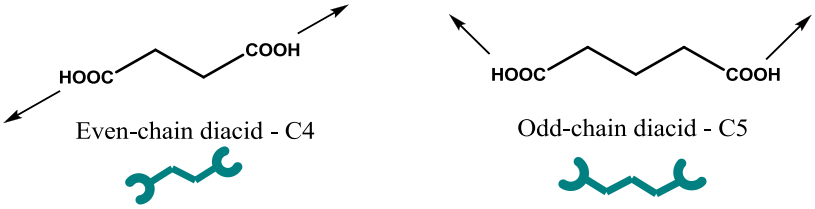

Figure 2.4 Binding site orientation in even and odd-chain aliphatic diacids

Depending upon the choice of the acceptor (**3N** or **4N**) and donor (even or odd diacids) combination to form a co-crystal, there are four different assemblies that could potentially be formed, Figure 2.5.

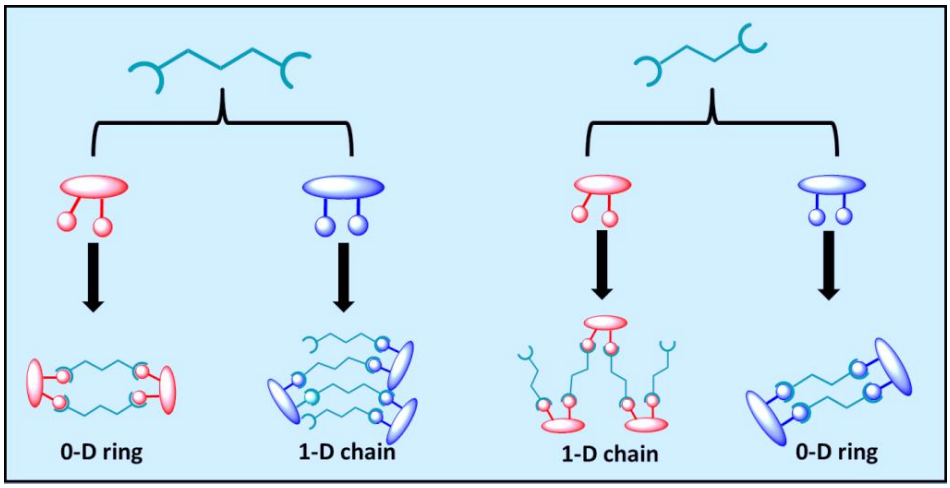

Figure 2.5 Possible architectures from building blocks 3N and 4N

Thus, the goals of this section are to;

1. Synthesize the two acceptors, **3N** and **4N**.

2. Test the potential of **3N** and **4N** for forming co-crystals with odd and even-chain diacids.
3. Grow single crystals, analyze them and elucidate any structural consistency.
4. Determine the effect of molecular geometry of the interacting species on the resulting supramolecular architectures.

2.2 Experimental

2.2.1 Synthesis

All chemicals, unless noted, were purchased from Sigma Aldrich and used without further purification. Melting points were determined on a Fisher- Johns melting point apparatus. ^{1}H and ^{13}C NMR spectra were recorded on a Varian Unity plus 400 MHz or 200 MHz spectrometer in $CDCl_3$ or D_6-DMSO. Infrared spectroscopy (IR) was done on a Nicolet 380 FT-IR.

2.2.1.1 Synthesis of (N-(3-pyridin-2-yl) nicotinamide), 3N[8]

The synthesis of **3N** was carried out using a modified procedure.[8] Nicotinic acid (1.45 g, 11.79 mmol) and triethylamine (1.92 ml, 13.77 mmol) were dissolved in 20 mL of chloroform. Thionyl chloride (1.2 ml, 16.52 mmol) was added drop wise under a dinitrogen atmosphere maintaining the temperature between 5 and 10 °C. After the addition was complete, the mixture was heated under reflux for 3 h at the end of which a brown solution was obtained. The mixture was cooled to room temperature, then a solution of amino pyridine (1.29 g, 13.34 mmol), triethylamine (1.01 g, 10 mmol), and acetonitrile (20 mL) was added in situ and stirred at room temperature overnight. The organic layer was washed with water, and the solvent was removed, followed by column chromatography to yield an off-white powder as the product. Yield 35%, mp 142−145 °C (lit. 141−143 °C).[9] ^{1}H NMR (δH, 400 MHz, DMSO): 11.094 (s, N−H 1H), 9.135 (s, 1H), 8.761 (d, 1H), 8.409 (d, 1H), 8.340 (d, 1H), 8.120 (d, 1H), 7.845 (t, 1H), 7.541 (t, 1H), 7.189 (t, 1H).

2.2.1.2 Synthesis of (N-(4-pyridin-2-yl) isonicotninamide), 4N[8]

The synthesis of **4N** was carried out using a modified procedure.[8] Isonicotinic acid (1.21 g, 9.82 mmol) and triethylamine (1.6 ml 11.47 mmol) were dissolved in 20 mL of chloroform. Thionyl chloride (1 ml, 13.76 mmol) was added drop wise under a dinitrogen atmosphere

maintaining the temperature between 5 and 10 °C. After the addition was complete, the mixture was heated under reflux for 3 h at the end of which a brown solution was obtained. The mixture was cooled to room temperature, then a solution of amino pyridine (1.08 g, 11.47 mmol), triethylamine (1.6 ml, 11.47 mmol), and acetonitrile (20 mL) was added in situ and stirred at room temperature overnight. The organic layer was washed with water, and the solvent was removed. Column chromatography gave a white powder as the product. Yield 41%, mp 138−140 °C (lit. 136−138 °C).[10] ^{1}H NMR (δH, 400 MHz, MeOD): 8.748 (s, 2H), 8.363 (s, 1H), 8.245 (d, J = 8.2 Hz, 1H), 7.902−7.801 (m, 3H), 7.208−7.153 (m, 1H).

2.2.2 IR spectroscopy screening of co-crystals

The ligands **3N** and **4N** were initially combined with even and odd-chain diacids to prepare co-crystal formation using solvent-drop assisted grinding. **3N/4N** and the co-formers were combined in a 1:1 stoichiometry in a motor and pestle. A drop of methanol was added and the mixture was ground for 30 seconds. The resulting product was screened using IR spectroscopy to confirm co-crystal formation via two broad O-H···N stretches in the 1800-2500 cm^{-1} region and also a significant shift in the acid C=O stretch. All samples that showed a positive hit for co-crystal formation were then subjected to slow evaporation experiments to grow single crystals suitable for X-ray diffraction analysis.

2.2.3 Synthesis of co-crystals using slow evaporation

2.2.3.1 (N-(3-pyridin-2yl)nicotinamide) malonic acid (1:1), 3N-MA

A solution of **3N** (10 mg, 0.05 mmol) in 2 mL of ethyl acetate was mixed with malonic acid (5.23 mg, 0.05 mmol) in 2 mL of ethyl acetate and warmed. Transparent rod-like crystals were obtained within few weeks. Mp 125−127 °C.

2.2.3.2 (N-(3-pyridin-2yl)nicotinamide) glutaric acid (1:1), 3N-GA

A solution of **3N** (10 mg, 0.05 mmol) in 2 mL of ethyl acetate was mixed with glutaric acid (6.6 mg, 0.05 mmol) in 2 mL of isopropanol and warmed. Transparent rod-like crystals were obtained within 40 days. Mp 94-97 °C.

2.2.3.3 (N-(3-pyridin-2yl)nicotinamide) pimelic acid (1:1), 3N-PA

A solution of **3N** (10 mg, 0.05 mmol) in 2 mL of ethyl acetate was mixed with pimelic acid (8.0 mg, 0.05 mmol) in 2 mL of ethyl acetate and warmed. Transparent rod-like crystals were obtained. Mp 119−120 °C.

2.2.3.4 (N-(3-pyridin-2yl)nicotinamide) azelaic acid (1:1), 3N-AzA

A solution of **3N** (10 mg, 0.05 mmol) in 2 mL of ethyl acetate was mixed with azelaic acid (9.41 mg, 0.05 mmol) in 2 mL of ethyl acetate and warmed. Needle-like crystals were formed. Mp 90−93 °C.

2.2.3.5 (N-(3-pyridin-2yl)nicotinamide) succinic acid (1:1), 3N-SA

A solution of **3N** (10 mg, 0.05 mmol) in 2 mL of ethyl acetate was mixed with succinic acid (5.9 mg, 0.05 mmol) in 2 mL of ethyl acetate and warmed. Transparent needle-shaped crystals were obtained. Mp 145−147 °C.

2.2.3.6 (N-(3-pyridin-2yl)nicotinamide) adipic acid (1:1), 3N-AA

A solution of **3N** (10 mg, 0.05 mmol) in 2 mL of ethyl acetate was mixed with adipic acid (7.31 mg, 0.05 mmol) in 2 mL of ethyl acetate and warmed. Transparent block-shaped crystals were formed. Mp 140−142 °C.

2.2.3.7 (N-(3-pyridin-2yl)nicotinamide) sebacic acid (1:1), 3N-SeA

A solution of **3N** (10 mg, 0.05 mmol) in 2 mL of ethyl acetate was mixed with sebacic acid (10.11 mg, 0.05 mmol) in 2 mL of ethyl acetate and warmed. Needle-shaped crystals were formed in four weeks. Mp 104−106 °C.

2.2.3.8 (N-(4-pyridin-2yl)isonicotinamide) glutaric acid (1:1), 4N-GA

A solution of **4N** (10 mg, 0.05 mmol) in 2 mL of ethyl acetate was mixed with glutaric acid (6.6 mg, 0.05 mmol) in 2 mL of ethyl acetate and warmed. Transparent rod-like crystals were obtained within 20 days. Mp 127−129 °C.

2.2.3.9 (N-(4-pyridin-2yl)isonicotinamide) pimelic acid (1:1), 4N-PA

A solution of **4N** (10 mg, 0.05 mmol) in 2 mL of ethyl acetate was mixed with pimelic acid (8.0 mg, 0.05 mmol) in 2 mL of ethyl acetate and warmed. Transparent needle-like crystals were obtained in one month. Mp 123−125 °C.

2.2.3.10 (N-(4-pyridin-2yl)isonicotinamide) azelaic acid (1:1), 4N-AzA

A solution of **4N** (10mg, 0.05mmol) in 2 ml of ethyl acetate was mixed with azelaic acid (9.41mg, 0.05 mmol) in 2 ml ethyl acetate and warmed. Transparent needle-like crystals were formed after 45 days. Mp 92-95 ^{o}C.

2.2.3.11 (N-(4-pyridin-2yl)isonicotinamide) succinic acid (1:1), 4N-SA

A solution of **4N** (10mg, 0.05mmol) in 2 ml of ethyl acetate was mixed with succinic acid (5.9mg, 0.05mmol) in 2 ml ethyl acetate and warmed. Transparent needles were obtained in 2 months. Mp 122-125 ^{o}C.

2.2.3.12 (N-(4-pyridin-2yl)isonicotinamide) adipic acid (1:1), 4N-AA

A solution of **4N** (10mg, 0.05mmol) in 2 ml of ethyl acetate was mixed with adipic acid (7.31mg, 0.05mmol) in 2 ml ethyl acetate and warmed. Transparent block-shaped crystals were formed in three weeks. Mp 142-145 ^{o}C.

2.2.3.13 (N-(4-pyridin-2yl)isonicotinamide) suberic acid (1:1), 4N-SuA

A solution of **4N** (10mg, 0.05mmol) in 2 ml of ethyl acetate was mixed with suberic acid (8.71mg, 0.05mmol) in 2 ml ethyl acetate and warmed. Transparent rod-shaped crystals were obtained within a few weeks. Mp 133-135 ^{o}C.

2.2.3.14 (N-(4-pyridin-2yl)isonicotinamide) sebacic acid (1:1), 4N-SeA

A solution of **4N** (10mg, 0.05mmol) in 2 ml of ethyl acetate was mixed with sebacic acid (10.11mg, 0.05mmol) in 2 ml ethyl acetate and warmed. Transparent rod-like crystals were formed within a month. Mp 104-107 ^{o}C.

2.3 Results

With the diacids, seven crystal structures were obtained out of eight co-crystallization experiments for **3N** and **4N,** respectively. Although IR spectroscopy confirmed a co-crystal for **3N-SuA** and **4N-MA** combination during the solvent assisted grinding method, single crystals suitable for X-ray diffraction analysis could not be grown for **3N-SuA** and **4N-MA**. Table 2.1 lists the IR stretches for O-H···N hydrogen bonds and the C=O stretch in the acid and corresponding co-crystal. Detailed hydrogen bond geometries for **3N** and **4N** co-crystals with the diacids are listed in Table 2.2 and 2.3, respectively.

Table 2.1 Summary of IR spectroscopy data for 3N and 4N co-crystals

Compound	O-H···N stretches (cm^{-1})	C=O stretch (cm^{-1}) (acid)	C=O stretch (cm^{-1}) (co-crystal)
3N-MA	2439; 1871	1693	1701
3N-GA	2450; 1850	1682	1680
3N-PA	2487; 1877	1683	1686
3N-AzA	2495; 1887	1682	1684
3N-SA	2406; 1887	1686	1679
3N-AA	2430; 1895	1683	1695
3N-SeA	2509; 1886	1682	1683
4N-GA	2492; 1862	1682	1687
4N-PA	2357; 1883	1683	1687
4N-AzA	2488; 1875	1682	1683
4N-SA	2481; 1890	1686	1685
4N-AA	2492; 1862	1683	1687
4N-SuA	2471; 1907	1684	1683
4N-SeA	2483; 1877	1682	1684

Table 2.2 Hydrogen bond geometries in 3N co-crystals[a]

Structure	D-H...A	D-H/A	H...A/A	D...A/A	D-H-N/°
3N-MA	N17 H17 O32	0.921(16)	2.225(16)	3.1144(13)	162.1(13)
	O31 H31 N21	0.969(16)	1.647(16)	2.5945(13)	164.8(14)
	O33 H33 N11_#1	0.971(17)	1.666(17)	2.6344(13)	174.9(15)
3N-GA	O31 H31 N11	0.958(16)	1.703(17)	2.6573(12)	173.6(15)
	N17 H17 O36_#1	0.860(14)	2.005(14)	2.8599(11)	172.6(13)
	O35 H35 N21_#2	0.940(17)	1.772(17)	2.7045(11)	171.0(14)
3N-PA	N17_1 H17_1 O32_1	0.90(2)	2.08(2)	2.975(2)	172.3(19)
	N17_2 H17_2 O32_2	0.89(2)	2.06(2)	2.943(2)	172(2)

	O31_1 H31_1 N21_1	1.04(2)	1.63(2)	2.6672(19)	172.5(19)
	O31_2 H31_2 N21_2	0.88(2)	1.78(2)	2.6611(19)	176(2)
	O37_1 H37_1 N11_2	0.91(2)	1.77(2)	2.672(2)	172.1(19)
	O37_2H37_2 N11_1_#1	1.01(2)	1.64(2)	2.647(2)	172.7(18)
3N-AzA	O31 H31 N11	1.00(2)	1.71(2)	2.7055(17)	171.3(18)
	N17 H17 O40_#1	0.906(19)	2.074(19)	2.9785(17)	176.7(16)
	O39 H39 N21_#2	0.95(2)	1.71(2	2.6491(17)	169.6(19
3N-SA	O31 H31 N11	0.96(2)	1.70(2)	2.6581(19)	172(2)
	N17 H17 O35_#1	0.85(2)	2.12(2)	2.9674(19)	170(2)
	O34 H34 N21_#1	0.90(2)	1.79(2)	2.6702(18)	169(2)
3N-AA	O31 H31 N11	0.909(17)	1.780(17)	2.6832(12)	172.0(14)
	N17 H17 O36_#1	0.924(14)	2.009(14)	2.9271(11)	172.2(12)
	O37 H37 N21_#1	0.970(17)	1.721(17)	2.6785(11)	168.6(14)
3N-SeA	O31 H31 N11	0.898(18)	1.795(18)	2.6898(14)	174.4(16)
	O41 H41 N21_#1	0.89(2)	1.79(2)	2.6579(14)	166.3(18)
	N17 H17 O42_#1	0.88	2.05	2.9131(13)	168.0

[a]Symmetry codes: **3N−MA**: #1 x,1 − y,−0.5 + z. **3N-GA**: #1 x, -y+1/2, z+1/2. #2 x, -y+1/2, z-1/2. **3N−PA**: #1 −2 + x, 1 + y, 1 + z. **3N−AzA**: #1 −0.5 −x, 0.5 + y, 0.5 − z. #2 −0.5 − x, −0.5 + y, 0.5 − z. **3N−SA**: #1 −x, 1 − y, 1 − z. **3N−AA**: #1 −x, 1 − y, −z. **3N−SeA**: #1 2 − x, 1 − y, 1 − z.

Table 2.3 Hydrogen bond geometries in 4N **co-crystals**[b]

Structure	D-H...A	D-H/A	H...A/A	D...A/A	D-H-N/o
4N-GA	O31 H31 N11	0.962(17)	1.712(17)	2.6713(11)	174.6(14)
	N17 H17 O36_#1	0.855(14)	2.164(14)	3.0103(11)	170.7(13)
	O35 H35 N21_#1	0.898(15)	1.786(15)	2.6570(11)	162.9(15)
4N-PA	N17 H17 O32	0.90(3)	2.08(3)	2.970(3)	173(2)
	O31 H31 N21	0.95(3)	1.74(3)	2.679(3)	169(3)
	O37 H37 N11	1.10(3)	1.57(3)	2.665(3)	172(2)
4N-AzA	O31 H31 N21	0.942(15)	1.738(15)	2.6756(11)	173.6(13)

	N17 H17 O32	0.862(14)	2.063(14)	2.9200(12)	172.7(12)
	O39 H39 N11_#1	0.957(15)	1.785(15)	2.7413(12)	176.3(13)
4N-SA	N17_1 H17_1 O52_1	0.89(2)	2.12(2)	3.005(2)	174(2)
	N17_2 H17_2 O52_2	0.92(2)	2.13(2)	3.050(2)	174.8(19)
	N17_3 H17_3 O52_3	0.91(2)	2.09(2)	3.001(2)	176.5(18)
	O51_1 H51_1 N21_1	0.97(2)	1.70(2)	2.661(2)	170(2)
	O51_2 H51_2 N21_2	0.96(2)	1.75(2)	2.691(2	165(2)
	O51_3 H51_3 N21_3	1.00(2)	1.69(2)	2.681(2)	170(2)
	O54_1 H54_1 N41_1	0.98(2)	1.72(2)	2.685(2)	171(2)
	O54_2 H54_2 N41_2	0.97(2)	1.74(2)	2.679(2)	162.4(19)
	O54_3 H54_3 N41_3	0.94(2)	1.79(2)	2.702(2)	165(2)
	O61_1 H61_1 N11_1	0.96(2)	1.72(2)	2.667(2)	173(2)
	O61_2 H61_2 N11_2	0.93(2)	1.75(2)	2.668(2)	170(2)
	O61_3 H61_3 N11_3	0.97(2)	1.72(2)	2.683(2)	173(2)
	O64_1 H64_1 N31_1_#1	0.90(2)	1.80(3)	2.688(2)	168(2)
	O64_2 H64_2 N31_2_#1	0.93(2)	1.74(2)	2.670(2)	175(2)
	O64_3 H64_3 N31_3 _#1	0.94(3)	1.72(3)	2.659(2)	170(2)
4N-AA	N17 H17 O42	0.856(18)	2.058(18)	2.9131(14)	177.4(17)
	O31 H31 N11	0.98(2)	1.73(3)	2.6945(15)	169(2)
	O41 H41 N21	0.94(2)	1.74(2)	2.6772(14)	172.3(19)
4N-SuA	O31 H31 N11	1.03(2)	1.69(2)	2.7133(15)	179.3(18)
	N17 H17 O39_#1	0.850(16)	2.077(16)	2.9228(13)	173.6(14)
	O38 H38 N21_#2	1.120(17)	1.541(17)	2.6583(13)	175.3(14)
4N-SeA	O31 H31 N11	0.999(15)	1.674(15)	2.6693(12)	174.2(13)
	N17 H17 O41_#1	0.855(14)	2.002(14)	2.8556(12)	176.2(13)
	O40 H40 N21_#2	1.013(15)	1.626(15)	2.6327(12)	172.0(13)

[b]Symmetry codes: **4N−GA**: #1 1 − x,−y, 1 − z. **4N−PA**: #1 2.5 − x, −0.5 + y, 1.5 − z. **4N−AzA**: #1 −1 − x, −y, 1 − z. **4N−SA**: #1 −1 + x, −1 + y, z. **4N−SuA**: #1 0.5 − x, −0.5 + y, 1.5 − z. #2 0.5 − x, 0.5 + y, 1.5 − z. **4N−SeA**: #1 0.5 − x, 0.5 + y, 1.5 − z. #2 0.5 − x, −0.5 + y, 1.5 − z.

2.3.1 Structural description of co-crystals

2.3.1.1 Crystal structure of 3N:MA

A co-crystal is formed between **3N** and malonic acid via two different primary hydrogen bonds; O-H···N(py), 2.594(13) Å and O-H···N(aminopy), 2.634(13) Å on either side of the diacid. The resulting structure is a 1-D infinite chain-like architecture (Fig 2.6).

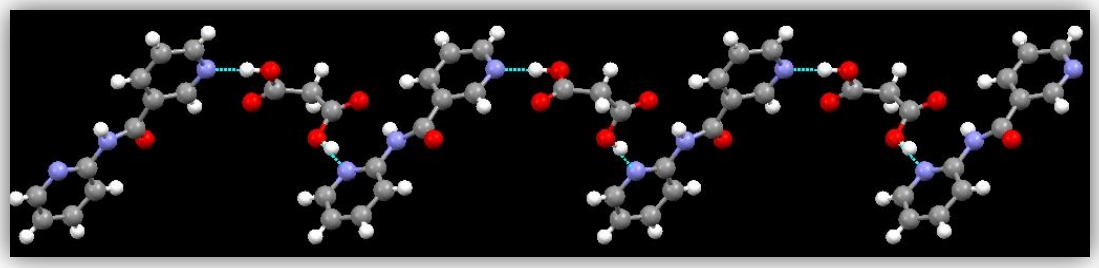

Figure 2.6 1-D chain formed in the co-crystal of 3N:MA

2.3.1.2 Crystal structure of 3N:GA

The crystal structure of **3N:GA** shows a co-crystal formed between **3N** and GA via two unique hydrogen bonds, O-H···N(py) and O-H···N(aminopy) with bond distances of 2.657(12) and 2.704(11) Å, respectively. The resulting architecture is an infinite 1-D zig-zag chain (Fig 2.7).

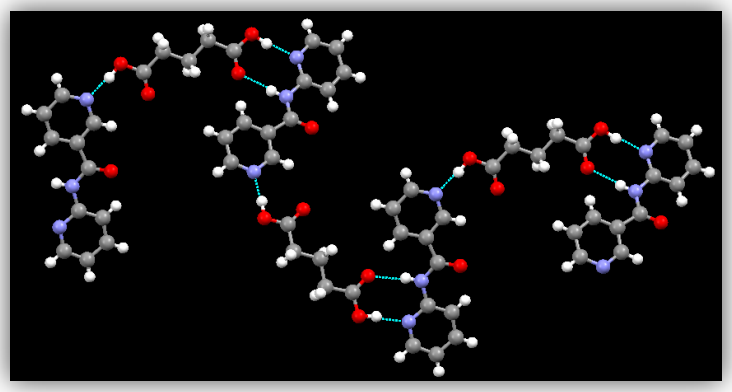

Figure 2.7 1-D zig-zag chain in the 3N:GA **co-crystal**

2.3.1.3 Crystal structure of 3N:PA

In the **3N:PA** co-crystal, primary synthons formed are the O-H···N(py) and O-H···N(aminopy) hydrogen bond with bond distances of 2.647(2) Å and 2.661(19) Å, respectively, resulting in a 1-D planar chain-like structure (Fig 2.8).

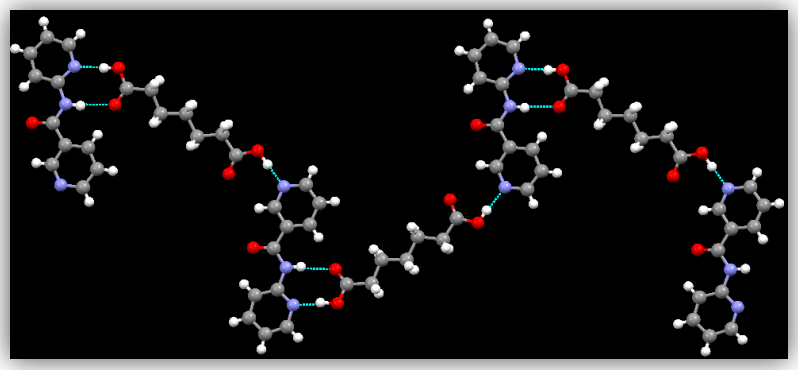

Figure 2.8 1-D infinite chains formed in the 3N:PA **co-crystal**

2.3.1.4 Crystal structure of 3N:AzA

In **3N:AzA**, azelaic acid interacts on both sides with **3N** via COOH-N(py), 2.705(17) Å and COOH-N(aminopy), 2.649(17) Å hydrogen bonds. It is interesting to note that unlike in **3N:MA**, **3N:GA** and **3N:PA**, in **3N:AzA**, the O-H···N bond distance for acid-pyridine interaction is shorter than the acid-aminoyridine interaction. The resulting architecture resembles infinite corrugated chains (Fig 2.9).

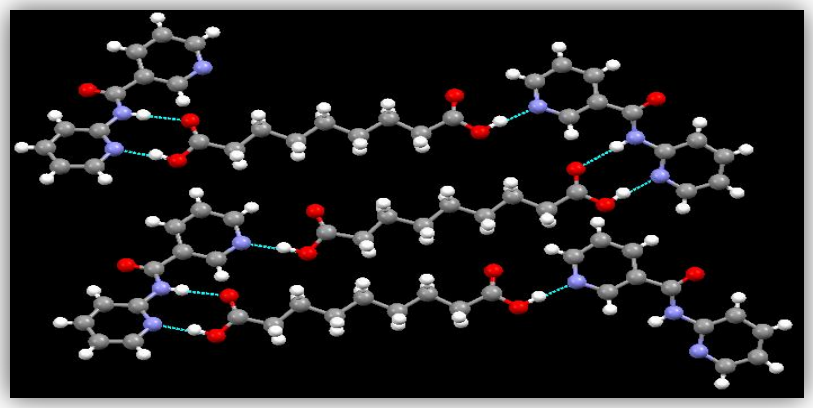

Figure 2.9 1-D corrugated chains in the 3N:AzA **co-crystal**

2.3.1.5 Crystal structure of 3N: SA

In **3N:SA** co-crystal the primary synthons are the robust O-H···N(py), 2.658(19) Å and O-H···N(aminopy), 2.670(18) Å hydrogen bonds that result in the formation of tetrameric rings (Fig 2.10).

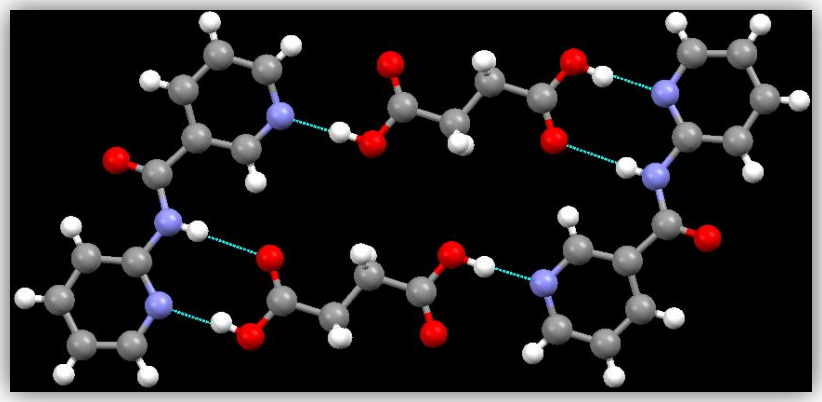

Figure 2.10 0-D ring in the 3N:SA **co-crystal**

2.3.1.6 Crystal structure of 3N:AA

The crystal structure of **3N:AA** shows a 1:1 co-crystal between **3N** and adipic acid. O-H···N(py), 2.683(12) Å and O-H···N(aminopy), 2.678(11) Å are the primary interactions that direct the assembly of tetrameric 0-D ring (Fig 2.11).

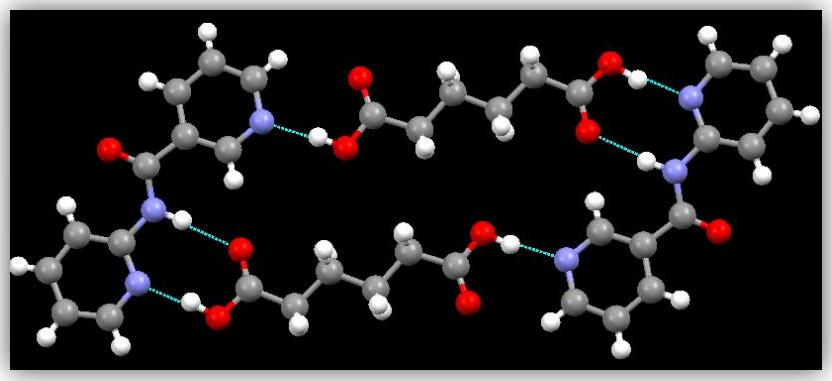

Figure 2.11 0-D ring architecture in the 3N:AA **co-crystal**

2.3.1.7 Crystal structure of 3N:SeA

The crystal structure of **3N:SeA** consist of a 1:1 co-crystal between **3N** and sebacic acid. The acid binds to **3N** on either sides via short O-H···N(py), 2.689(14) Å and O-H···N(aminopy), 2.657(14) Å hydrogen bonds. The resulting assembly is a tetrameric ring (Fig 2.12).

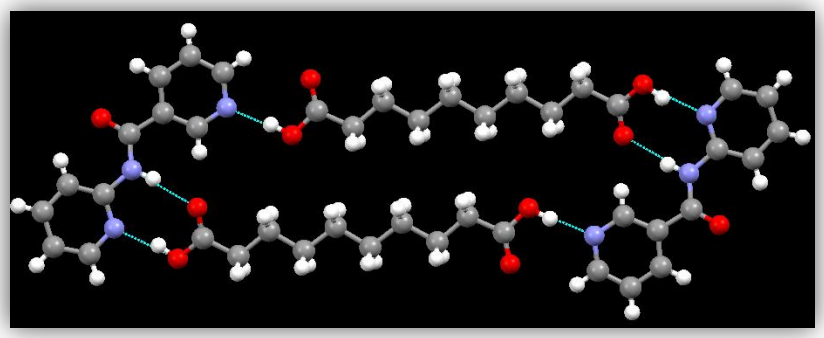

Figure 2.12 0-D ring architecture in the co-crystal of 3N:SeA

2.3.1.8 Crystal structure of 4N:GA

The crystal structure of **4N:GA** shows a 1:1 co-crystal formed using both O-H···N(py), 2.671(11) Å and O-H···N(aminopy), 2.657(11) Å hydrogen bonds. The interactions result in 0-D rings (Fig 2.13).

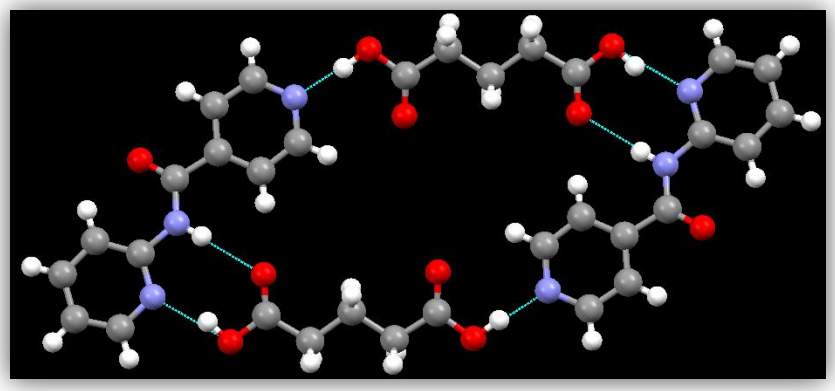

Figure 2.13 0-D tetrameric ring in the 4N:GA **crystal structure**

2.3.1.9 Crystal structure of 4N:PA

The crystal structure of **4N:PA** displays an infinite 1-D zig-zag chain formed via O-H···N(py), 2.665(3) Å and O-H···N(aminopy), 2.679(3) Å hydrogen bonds (Fig 2.14).

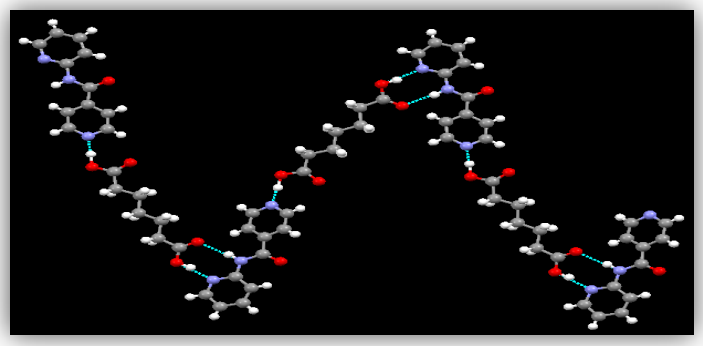

Figure 2.14 1-D zig-zag chains formed in the 4N:PA **co-crystal**

2.3.1.10 Crystal structure of 4N:AzA

The crystal structure of **4N:AzA** is a 1:1 co-crystal formed between **4N** and azelaic acid via O-H···N(py), 2.741(12) Å and O-H···N(aminopy), 2.676(11) Å hydrogen bonds (Fig 2.15). The acid-pyridine bond distance is comparatively longer than the acid-aminopyridine bond distance. The resulting assembly is a tetrameric ring.

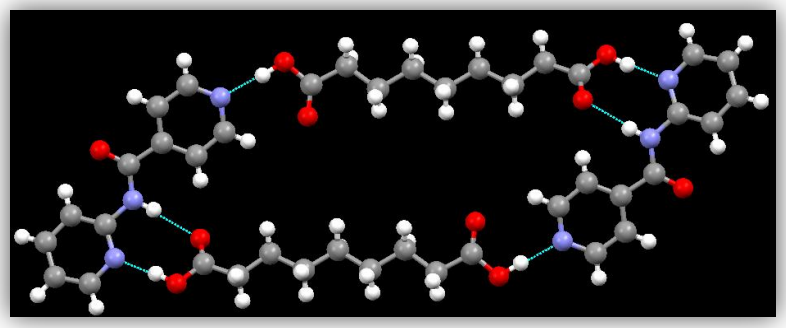

Figure 2.15 0-D tetrameric ring in the 4N:AzA **co-crystal**

2.3.1.11 Crystal structure of 4N:SA

The crystal structure of **4N:SA** displays infinite 1-D zig-zag planar chains formed using strong hydrogen bond interactions, *i.e.* O-H···N(py), 2.688(2) Å and O-H···N(aminopy), 2.660(2) Å (Fig 2.16).

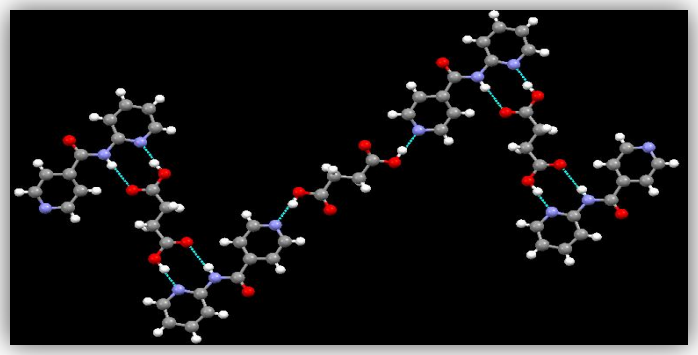

Figure 2.16 Infiite 1-D zig-zag chains formed in 4N:SA **co-crystal**

2.3.1.12 Crystal structure of 4N:AA

The crystal structure of **4N:AA** displays infinite 1-D corrugated chains formed via intermolecular O-H···N(py), 2.695(15) Å and O-H···N(aminopy), 2.677(14) Å hydrogen bonds (Fig 2.17).

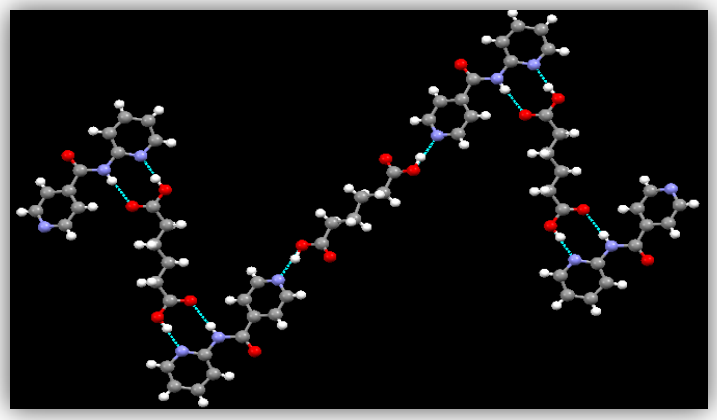

Figure 2.17 1-D infinite corrugated chains in 4N:AA **co-crystal structure**

2.3.1.13 Crystal structure of 4N:SuA

The crystal structure of **4N:SuA** displays 1-D corrugated chain formed via strong intermolecular hydrogen bond interactions on either sides of suberic acid, *i.e.* O-H···N(py), 2.713(15) Å and O-H···N(aminopy), 2.658(13) Å (Fig 2.18).

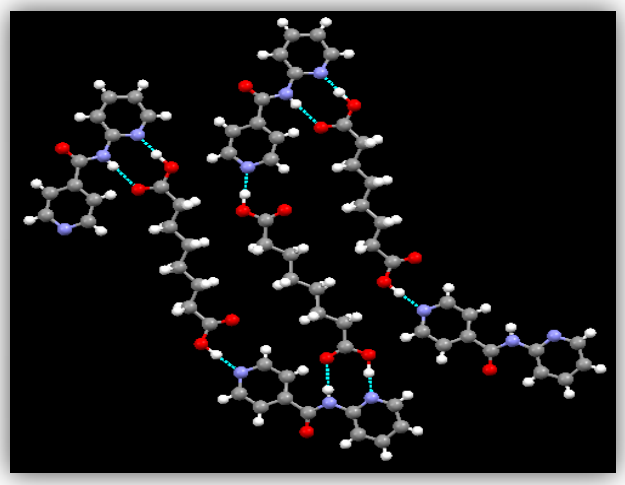

Figure 2.18 1-D corrugated chain-like assembly in 4N:SuA **co-crystal**

2.3.1.14 Crystal structure of 4N:SeA

In **4N:SeA** co-crystal, the primary synthons O-H···N(py), 2.669(12) Å and O-H···N(aminopy), 2.633(12) Å hydrogen bonds drive the assembly into an infinite 1-D corrugated chain-like architecture (Fig 2.19).

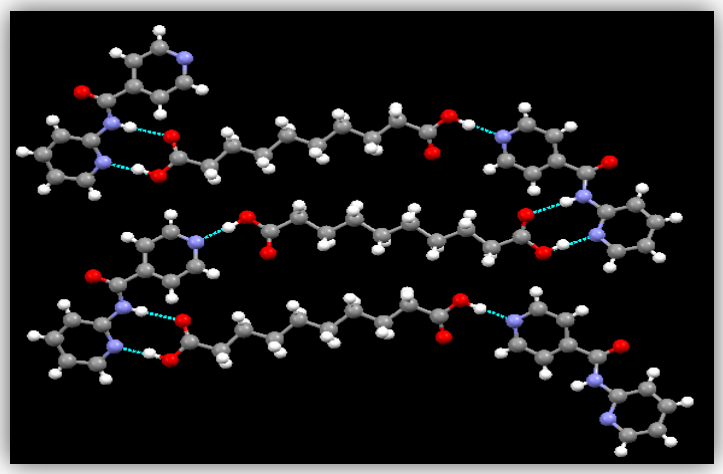

Figure 2.19 1-D corrugated chains in 4N:SeA **crystal structure**

2.3.2 Isostructural co-crystals

Isostructural crystals have the same space group and similar cell dimensions. A summary of the unit cell parameters for the crystal structures of **3N** and **4N** co-crystals are given in Table 2.4 and 2.5, respectively.

Table 2.4 Unit cell parameters of 3N **co-crystals**

Co-crystal	***3N:MA***	***3N:GA***	***3N:PA***	***3N:AzA***	***3N:SA***	***3N:AA***	***3N:SeA***
Crystal system	Monoclinic	Monoclinic	Triclinic	Monoclinic	Triclinic	Triclinic	Triclinic
Space group, Z	C2/c, 8	P 2(1)/c, 4	P-1, 4	P2(1)/n, 4	P-1, 2	P-1, 2	P-1, 2
a, Å	31.2168(18)	7.2374(6)	7.5711(5)	13.5588(13)	4.8289(5)	8.9361(8)	7.5703(8)
b, Å	4.7940(3)	11.1991(10)	11.9820(8)	9.4660(10)	11.1223(11)	9.8031(9)	9.6882(10)
c, Å	22.7743(13)	19.5063(17)	20.1758(13)	15.8384(15)	14.3787(14)	9.8270(9)	13.9977(14)
α, °	90.00	90.00	82.560(4)	90.00	67.856(4)	83.130(2)	85.455(4)
β, °	128.375(2)	90.267(3)	80.081(4)	105.946(4)	89.550(4)	74.507(3)	81.210(4)
γ, °	90.00	90.00	85.195(4)	90.00	87.878(4)	79.462(2)	79.358(4)
Volume, Å^3	2671.9(3)	1581.01	1784.2(2)	1954.6(3)	714.79(12)	813.31(13)	995.74(18)

Table 2.5 Unit cell parameters of 4N **co-crystals**

Co-crystal	***4N:GA***	***4N:PA***	***4N:AzA***	***4N:SA***	***4N:AA***	***4N:SuA***	***4N:SeA***
Crystal system	Triclinic	Monoclinic	Triclinic	Triclinic	Monoclinic	Monoclinic	Monoclinic
Space group, Z	P-1, 2	P2(1)/n, 4	P-1, 2	P-1, 12	P2(1)/c, 4	P2(1)/n, 4	P2(1)/n, 4
a, Å	5.1663(6)	7.5855(12)	5.6707(3)	11.2578(7)	11.9508(11)	11.4438(7)	11.0319(11)
b, Å	9.9211(10)	21.675(3)	10.8221(6)	19.6623(11)	19.8752(19)	10.1874(5)	9.9500(9)
c, Å	15.8829(17)	11.1031(16)	17.0848(10)	19.8130(12)	7.3996(8)	16.5671(9)	18.7354(18)
α, °	75.339(3)	90.00	104.161(2)	93.236(3)	90.00	90.00	90.00
β, °	82.551(3)	96.050(9)	94.599(2)	91.236(3)	105.384(4)	95.023(3)	90.323(4)
γ, °	78.820(3)	90.00	104.840(2)	90.298(3)	90.00	90.00	90.00
Volume, Å^3	769.84(14)	1815.4(5)	971.22(9)	4377.6(5)	1694.6(3)	1924.02(18)	2056.5(3)

The following co-crystals are isostructural and their volume increases in proportion to the increase in number of carbon atoms in the acid chain;

- **3N:GA** and **3N:AzA**
- **4N:G**A and **4N:AzA**
- **4N:AA**, **4N:SuA** and **4N:SeA**

The melting points of isostructural co-crystals within the same series show a decreasing trend with an increase in the number of carbon atoms in the corresponding diacids (Section 2.2.3).

2.4 Discussion

2.4.1 Co-crystals vs salts

All co-crystals were constructed using hydrogen bonds between an acid and a pyridine acceptor. This reaction however, could have also resulted in the formation of salts, wherein a

proton gets transferred from the acid to the pyridine nitrogen. This would result in an $O^{-}\cdots H\text{-}N^{+}$ charge assisted interaction instead of a neutral O-H···N hydrogen bond. IR spectroscopy and single crystal structural data were used to interpret our results and confirm the formation of co-crystals.

2.4.1.1 Characterization using IR spectroscopy

In our set of experiments we have obtained 14/14 co-crystals, *i.e.* 100% supramolecular yield. All fourteen co-crystallization experiments were first screened using IR spectroscopy. Co-crystal formation was confirmed by two broad stretches in the 1800-2500 cm^{-1} region, representing the intermolecular O-H···N hydrogen bond (Fig 2.20). In addition, the C=O stretch in all cases was above 1670 cm^{-1} (Table 2.1) which further confirms co-crystal formation and not salts, since in salts the C-O stretch which is now a part of the COO- anion shows up lower than 1670 cm^{-1} .

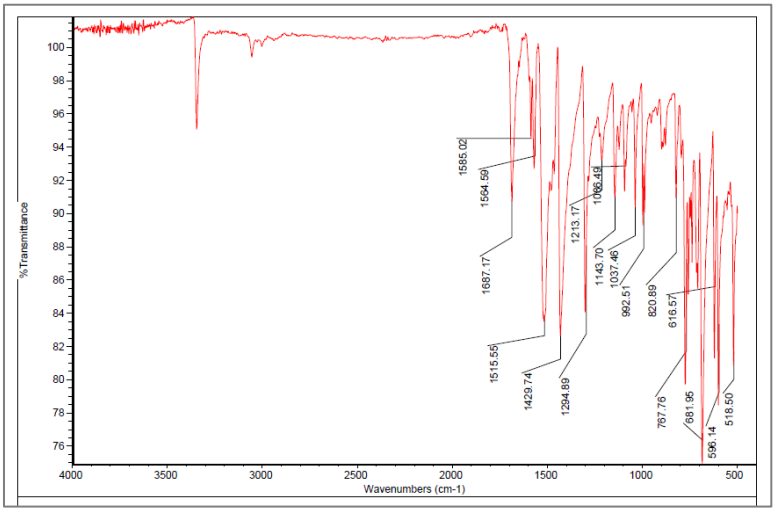

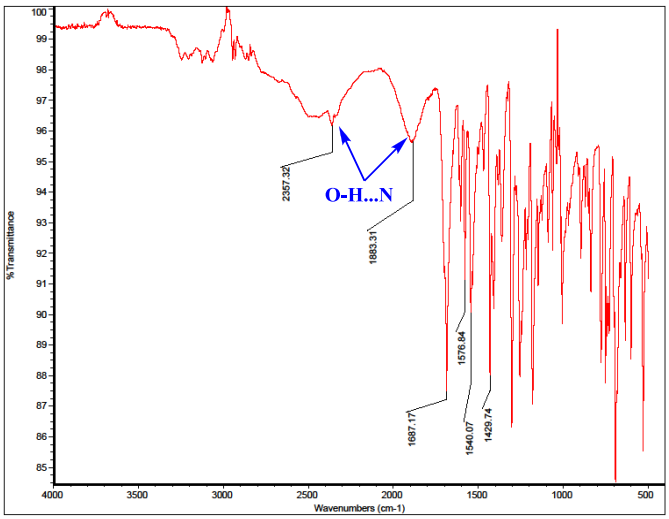

Figure 2.20 IR spectra of 4N **(top) and** 4N:AA **(bottom) indicating the two broad O-H...N stretches**

2.4.1.2 Characterization using structural data analysis

Apart from the IR spectroscopy data, a closer look at the two C-O bond lengths of the acid moiety as well as the endocyclic C-N-C bond angle confirm co-crystal formation in all cases.[11] In order to compare the C-O bond distances in neutral acid and a salt a CSD search was performed on carboxylic acids (7807 hits) and ionic carboxylates (98 hits). In neutral acid moiety the average C=O bond distance is 1.21(6) Å and the average C-O bond distance is 1.31(2) Å. While in ionic species, the two C-O stretches in the carboxylate anion (COO^-) get a double bond character due to electron pair delocalization and hence have the same bond distance, *i.e.*1.24 (13) Å, Fig 2.21. An analysis of our crystal structures indicate that the C=O bond distance fall in the range of 1.205-1.213Å while the C-O bond distance falls in the range of 1.301-1.328Å, which is indicative of a neutral carbonyl group and thus a co-crystal formation, Tables 2.2 and 2.3. CSD search was also performed on neutral (17668 hits) and ionic (2443 hits) C-N-C bond angle in pyridine type compounds. The C-N-C bond angle for the protonated form was above 120°, *i.e.*122.5°(sd=1.5), while the non-protonated C-N-C bond angle is below 120°, *i.e.*118.1° (sd=2.3), Fig 2.21. In our crystal structures, the C-N-C bond angle values fall in the range of 116.21-118.78° which represents the non-protonated form of pyridine moiety.

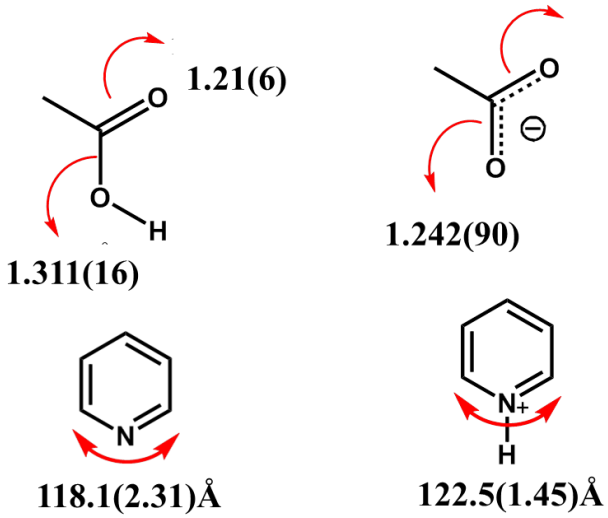

Figure 2.21 Comparing C-O and C=O bond distances and C-N-C bond angles in neutral (left) vs ionic moities (right)

2.4.2 Hetero- synthons directing the co-crystal assembly

All fourteen co-crystals were constructed using the robust O-H···$N_{(py)}$ (acid-pyridine) and O-H···$N_{(ampy)}$ (acid-aminopyridine) hydrogen bonds to form either 0-D rings or 1-D chains. A CSD search of the acid-pyridine heterosynthon gave a total of 1125 hits with the O-N bond distance (in O-H···$N_{(py)}$) in the range of 2.5-3.50 Å (Fig 2.22) and average value of 2.73(9) Å. In our data set, the O-N bond distances in O-H···N(py) hydrogen bond interactions fall in the range of 2.59-2.74 Å, with an average value of 2.63 Å. A CSD search on the acid-aminopyridine heterosynthon gave a total of 87 hits with O-N distances in the range of 2.538-3.452 Å (Fig 2.23) and an average of 2.797(63) Å. In our data set, the O-N bond distances in O-H···N(aminopy) hydrogen bond interactions fall in the range of 2.632-2.704 Å, with an average value of 2.618 Å. The values of O···N bond distances in our set of co-crystals fall well within the range of literature values and are very comparable. The number of hits in the database coupled with our consistent results signify the robustness and reliability of the acid-pyridine and acid-aminopyridine heterosynthons in constructing supramolecular architectures.

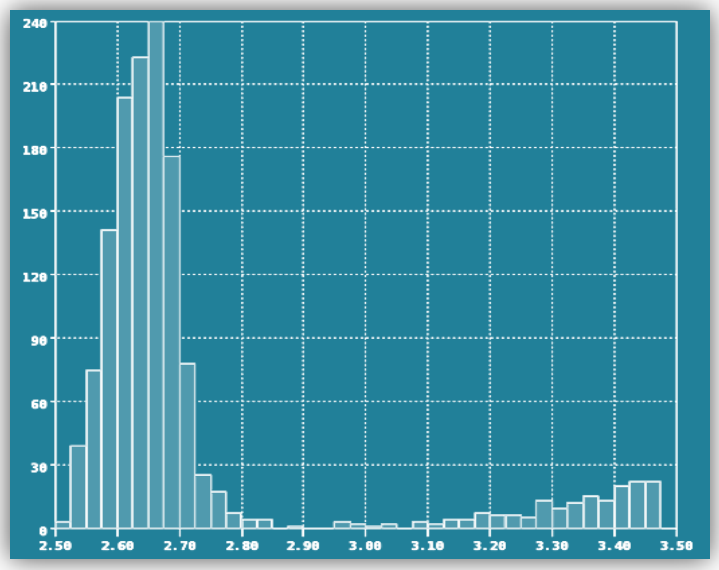

Figure 2.22 Histogram showing O-$N_{(py)}$ bond distance in acid-pyridine heterosynthon

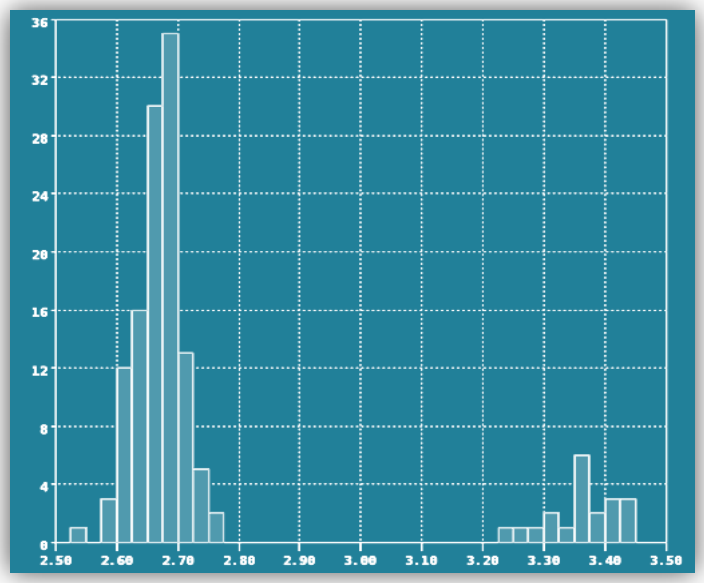

Figure 2.23 Histogram showing O-$N_{(ampy)}$ bond distance in acid-aminopyridine heterosynthon

2.4.3 Assessing the co-crystal assemblies

In order to examine the role of binding site complementarity in directing the supramolecular solid-state structure, two isomeric pyridine based acceptors **3N** and **4N** were combined with four even and four odd-chain diacids, respectively. Out of the sixteen

combinations, we successfully obtained crystal structures for fourteen co-crystals. Two distinctly different types of supramolecular assemblies were formed depending upon the choice of the interacting pairs. The primary driving force in all crystal structures was the acid-pyridine and acid-aminopyridine heterosynthons. However, the final structural outcome was an infinite 1-D chain in **3N:odd** (Fig 2.24) and **4N:even** (Fig 2.25) diacid pairs, and a 0-D cyclic assembly in **3N:even** (Fig 2.26) and **4N:odd** (Fig 2.27) diacid pairs (**4N:PA**, Figure 2.27 was the only outlier that formed chains instead of the expected ring in **4N:odd series**). As we are dealing with relatively weak and reversible forces, the preferential construction of 1-D or 0-D assembly within selected pairs is clearly indicative of the geometric complementarity that exists between the given acid-base pairs. Thus, the observed outlier may be a polymorph as we do not see any reason why **4N** and pimelic acid combination should behave differently from the others in the same series.

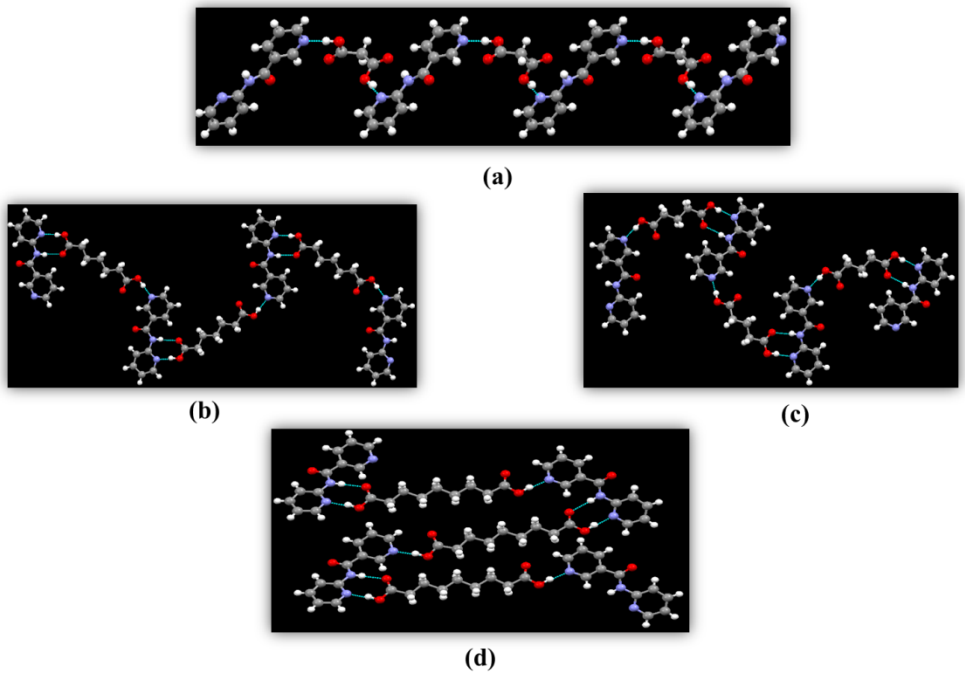

Figure 2.24 1-D chains in 3N:odd **co-crystals a)** 3N:MA **b)** 3N:GA **c)** 3N:PA **and d)** 3N:AzA

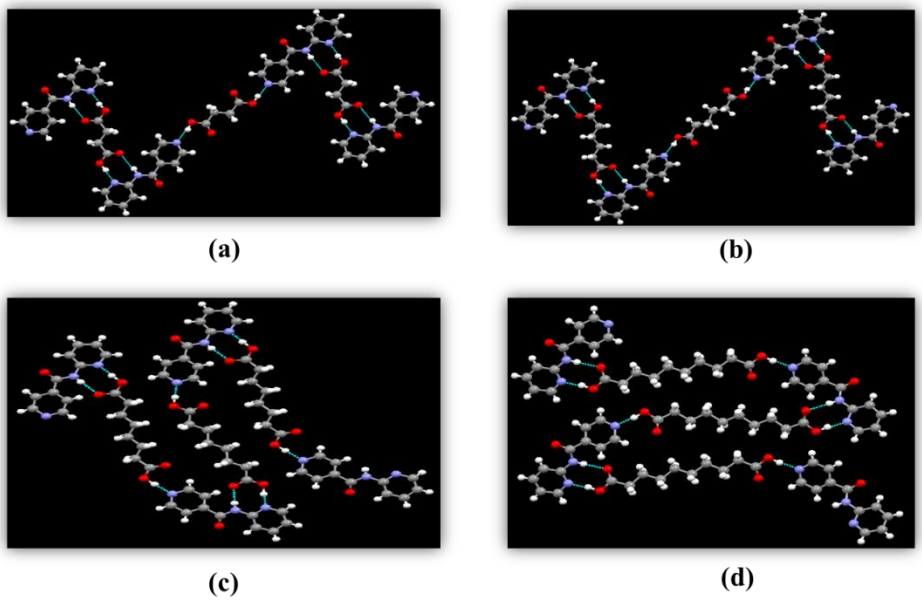

Figure 2.25 1-D chains in 4N:even **co-crystals a)** 4N:SA **b)** 4N:AA **c)** 4N:SuA **and d)** 4N:SeA

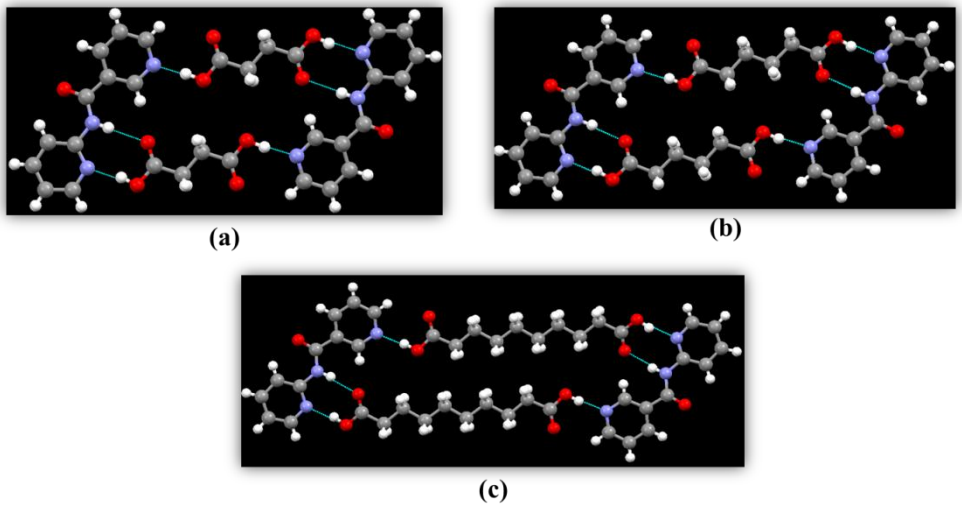

Figure 2.26 0-D rings in 3N:even **co-crystals a)** 3N:SA **b)** 3N:AA **and c)** 3N:SeA

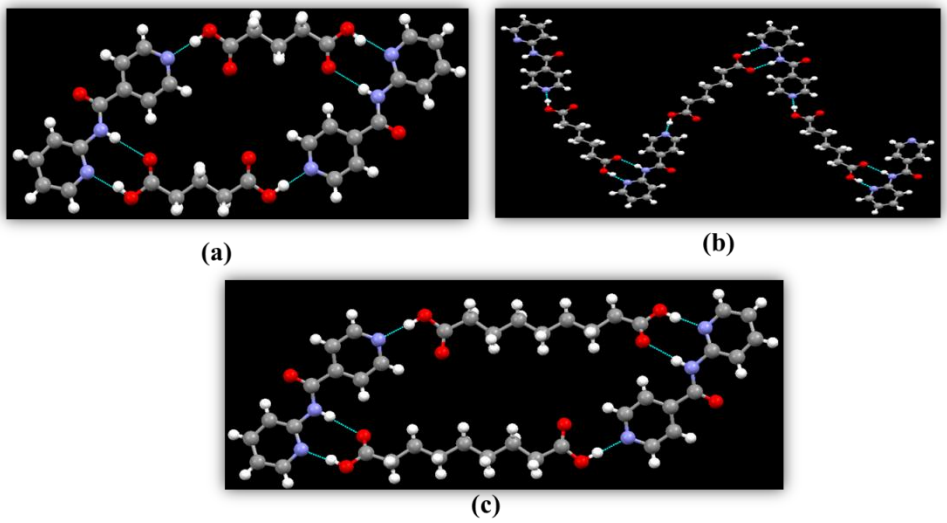

Figure 2.27 0-D rings in co-crystals of a) 4N:GA **b) 1-D chain in** 4N:PA **and c)** 4N:AzA**,**

Another interesting observation to note is the orientation of the carbonyl group and pyridine nitrogen in **3N:odd** diacid series where they are 'syn' with respect to each other in **3N:MA**, **3N:GA** and **3N:PA** co-crystals but 'anti' in the **3N:AzA** co-crystal. This discrepancy however does not seem to have any effect on the resulting assembly, *i.e.* all four co-crystals in the series give 1-D chains.[12]

We can conclude that although the primary recognition between the acid and pyridyl moiety occurs through the formation of O-H···N hydrogen bond, the assembly process is governed by the number of carbon atoms in the diacid chain and the precise orientation of binding sites in the co-crystallizing agents. Along similar lines, Pedireddi et.al,[13] designed an experiment to check the dependence of the resulting crystal structure on the number of carbon atoms in the diacid chains, Using 4,4'-bipyridine as the acceptor and odd-even chain di-carboxylic acids (malonic, glutaric and adipic acid) as the donor, they had postulated two distinct types of architectures; chains with even diacid and rings with odd diacid. However, contrary to their expectations 4,4'-bipyridine formed chains with malonic, glutaric and adipic acid, irrespective of the number of carbon atoms in the diacid backbone. The difference between their acceptor system and ours is the orientation of the binding sites. In 4,4'-bipyridine, the binding sites are co-linear whereas in our system they are parallel (**3N**) and at an angle of 60° (**4N**) (Fig 2.28).

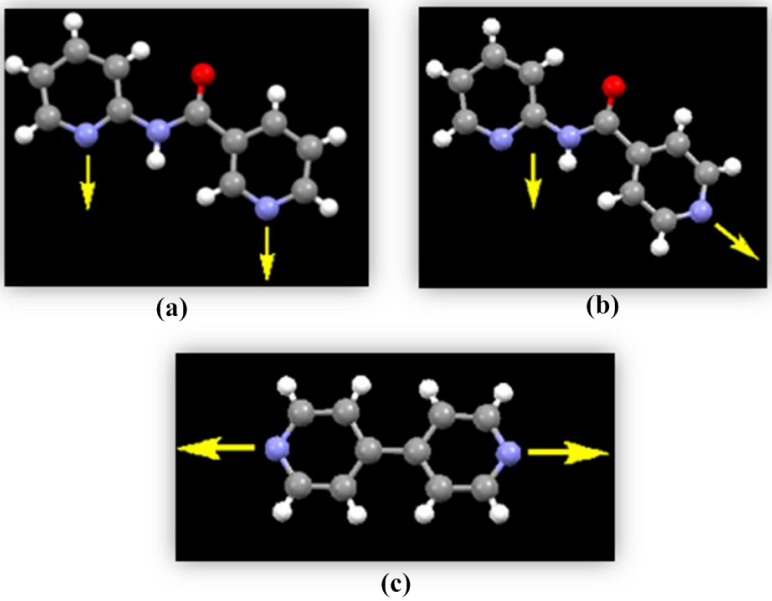

Figure 2.28 Arrows indicating the orientation of binding sites in a) 3N **b)** 4N **c) 4,4'-bipyridine**

2.5 Conclusion

In conclusion, we have synthesized two acceptors **3N** and **4N** using slightly modified literature procedures and performed co-crystallization experiments to examine the potential of the ligands for forming co-crystals with a series of diacids. A remarkable degree of structural consistency is observed within the given groups of interacting species. We postulated two different types of architectures, chains and rings for the combination of **3N**/**4N** with odd/even dicarboxylic acid. Based on our structural analysis of fourteen co-crystals, rings were formed when **3N** was combined with even diacids and when **4N** was combined with odd diacids. On the other hand, chains were formed with **3N:odd** diacids and **4N:even** diacids pairs. A correlation is observed between the molecular geometries of interacting species and the resulting assembly (Fig 2.29).

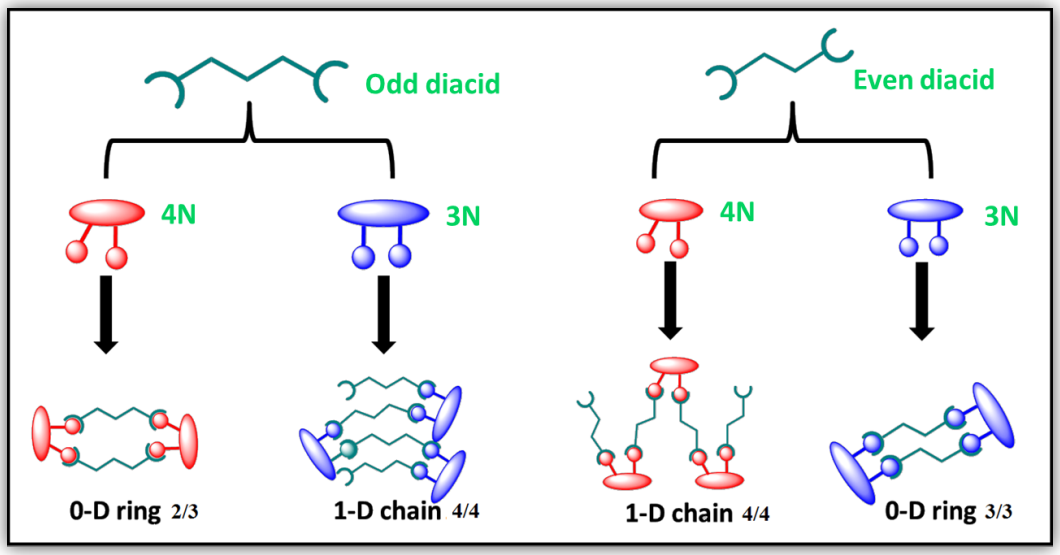

Figure 2.29 Results of the postulated structural outcome

We have thus identified a reliable supramolecular method for constructing solid-state architectures with a high degree of structural control and reproducibility using a simple mix and match strategy.[12]

---

1 . Desiraju, *Angew. Chern*., *Int. Ed. Engl*., **1995**, 34, 23 11

2 Aakeröy, C.B., *Acta Cryst.,* **1997,** B 53, 569

3 Aakeröy, C.B.; Beatty, A.M.; Tremayne, M.; Rowe, D. *Cryst. Growth Des*. **2001**, 1, 377; Dale, S. H.; Elsegood, M. R. J.; Hemmings, M.; Wilkinson, A. L. *CrystEngComm.* **2004**, 6, 207; Hguyen, T. L.; Fowler, F. W.; Lauher, J. W. *J. Am.Chem. Soc.* **2001**, 123, 11057; Aakeröy, C.B.; Panikkattu, S.; Dehaven, B.; Desper, J.; *CrystEngComm,* **2013**,15, 463-470

4 Vishweshwar, P.; Nangia, A.; Lynch, V. M. *J. Org. Chem.* 2002, 67, 556; Leiserowitz, L.; Nader, F. *Acta Crystallogr., Sect. B*: *Struct. Sci*. **1977,** 33, 2719; Huang, C. M.; Leiserowitz, L.; Schmidt, G. M. J. *J. Chem. Soc., Perkin Trans*. 2, **1973**, 5, 503

5 Huang, K. S.; Britton, D.; Etter, M.C.; Byrn, S. R. *J. Mater. Chem*. **1997,** 7, 713; MacGillivray, L. R.; Reid, J. L.; Ripmeester, J. A. *J. Am. Chem. Soc*. **2000**, 122, 7817

6 Lehn, J. M., *Science*, **2002**, 295, 2400; Desiraju, G. R., *Acc. Chem. Res.,* **2002**, 35, 565–573; Wenger, M. and Bernstein, J. *Angew. Chem., Int. Ed*., **2006**, 45, 7966–7969; Childs, S. L.; Hardcastle, K. I. *CrystEngComm*. **2007**, 9, 64

7 Steed, J. W and Atwood, J. L., *Supramolecular Chemistry*, John Wiley and Sons, Ltd., 2nd edn, **2009**

8 Kim, T. H.; Seo., *J. Chem. Mater*. **2007**, 19, 5815−5817

9 Kushner, S.; Dalalian, H.; Robert, T. C. *J. Org. Chem*. **1948**, 13, 834−836

10 Krishna, K.; Jose, D. A.; Dastidar, P.; Das, A. *Langmuir*. **2004**, 20, 10413−10418

11 Aakeröy, C. B.; Fasulo, M. E and Desper, J., *Mol Pharmaceutics*., **2007**, 4, 317-322

12 Aakeröy, C.B.; Panikkattu, S.; DeHaven, B.; Desper, J., *Cryst. Growth Des*., **2012**, 12, 2579–2587

13 Pedireddi, V. R.; Chatterjee, S.; Ranganathan, A.; Rao, C. N.; *Tetrahedron.* **1998**, 54, 9457-9474

Chapter-3 Correlating molecular properties with physical properties of bulk solids

3.1 Introduction

The discovery and formulation of a new drug is an extremely expensive and time consuming process (Fig 3.1).[1] Poor oral bioavailability still remains one of the main reasons for why less than 1% of active compounds make it to the market.[2] Oral bioavailability is the fraction of an orally administered drug that reaches systemic circulation. A higher bioavailability means lower administered drug dosage is needed and this reduces the risk of side effects and toxicity. On the other hand, low bioavailability demands increased dosage of the drug and thus poor efficacy. Aqueous solubility and membrane permeability of the drug are the two important determinants of the overall oral bioavailability. Solubility is a key physicochemical parameter that needs to be addressed in the initial stages of the drug development process.[3] Table 3.1 briefly summarizes the definition of solubility according to United States Pharmacopeia (USP).[4]

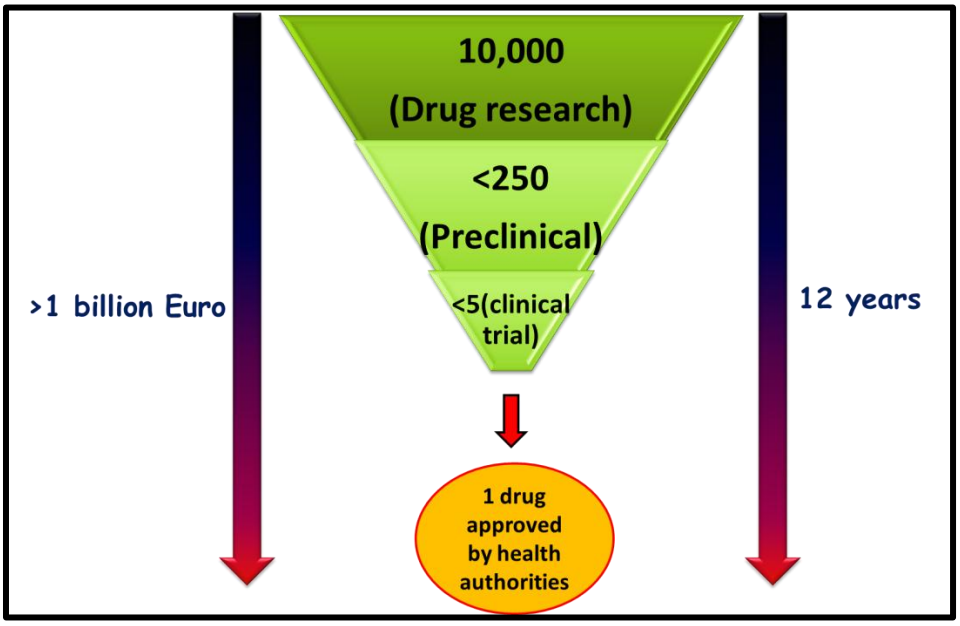

Figure 3.1 Drug development time line[1]

Table 3.1Solubility definition according to USP[4]

	Solubility range (mg/ml)
Very soluble (VS)	>1,000
Soluble(S)	33–100
Sparingly soluble (SPS)	10–33
Slightly soluble (SS)	1-10
Very slightly soluble (VSS)	0.1–1
Practically insoluble (PI)	<0.1

According to the Biopharmaceutical Classification System[5] (BCS), active pharmaceutical ingredient (API) can be divided into four classes: Class 1, drug candidates that have good solubility as well as good permeability; Class II, drugs that have good membrane permeability but poor solubility; Class III, drugs with poor permeability and higher solubility; Class IV, drugs that are poorly soluble as well as poorly permeable through the membrane. The problem of low solubility of API has been addressed in a number of ways such as micronization[6], salt formation[7], solubilization in co-solvents[8] and use of micellar solutions[9].

Figure 3.2 BCS classification of API's[5]

Recent advances in crystal engineering combined with the knowledge of reliable and predictable supramolecular synthons have led to extensive research in the design of

pharmaceutical co-crystals.[10] Pharmaceutical co-crystals are molecular complexes containing therapeutic molecules, *i.e.* an active pharmaceutical ingredient (API) along with co-former. Co-crystals are formed through non-covalent interactions (Fig 3.3), *i.e.* without making or breaking of covalent bonds, and hence this technique can be used to fine-tune physical properties of API via precise control over molecular assembly, without affecting the therapeutic activity.

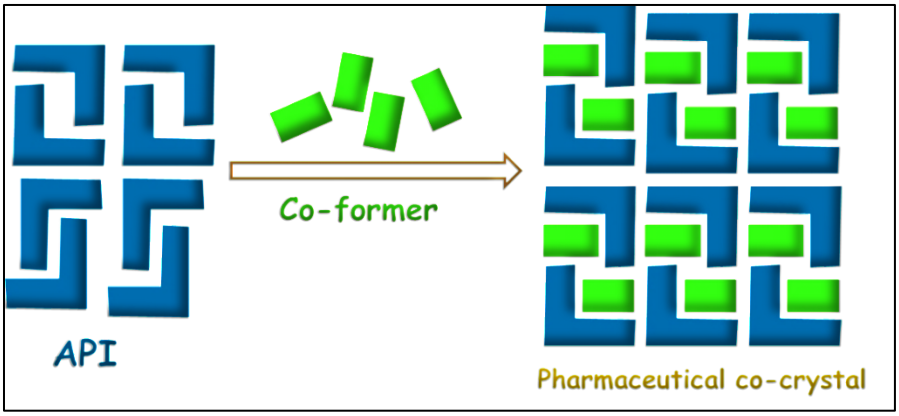

Figure 3.3 Schematic representation of a pharmaceutical co-crystal

The physical properties of crystalline materials are largely governed by the arrangement of molecules in the solid state. Alterations to this arrangement can bring about changes in the physical properties. Solubility of a given solute is based on free energy of solubilization, which is a combination of two factors, *i.e.* crystal lattice interactions as well as solute-solvent interactions (solvation) given by the equation,

$$\Delta G_{solution} = \Delta G_{lattice} + \Delta G_{solvation}$$

where $\Delta G_{solution}$ represents the Gibbs free energy for the solubilization process, $\Delta G_{lattice}$ and $\Delta G_{solvation}$ are the free energies of lattice contribution and solvation, respectively.[11] Solubility can be altered by changes in the lattice energies and/or solvation energies. Co-crystals have the ability to alter both, and thus influence the associated lattice and solvation energy.

There are many examples in the literature where co-crystallizations have improved the solubility of API's.[12] One notable example is Itraconazole (BCS class II drug) co-crystals with 1,4-dicarboxylic acids (fumaric, succinic, malic and tartaric acid), which showed a 4-20 fold increase in the solubility as compared to the crystalline form of the drug itself.[13] Another example is the co-crystals of an anti-cancer drug (Fig 3.4a) with a series of even-chain dicarboxylic acids that shows an enhancement in solubility compared to the drug itself. The co-

crystal solubility decreases systematically with an increase in the hydrophobicity of the corresponding diacids.[14]

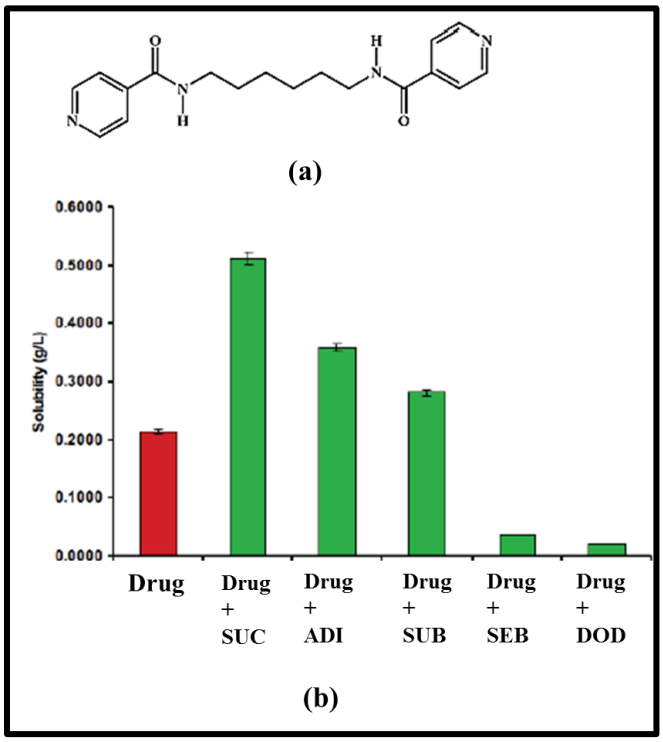

Figure 3.4 (a) Structure of the anti-cancer drug, (b) Aqueous solubility of the drug and its co-crystals with dicarboxylic acids [14]

In this study we attempt to use co-crystallization as a tool to systematically fine-tune the solubility of two pyridine based ligands, **3N** and **4N**. Both **3N** and **4N** are potential mimics of the API Imatinib, a BCS Class II drug. All three have common binding sites; the pyridine nitrogen atom and the amino-pyridine site (Fig 3.5). Based on our knowledge of supramolecular synthons, the co-formers of choice for **3N** and **4N** are the even (succinic, adipic, suberic and sebacic) and odd-chain (malonic, glutaric, pimelic and azelaic) dicarboxylic acids. In Chapter 2 we have demonstrated the potential of these ligands to form co-crystals with the diacids and have mapped out their structural landscape through single crystal analysis. Both the pyridine as well as amino-pyridine nitrogen atoms form hydrogen bonds with the diacids resulting in either a 0-D or 1-D assembly.

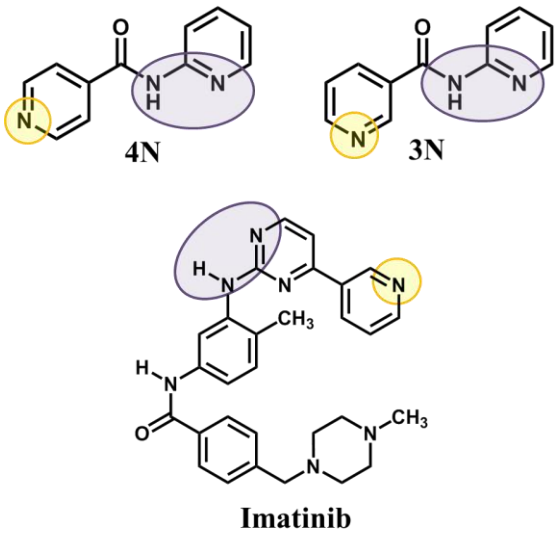

Figure 3.5 4N**,** 3N **and Imatinib displaying common functional groups**

In this study, we aim to map the solubility of **3N** and **4N** co-crystals and also understand any correlations that might exist between the solubility of a co-crystal and molecular property of individual component.

Our study will therefore cover the following points;

i) Effect of co-crystallization on the solubility behavior of the mimics.

ii) Correlation between co-crystal solubility and co-crystal melting point.

iii) Correlation between co-crystal solubility and co-former solubility.

iv) Effect of binding event on the resulting co-crystal solubilities using Isothermal Titration Calorimetry

3.2 Experimental

3.2.1 Synthesis

3.2.1.1 Synthesis of 3N and 4N

The syntheses of **3N** and **4N** are presented in Ch 2, Section 2.2.1.

3.2.1.2 Preparation of co-crystals for solubility studies

Co-crystals of **3N** and **4N** with the even chain diacids succinic C4, adipic C6, suberic C8 and sebacic acid C10 as well as odd-chain diacids malonic C3, glutaric C5, pimelic C7 and azelaic acid C9 were prepared via a solvothermal method.[15] The ligand and the acid were combined in a 1:1 ratio and refluxed in 25ml of methanol. After 40 min of heating, the resulting solution was cooled to 5 °C. The precipitated solid was filtered, dried and analyzed using IR spectroscopy to confirm co-crystal formation. The IR spectra of the bulk co-crystal matched the IR spectra of single crystals that were submitted for X-ray analysis. The PXRD patterns of the bulk and single crystal were also compared to confirm structural homogenity (Fig 3.6). The melting points of the co-crystals were determined on a Fisher- Johns melting point apparatus and are listed in Table 3.2.

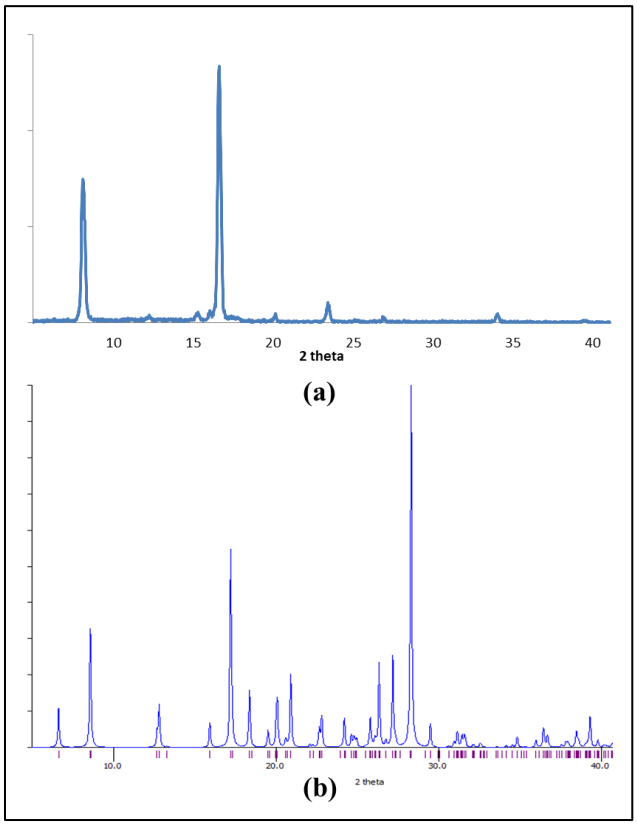

Figure 3.6 a) PXRD of bulk 3N:SA **co-crystal synthesized by solvothermal method and b) PXRD from single crystal of** 3N:SA

Table 3.2 Melting points of 3N **and** 4N **co-crystals in °C**

	3N	4N
Malonic acid C3	126	143
Glutaric acid C5	96	128
Pimelic acid C7	119	130
Azelaic acid C9	92	94
Succinic acid C4	146	124
Adipic acid C6	141	144
Suberic acid C8	127	134
Sebacic acid C10	105	106

3.2.2 Solubility measurements

3.2.2.1 Equilibrium solubility of 3N and 4N

In order to determine the equilibrium solubility of **3N** and **4N,** a saturated solution of **3N** was prepared by dissolving 0.125g of **3N** in 10ml of distilled water in a vial. The vial was sealed and stirred in a water bath to maintain constant temperature. After stirring for 12hrs at room temperature, the remaining solid was filtered and dried. The weight of the left over solid was recorded. The concentration of the filtrate was determined by the mass difference of **3N** in 10ml of the solvent. The experiment was carried out at different time intervals like 24hrs, 48hrs and 72hrs. Similar procedure was followed for **4N**.

The resulting concentrations were plotted against the corresponding time intervals and the equilibrium concentration and time was determined (Table 3.3, Figures 3.7 and 3.8).

Table 3.3 Concentration of 3N **and** 4N **at different time intervals**

Time (hrs)	3N Concentration (M)	4N Concentration (M)
12	0.0061	0.0251
24	0.0065	0.0273
48	0.0091	0.0294
72	0.0087	0.0298

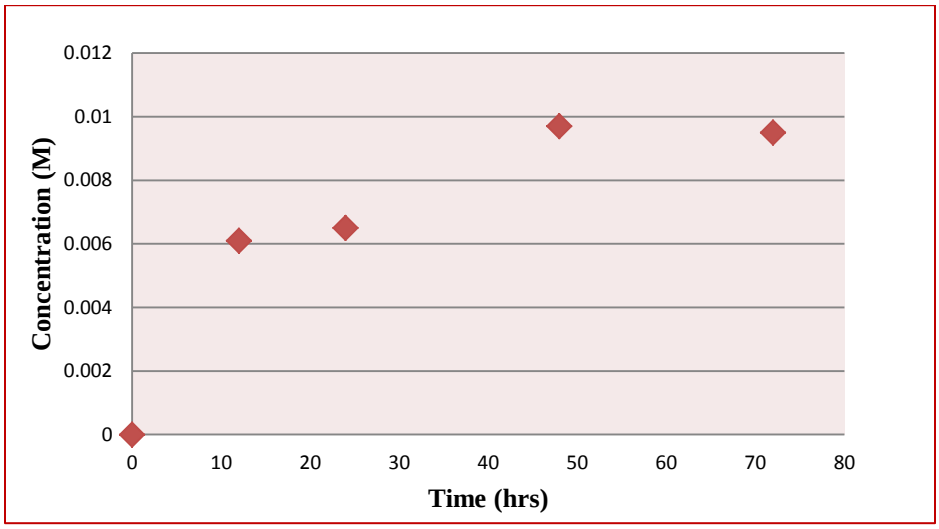

Figure 3.7 Concentration vs time in 3N

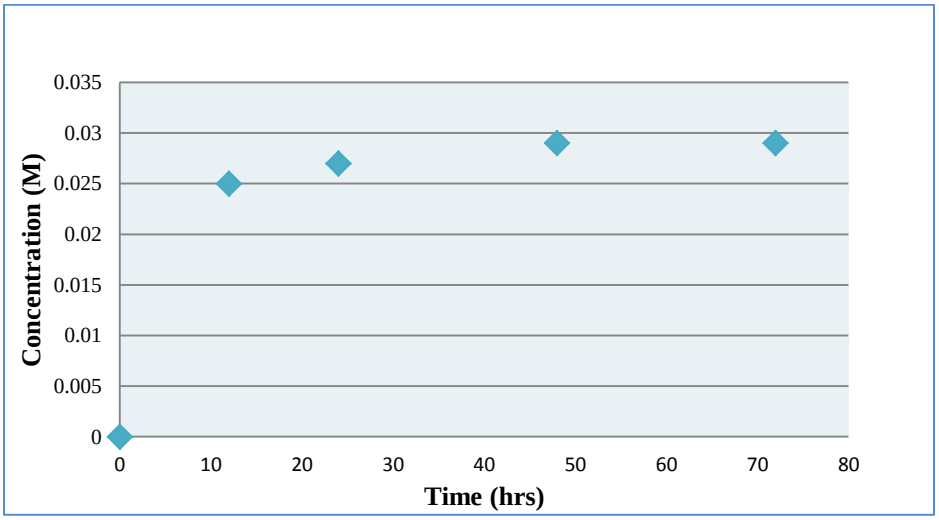

Figure 3.8 Concentration vs time in 4N

3.2.2.2 Calibration curve

To construct a calibration curve, the stock solution of ligand was subjected to serial dilutions and their corresponding absorbance was recorded (Fig 3.9 and 3.10). The equation of the line was used for determining the unknown concentration of the ligand during co-crystal solubility measurements.

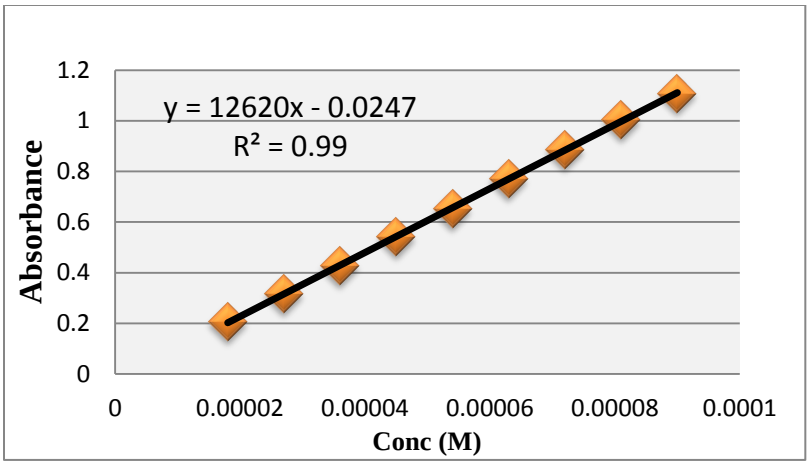

Figure 3.9 Calibration curve of 3N **at 72hrs**

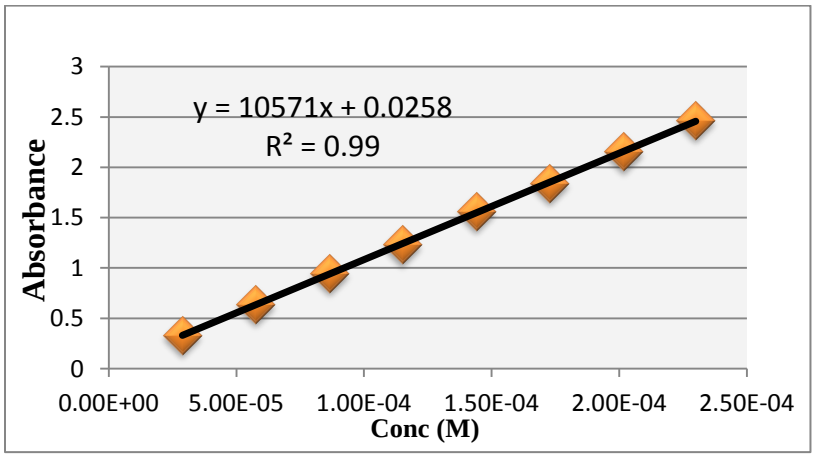

Figure 3.10 Calibration curve of 4N **at 72hrs**

3.2.2.3 Aqueous solubility measurement of 3N and 4N co-crystals

A suspension of the co-crystal (0.125g) was stirred in 10ml of distilled water in a sealed vial and placed in a water bath to maintain constant temperature. After stirring for 72hrs, the remaining solid was filtered off. A 0.2 ml aliquot of the filtrate was diluted to 10ml using distilled water (dilution factor = 50) and the absorbance of **3N**/**4N** was measured using UV-Vis spectroscopy, Shimadzu UV-1650-PC. The absorbance (y) values were used to calculate the corresponding concentrations (x) from the equation of line (y=mx+c) of the calibration curves. The calculated concentration was then multiplied by the dilution factor to get the final concentration and thus the solubility of the co-crystal.

3.2.3 Isothermal Titration Calorimetry (ITC)

Isothermal titration calorimetry (ITC) is a thermodynamic technique used to study interactions between molecules in the solution phase. When two molecules interact, heat is either released or gained by the system to form an energy-minimum stable complex. The amount of heat lost or gained is a measure of the strength of the interaction between the two species. This can be analyzed in terms of thermodynamic parameters like enthalpy change (ΔH), entropy change (ΔS), Gibbs free energy changes (ΔG) of the system. The binding constants (K_a) and binding stoichiometry (N) can also be calculated.[16]

2.2.3.1 Experimental details of ITC

In this study, ITC measurements were carried out for **3N** and **4N** with succinic and sebacic acid respectively. The sample and reference cell was rinsed with distilled water. The reference cell was filled with water (blank) and sample cell was filled with an aqueous solution of the donor (acids). The aqueous solution of the acceptor (**3N**/**4N**) was filled in a syringe (Table 3.4). After letting the system equilibrate for about 1hr, 8µl of the acceptor solution was injected into the sample cell at intervals of 400s between each injection. 30 such injections were made in total and the change in enthalpy was measured after each injection. The experiment was repeated twice.

Table 3.4 Details of the ITC experiment

	Mass (mg)	Vol (ml)	Conc (mM)
3N	23.90	10	11.99
4N	23.90	10	11.99
Succinic acid	0.18	10	0.15
Sebacic acid	0.31	10	0.15

Data analysis and data fit procedures were performed using the software *NanoAnalyze*. The signals from the experiment are plotted in µcal/sec as a function of time, interpreting the power needed to maintain the reference and sample cell at the same temperature. The number of pulses corresponds to the heat released/absorbed with injection of the ligand. These can be integrated to obtain the total heat change per injection

3.3 Results and discussion

3.3.1 Modulating the solubility of 3N and 4N

Based on the experimental measurements, the aqueous solubility of **3N** and **4N** are 1.692 mg/ml and 5.757 mg/ml respectively. **4N** is approximately 3.5 times more soluble than **3N**. These mimics can be considered to be slightly soluble compounds (Table 3.1). The solubility in mg/ml for **3N** and **4N** are listed in Table 3.5.

Table 3.5 Aqueous solubility of 3N **and** 4N **co-crystals**

	3N (mg/ml)	**4N(mg/ml)**
Malonic acid C3	7.376(60)	7.693(34)
Glutaric acid C5	3.376(227)	4.074(19)
Pimelic acid C7	2.899(66)	0.890(4)
Azelaic acid C9	1.857(117)	0.662(40)
Succinic acid C4	2.877(39)	4.131(45)
Adipic acid C6	0.661(19)	0.922(13)
Suberic acid C8	0.460(45)	0.301(56)
Sebacic acid C10	0.113(5)	0.211(4)

The experimental results indicate that the solubility of **3N** and **4N** can be modulated systematically via co-crystallizations with diacids (Fig 3.11 and 3.12, Table 3.5). In the series of even-chain diacid co-crystals with **3N**, the shortest diacid, *i.e.* C4, displays a solubility four times higher than that of **3N** itself. The remaining three co-crystals have solubility lower than **3N**. However, with 3N:odd-diacid co-crystals, we have achieved a higher (four-fold) or similar solubility for all co-crystals (Fig 3.11).

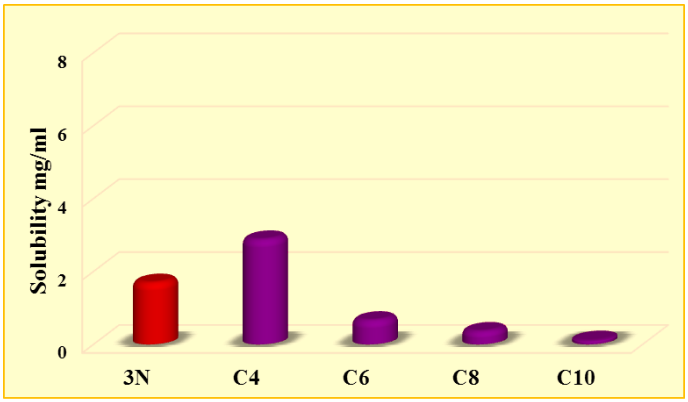

(a)

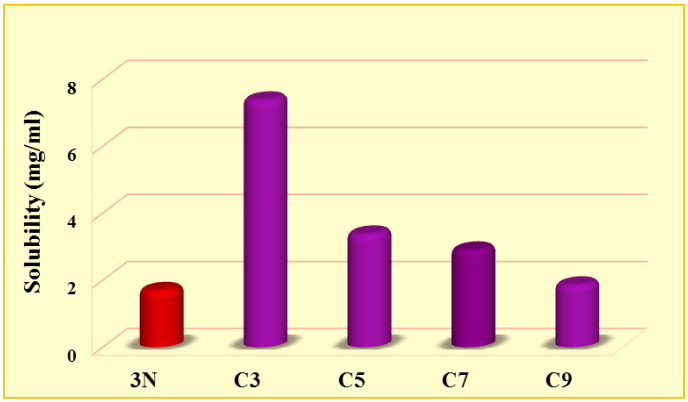

(b)

Figure 3.11 Aqueous solubility of 3N **and** 3N **co-crystals with even chain diacids (a), and odd chain diacids (b).**

In co-crystals of **4N** with even-chain diacids, the solubility is reduced systematically from C4 to C10 with increasing hydrophobicity of the diacid. However in co-crystals of **4N** with odd-chain diacids, C-3 shows higher solubility than that of **4N**. The other compounds in the series show a systematic decrease in the solubility (Fig 3.12).

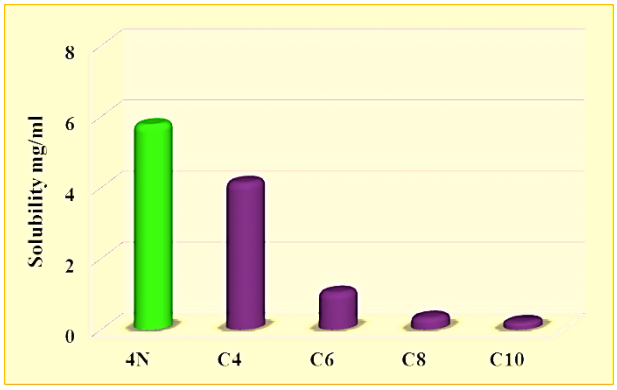

(a)

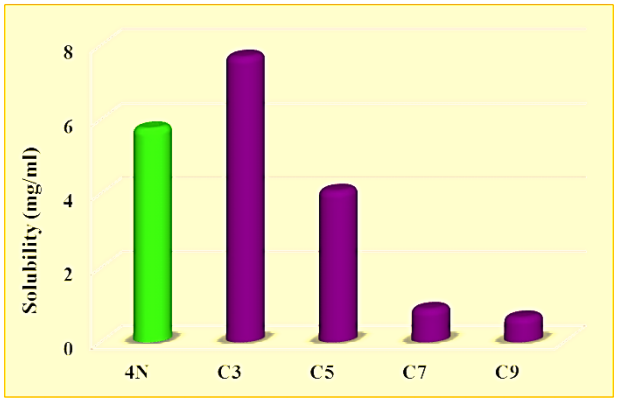

(b)

Figure 3.12 Aqueous solubility of 4N **and** 4N **co-crystals with even chain diacids (a), and odd chain diacids (b).**

Our results demonstrate the potential of co-crystallization as a tool for modifying the solubility of an organic molecular solid, *i.e.* the solubility can either be lowered or improved depending on the choice of co-crystallizing agents. The solubility decreases with increasing hydrophobicity of the acid co-former.

3.3.2 Correlation between solubility and melting point of co-crystals

The melting point is a very important physical property of crystalline materials. In pharmacy, the general solubility equation is widely used to estimate the aqueous solubility of solutes. This equation takes into account two factors, *i.e.* melting point and partition co-efficient of the solute.[17] While these predictions can be made for single component systems, the literature remains sparse when making such correlations in multi-component systems like co-crystals. There are two contrasting views in terms of correlating solubility and melting point. While some propose that they are correlated, few others believe that they are independent of each other.[18,19]

Solubilizing a co-crystal involves two main processes, (i) breaking of the non-covalent interaction in a co-crystal to release the solute from the crystal lattice and (ii) solvation of the released solute molecule. Both these factors contribute to the free energy of solvation.[20] Hence, since solvation also plays a role in solubilizing molecules, accurate prediction of solubility based on thermal properties alone can prove inaccurate and unreliable. There are several examples in the literature that demonstrate how melting point of a co-crystal is not an accurate measure in predicting aqueous solubility.[19] For instance, a recent study on co-crystals of AMG-517 with structurally diverse co-formers found no correlation between the melting points and log of solubility of the co-crystals.[21] In another example, the experimental solubility values of Gabapentin-Lactam (GBPL) co-crystals were found to be different from the calculated ideal solubility values that was measured based on thermal properties of the co-crystal using the equation,

$$\log \chi \text{ideal} = \frac{\Delta \text{Hf}}{2.303R}\left(\frac{Tf-T}{TfT}\right),$$

where χideal is the ideal mole fraction solubility at temperature T, T_f is the fusion temperature and ΔH_f is the enthalpy of fusion.

Along similar lines, in our studies we observe no correlation between the melting points of **3N**/**4N** co-crystals and their corresponding solubility (Figures 3.13 and 3.14). This further proves the inadequacy of thermal properties for reliably predicting co-crystal solubility.

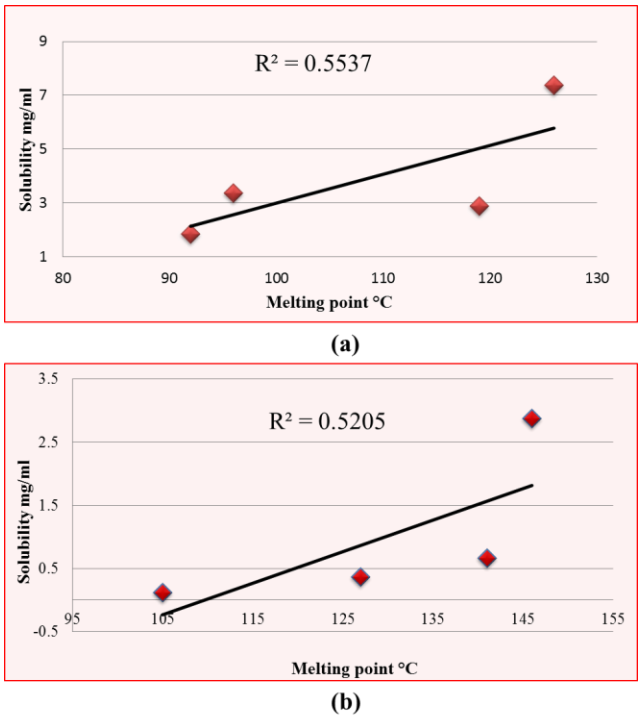

Figure 3.13 Melting point vs Solubility a) 3N:odd-chain diacid and b) 3N:even-chain diacid

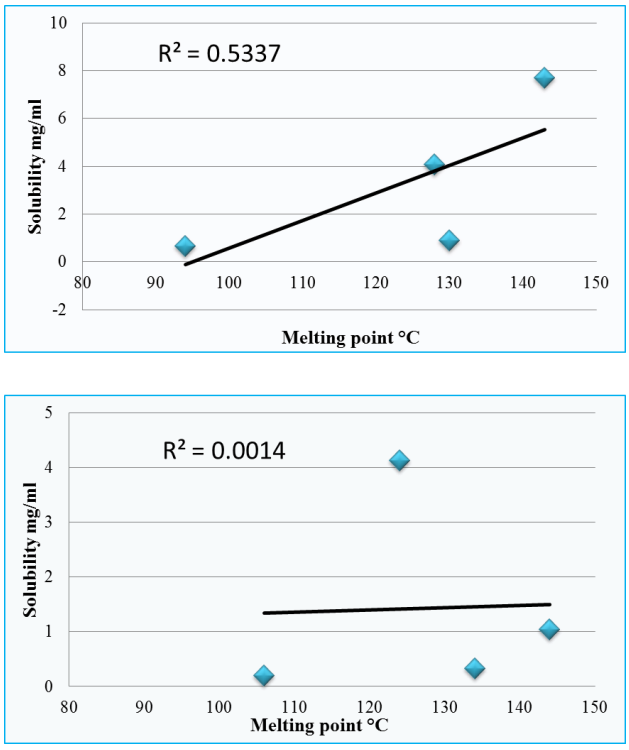

Figure 3.14 Melting point vs Solubility a) 4N:odd-chain diacid and b) 4N:even-chain diacid

3.3.3 Correlation of solubility of the co-crystal and solubility of co-former

Similar to the analysis conducted by Nair et al, our results show that with the increase in the solubility of the co-crystal former there is an increase in the solubility of co-crystal.[19] Our data indicate a possible correlation between the co-crystal solubility and co-former solubility in all four sets of experiments, *i.e.* **3N:odd, 3N:even, 4N:odd** and **4N:even**, (Fig 3.15 and Fig 3.16).

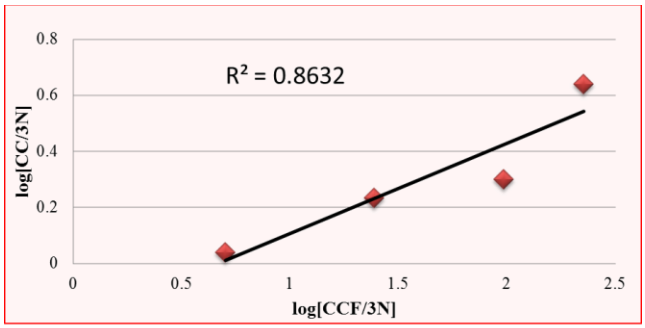

(a)

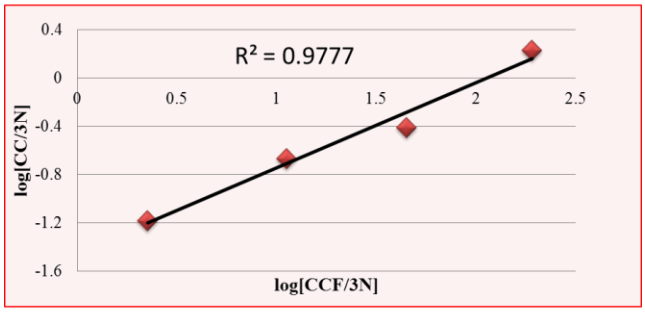

(b)

Figure 3.15 Correlation of co-crystal and co-former solubility in a) 3N:odd system and b) 3N:even system

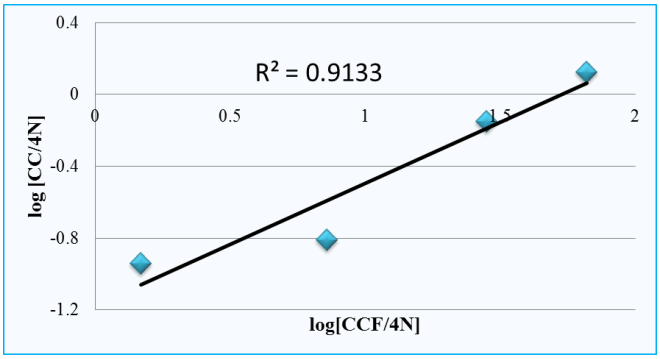

(a)

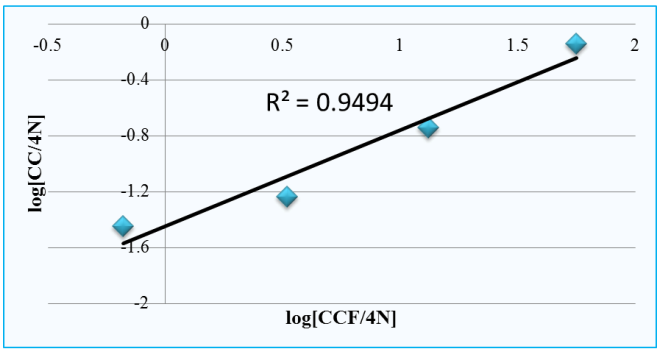

(b)

Figure 3.16 Correlation of co-crystal and co-former solubility in a) 4N:odd system and b) 4N:even system

Our experimental data clearly demonstrates the ability to reliably alter the solubility of a given co-crystal based upon the solubility of the co-former. This provides a good pathway to fine-tune solubility in a systematic manner based upon the desired function.

3.3.4 Investigating the binding event in solution

In solid state, the hydrogen-bonding patterns are well-defined; however in solutions the patterns are less-easily established. We used ITC to analyze the thermodynamic output that results from intermolecular interactions between our acceptors **3N**/**4N** and donors **SA**/**SeA** in the solution state**.** A concentrated solution of the acceptor was titrated into a dilute solution of the donor. During the first injection, most of the acceptor ligand interacts with the available donor acids in the solution. The interaction is exothermic as indicated by the nature of the curve in Fig 3.17(a) (sample curve of **3N** and succinic acid titration). With subsequent additions, the number of free available acid molecules reduces and hence the corresponding heat liberated also decreases exponentially. Towards the final injections, there are no more free acid available for binding which is reflected in the curve since no more heat is released. The heat resulting from

each individual injection is then integrated with respect to time and plotted against the molar ratio of the two components. These values are fitted using the independent model from the software *NanoAnalyze* to get output in terms of enthalpy change (ΔH), association constant (K_a) (Fig 3.17b). Since the acid and base combine in a 1:1 ratio (as seen in our crystal structure in Ch. 2), the stoichiometry (N) was fixed in the range of 0.9 to 1.1. To test the consistency of the data, another trial was performed under similar conditions. Table 3.6 displays the results of various thermodynamic parameters that were calculated using the equations, $\Delta G = -RT\ln K_a$ (to obtain the free energy change (ΔG) and $\Delta G = \Delta H - T\Delta S$; to obtain ΔS.

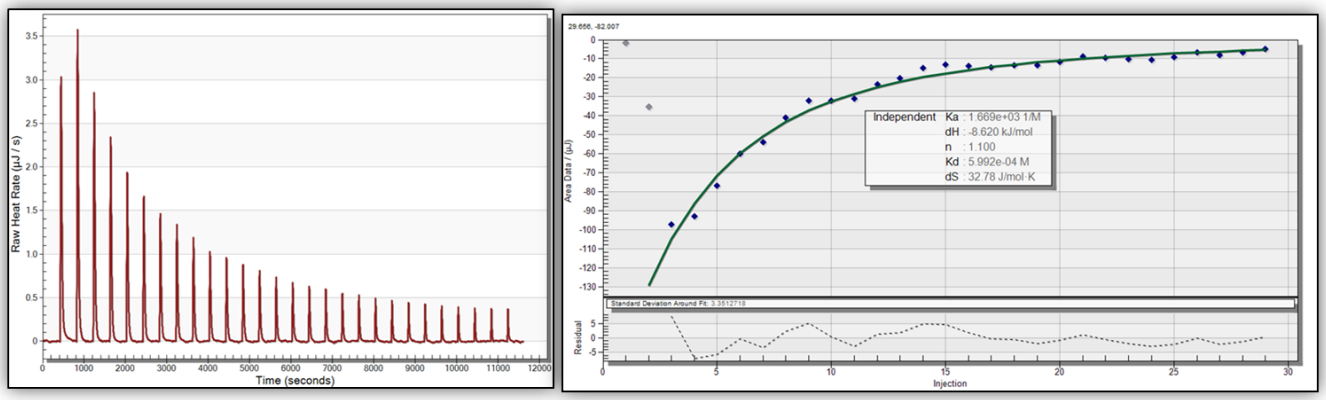

(a) **(b)**

Figure 3.17 a) ITC titration curve of 3N and succinic acid (b) Thermodynamic fit parameters.

Table 3.6 Thermodynamic parameters based on ITC

	3N:SA		4N:SA		3N:SeA		4N:SeA	
	#1	**#2**	**#1**	**#2**	**#1**	**#2**	**#1**	**#2**
ΔG (kJ)	-17.6	-17.2	-17.8	-17.9	-19.6	-19.7	-20.4	-20.5
ΔH (kJ/mol)	-14.1	-10.5	-8.6	-7.9	-3.2	-3.1	-9.9	-8.2
ΔS (J/mol.K)	11.9	22.4	30.7	33.5	55.3	56.3	35.4	41.5

A normal hydrogen bond enthalpy can range from anywhere between 10-65 kJ/mol.[22] The observed enthalpy in our system is a result of several factors that can be explained as follows;

In order for a heteromeric interaction to occur between the ligand and acid in solution phase, there are two processes that should be overcome, i.e. (i) the bonds between the acid

dimers in the solution must be broken and (ii) the water molecules surrounding the acid must be removed (de-solvation). Both these factors are endothermic and entropically favorable. In our ITC experiments, since very dilute acid solutions were used, most of the acid molecules would be present as monomers and thus the second process (de-solvation) will have a more significant effect on the resulting enthalpy.

When new heteromeric hydrogen bond are formed between the free ligand and acid, it is an exothermic process and entropically unfavorable. The thermodynamic effects observed are the net effect of the breaking of old hydrogen bonds in homomeric dimer and formation of new hydrogen bonds in heteromeric dimers. In our system, the ligands under consideration are structurally similar (**3N** and **4N**, Fig 3.5) and the diacids used only differ in the number of methylene groups between the two ends. Increased carbon chain length from succinic (C4) to sebacic (C10) contributes to increasing hydrophobicity in the system. Hence, since the binding events are very similar (acid-pyridine and acid-aminopyridine) we do not expect to see any significant differences in the overall free energy of the system, which is confirmed by the comparable ΔG values in the different combinations under study (Table 3.6). This proves that the face to face interaction at the hydrogen bonding site is similar in all cases and hence does not have any influence on the resulting solubility differences observed for the co-crystals. Thus, hydrophobicity of the acid co-former plays a crucial role in modulating the solubility of a given co-crystal. Increasing hydrophobicity of the acid chain length corresponds to decreasing solubility, which is exactly what we find in the previous section 3.2.3 in the form of a good reliable correlation between co-crystal solubility and co-former solubility.

3.4 Conclusions

We have demonstrated a systematic way to alter the solubility of two API mimics using co-crystallizations. In some cases a higher solubility than the mimic was achieved (beneficial for pharmaceutical drugs with poor solubility issues), while in some cases the solubility was decreased (beneficial for slow release applications). It was found that melting point of the co-crystal and its solubility cannot be correlated. ITC experiments show similar free energy values (ΔG) for different co-crystal combinations (including shortest and longest chain diacid used in this study) indicating that the binding interaction is very similar in all cases and does not contribute to the observed solubility differences. We successfully demonstrated a correlation

between the co-crystal solubility and co-former solubility. Higher hydrophobicity of the co-former results in lower solubility of the co-crystal. Co-crystals thus offer a unique opportunity for developing new solid forms wherein the physical properties can be tuned in a predictable to give the desired result.

---

1 http://www.bayerpharma.com/en/research-and-development/processes/index.php

2 Waterbeemd, H.; Smith D. A.; , Beaumont, K.; Walker, D. K., *J. Med. Chem.* **2001** 44, 1313-1333

3 Thomas, V. H.; Bhattachar, S.; Hitchingham, L.; Zocharski, P.; Naath, M.; Surendran, N.; Stoner, C.; Kattan, A., **2006** *Informa* UK Ltd ISSN 1742-5255.

4 Stegemann,S.; Leveiller, F.; Franchi, D.; Jong, H. D.; Linden, H., *European Journal of Pharmaceutical Sciences* 31, **2007**, 249-261.

5 Yu, L. X.; Amidon, G. L.; Polli, J. E.; Zhao, H.; Mehta, M. U.; Conner, D. P.; Shah, V. P.; Lesko, L.J.; Chen, M. L.; Lee, V. H.; Hussain, A. S., *Pharm. Res.,* **2002**, 19, 921

6 Chaumeil, J. C., *Exp. Clin. Pharmacol*., **1998**, 20, 211

7 Bica, K.; Shamshina, J.; Hough, W.; MacFarlane, D. R. and Rogers, R. D., *Chem. Commun*., **2011**, 47, 2267-2269; Lam, K. W.; Xu, J. and Ka M. Ng., *Ind. Eng. Chem. Res.,* **2010**, 49, 12503–12512: Agharkar, S.; Lindenbaum, S.; Higuchi, T., *J. Pharm Sci.,* **1976**, 65, 747

8 Aim. K.; Dannenfelser, R. M.; Zienlinski, J.; Wang, B., *J Pharm. Sci.,* **2004**, 93, 2244

9 Torchillin, V. P. *Pharm. Res.,* 2007, 24, 1; Rajewski, R. A.; Stella, V. J. *J. Pharm. Sci.,* **1996**, 85, 1142; Humberstone, A. J.; Charman, W. N. *Adv. Drug Deliv. Rev*., **1997**, 25, 103.

10 Trask, A. V.; Motherwell, W. D. S.; Jones, W. *Cryst. Growth Des*. **2005**, 5, 1013-1021; Brader, M. L.; Sukumar, M.; Pekar, A. H.; McClellan, D. S.; Chance, R. E.; Flora, D. B.; Cox, A. L.; Irwin, L.; Myers, S. R. *Nat. Biotechnol*. 2002, 20, 800-804; Good D. J;

Rodrıguez-Hornedo N., **2010**. *Cryst Growth Des*., 10, 1028–1032; Gao Y, Zu H, Zhang J. **2011**. *J PharmPharmacol.,* 63, 483–490; Permumalla S. R, Sun C. C. *CrystEngComm,* **2012**, 14, 3851–3853

11 Serajuddin, A. T. M.; *Adv Drug Delivery Rev*., **2007**, 59, 603-616; Avdeef, A.; *Adv. Drug Delivery Rev.,* **2007**, 59, 568-590.

12 Basavoju, S.; Boström, D.; Velaga, S. P. *Pharm. Res.* **2008**, 25, 530; Childs, S.L.; Rodríguez-Hornedo, N.; Reddy, S.-L.; Jayasankar, A.; Maheswari, C.; McCausland, L.; Shipplett, R.; Stahly, B. C. *CrystEngComm.* **2008**, 10, 856; Hickey, M. B.; Peterson, M. L.; Scoppettuolo, L. A.; Morrisette, S. L.; Vetter, A.; Guzmán, H.; Remenar, J. F.; Zhang, Z.; Tawa, M. D.; Haley S.; Zaworotko, M. J.; Almarsson, Ö. *Eur. J. Pharm. Biopharm*. **2007**, 67, 112; Fleischman, S. G.; Kuduva, S. S.; McMahon, J. A.; Moulton, B.; Walsh, -B.R.D.; Rodríguez-Hornedo, N.; Zaworotko, M. J. *Cryst. Growth Des.* **2003**, 3, 909

13 Remenar, J. F.; Morissette, S. L.; Peterson, M. L.; Moulton, B.; MacPhee, J. M.; Guzmán, H. R. and Almarsson, O. *J. Am. Chem. Soc.* **2003** , 125, 8456-8457.

14 Aakeröy, C. B.; Forbes, S.; Desper, J.; *J. Am. Chem. Soc*., **2009**, 12, 17048-17049

15 Nehm, S. J.; Rodríguez-Spong, B.; Roderíguez-Hornedo, N. *Cryst. Growth Des.* **2006**, 6, 592

16 Saboury, A. A. *J. Therm. Anal. Cal.* **2004**, 77, 997; Banerjee, M.; Poddar, A.; Mitra, G.; Surolia, A.; Owa, T.; Bhattacharyya, B. *J. Med Chem*. **2005**, 48, 547; Wiseman, T.; Williston, S.; Brandts, J. F.; Lin, L. N. *Analytical Biochemistry*, **1989,** 179, 131

17 Jain, N. and Yalkowsky, S. *Journal of Pharmaceutical Science*, **2001**, 90, 234-252; Abramowitz, R.; Yalkowsky, S. H.; *Pharm. Res.* **1990**, 7, 942-947

18 Stanton. M. K.; Bak. A., *Cryst. Growth Des*. **2008**, 8, 3856-3862

19 Good, D. J. and Rodriguez-Hornedo, N., *Cryst. Growth Des.,* **2009**, 9, 2252-2264; Stanton, M. K. and Bak, A., *Cryst. Growth Des*., **2008**, 8, 3856-3862

20 Maheshwari, C.; Andre, V.; Reddy, S.; Roy, Duarte, T.; Rodriguez, N., *CrystEngComm,* **2012**, 14, 4801-4811.

21 Stanton, M. K.; Tufekcic, S.; Morgan, C.; Bak, A., *Cryst. Growth Des.,* **2009,** 9, 1344-1352.

22 Perrin, C. L.; Nielson, J. B. *Annu. Rev. Phys. Chem*. **1997,** 48, 511

Chapter-4 Interdependence of structure and physical properties in co-crystals of azopyridines

4.1 Introduction

Organized synthesis of supramolecular assemblies in the solid state provides a handle to design functional materials with desired physical properties. Physical properties like thermal stability, solubility and dissolution behavior can be tuned via co-crystallization process, and with supramolecular control over solid state architectures[1], we can establish a correlation between properties and molecular structure in a predictable manner.[2] For example, even-chain dicarboxylic acids like succinic (**C4**), adipic (**C6**), suberic (**C8**) and sebacic, (**C10**) form 1-D chains and structural consistency is observed in their crystal structures with an increase in the number of methylene groups from **C4** to **C10** (Fig 4.1).[3] This consistency translates into a predictable structure-property relationship where the melting points decrease gradually with the increase in chain length of the diacids (Fig 4.2).

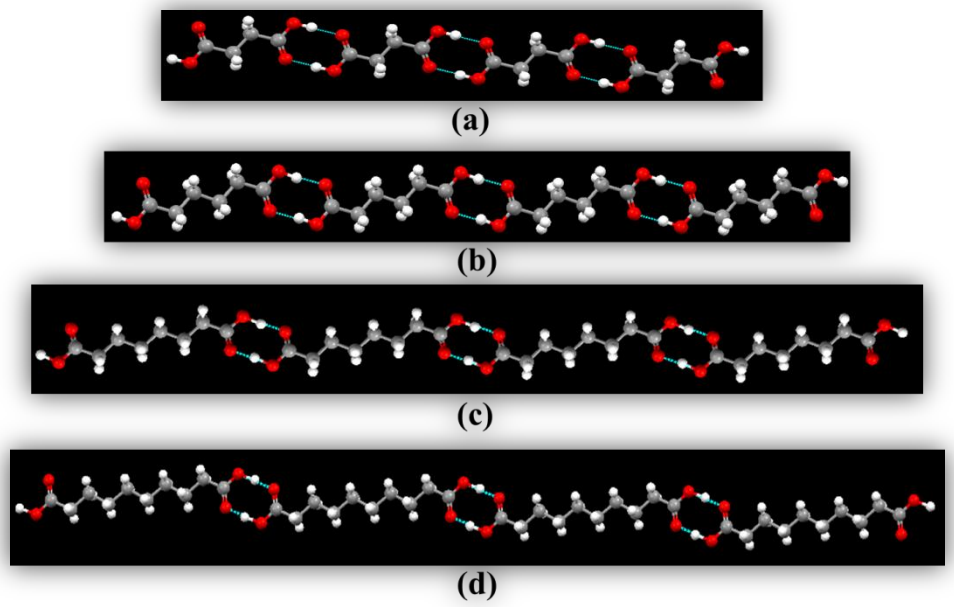

Figure 4.1[3] Structural consistency in even-chain dicarboxylic acid a) succinic[3a], C4 **b) adipic[3b],** C6 **c) suberic[3c],** C8 **d) sebacic acid[3d],** C10

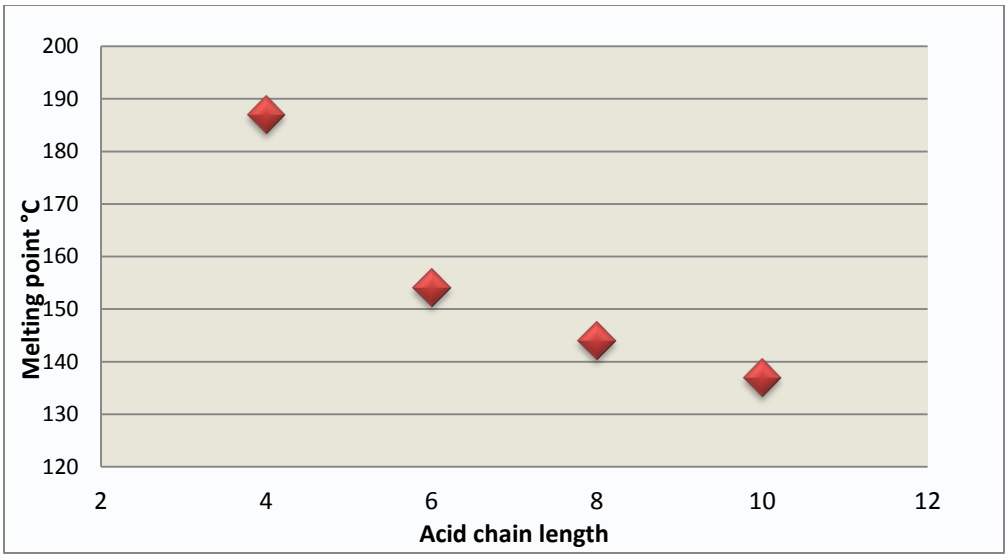

Figure 4.2 A gradual decrease with an increase in the chain length among even-chain dicarboxylic acid

Although stronger interactions drive the initial supramolecular assembly process, weaker intermolecular interactions play a crucial role in connecting discrete assemblies into 3-D solid-state architectures.[4] In our experiment we will highlight the influence of weaker secondary interactions in constructing assemblies of higher dimensionalities and also establish a possible structure-property correlation using co-crystallization techniques. For the experiment, we chose two pyridine-based isomeric acceptors, *i.e.* 3,3'-azopyridine (**3,3'-azpy**) and 4,4'-azopyridine (**4,4'-azpy**), Figure 4.3(a), and a set of four even chain aliphatic dicarboxylic acid; succinic, adipic, suberic and sebacic acid (with increasing number of carbon atoms in the backbone, Fig 4.3(b)) as hydrogen bond donors. Co-crystals of **4,4'-azpy** with succinic, adipic and sebacic acid were synthesized and reported previously by Wu et.al.[5] We have completed the series by including the co-crystal of **4,4'-azpy** with suberic acid.

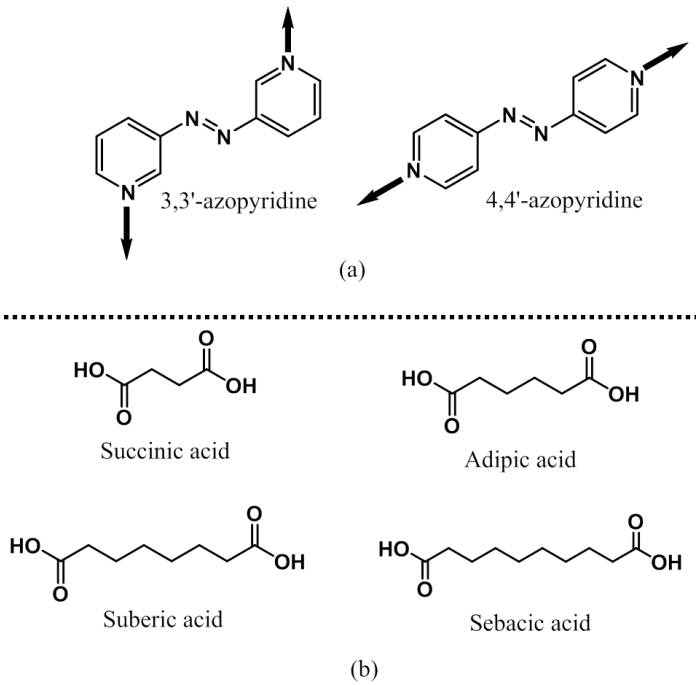

Figure 4.3 a) binding site orientation in 3,3'-azopyridine (anti-parallel) and 4,4'-azopyridine (co-linear); b) even chain dicarboxylic acid with increasing chain length

Molecular surface potential calculations using density functional theory (B3LYP, 6-31G++G** basis set) method showed that the charges on the nitrogen atoms were -174 kJ/mol and -172 kJ/mol for **3,3'-azpy** and **4,4'-azpy** respectively (Fig 4.4). A difference of 2 kJ/mol is unlikely to be significant and should not play any role in influencing the structure directing processes.

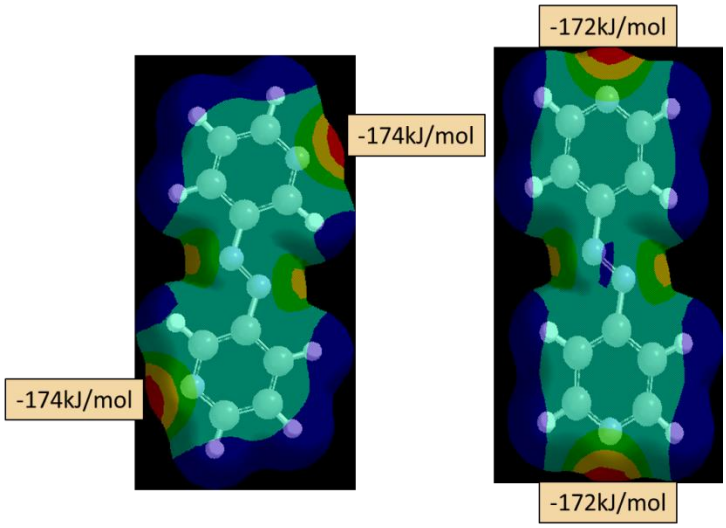

Figure 4.4 Surface potentials in 3,3'-azpy **and** 4,4'-azpy

However, the binding sites on the acceptors have a geometric bias, *i.e.* in **3,3'-azpy** they are oriented in an anti-parallel fashion, whereas in **4,4'-azpy** the binding sites are co-linear (Fig 4.3). The primary molecular recognition occurs at the acid-pyridine interface forming robust and reliable COOH···N hydrogen bonds. This key interaction will remain consistent in all crystal structures irrespective of the co-former chain length, but the secondary interactions will be greatly influenced by the chain length, increasing hydrophobicity of the acid donors and binding site orientation of the acceptors. We assume that infinite 1-D chains will be formed initially followed by their organization into 2-D sheets via weaker inter-chain interactions to give two different motifs (in phase and out of phase) in each of the two groups as postulated in Fig 4.5. In ***motif 1*** and ***3*** the chains are arranged in an out-of-phase fashion, while in ***motifs 2*** and ***4*** they have an in-phase arrangement.

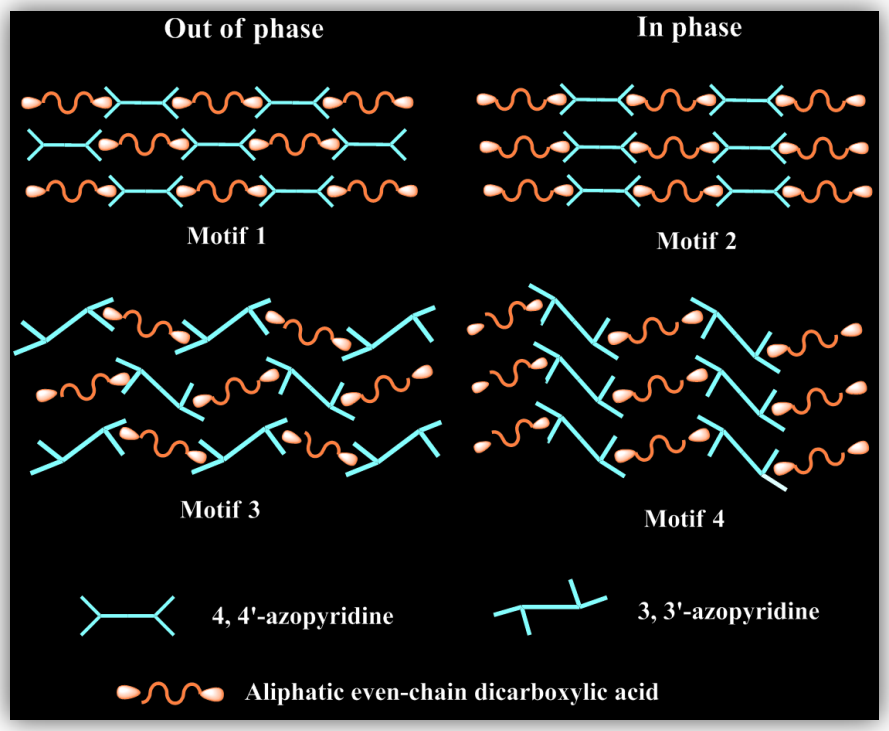

Figure 4.5 Postulated motifs for the combination of 3,3'-and 4,4'-azopyridine with aliphatic diacids

Our objectives of the study are to seek answers to the following questions;

i. Can we construct consistent and reliable assemblies in two groups of azopyridine co-crystals of dicarboxylic acids?

ii. Can we establish a reliable structure-property correlation in the given set of co-crystals?

iii. What is the effect of geometric bias on the overall molecular arrangement and physical property?

4.2 Experimental

4.2.1 Synthesis

All chemicals, unless noted, were purchased from Sigma Aldrich and used without further purification. Melting points were determined on a Fisher- Johns melting point apparatus. ^{1}H and ^{13}C NMR spectra were recorded on a Varian Unity plus 400 MHz or 200 MHz spectrometer in $CDCl_3$ or D_6-DMSO. Infrared spectroscopy (IR) was done on a Nicolet 380 FT-IR.

4.2.1.1 Synthesis of 3,3'-azopyridine, (3,3'azpy)[6]

The synthesis of **3,3'-azpy** was carried out using a previously reported procedure.[6] KOH (16.26g, 28.98mmol) was dissolved in 100ml of water and kept in an ice bath. Using a dropping funnel, bromine (5.24ml, 20.39mmol) was slowly added to the KOH solution with stirring, maintaining the temperature between 0-5 $^{\circ}C$. After the addition was complete, 3-amino pyridine (1.9g, 20.18mmol) dissolved in 40ml of cold water was slowly added to it. The resulting mixture was stirred in an ice-bath for 1-2 h. The solution was extracted into methylene chloride and the solvent was removed under reduced pressure. The resultant crude was subjected to column chromatography and the pure orange product was isolated in 46% yield. Mp 132-134 $^{\circ}C$ (lit. 136-140 $^{\circ}C$); ^{1}H NMR **(**δH, 400MHz, $CDCl_3$): 9.17 (d, 2H), 8.79 (s, 2H), 8.23 (d, 2H), 7.66 (t, 2H), appendix A.

4.2.1.2 Synthesis of 4,4'-azopyridine,(4,4'-azpy)[7]

The synthesis of **4,4'-azpy** was carried out using a slightly modified procedure.[7] 4-Amino pyridine (2.50g, 26.55mmol) was dissolved in 20ml water and kept cold in an ice bath. 6% NaOCl (50ml, 36.25mmol diluted with 50ml water) was added drop wise to the pyridine solution with constant stirring while maintaining the temperature between 0-5 ^{o}C. After stirring for 2-3 h in the ice-bath, the product was extracted into ether. After removing the solvent under reduced pressure, a small amount of hexane was added to the crude (to dissolve the product). Any

insoluble residue was discarded. The solvent was then removed under reduced pressure and pure bright-orange product was re-crystallized from methanol in 51% yield. Mp 106-109 ºC (lit.105-106 ºC); ^{1}H NMR (δH, 400MHz, $CDCl_3$): 8.88 (d, 4H), 7.76 (d, 4H), appendix A.

4.2.2 IR spectroscopy screening of co-crystals

3,3'-azpy and **4,4'-azpy** were screened with even-chain diacids using the solvent drop assisted grinding method. The acid and base were combined in 1:1 stoichiometry in a motor and pestle. A drop of methanol was added and the mixture was ground for 30 seconds. The resulting product was screened using IR spectroscopy to confirm co-crystal formation. All samples that showed a positive hit for co-crystal formation were then subjected to slow evaporation experiments to grow single crystals suitable for X-ray diffraction analysis.

4.2.3 Synthesis of co-crystals

Stoichiometric amounts of the acid and base were dissolved in suitable organic solvents and the co-crystals were synthesized using slow evaporation method. The details of co-crystal synthesis are listed in Table 4.1.

Table 4.1 Synthesis of 3,3'-and 4,4'-azopyridine co-crystals

Azopyridine:acid	Abbreviation	Mole ratio	Solvent and method	Condition	Melting point (°C)
3,3'-azopyridine: succinic acid	3,3'-azpy:SA	1:1	Ethanol- slow evaporation	Ambient temp for 7 days	144-146
3,3'-azopyridine:adipic acid	3,3'-azpy:AA	1:1	Ethanol- slow evaporation	Ambient temp for 14 days	149-151
3,3'-azopyridine:suberic acid	3,3'-azpy:SuA	1:1	Methanol-slow evaporation	Ambient temp for 5 days	133-136
3,3'-azopyridine:sebacic acid	3,3'-azpy:SeA	1:1	Methanol-slow evaporation	Ambient temp for 9 days	122-125
4,4'-azopyridine:succinic acid	4,4'-azpy:SA	1:1	Methanol-slow evaporation	Ambient temp for 7 days	205-209
4,4'-azopyridine:adipic acid	4,4'-azpy:AA	1:1	Methanol-slow evaporation	Ambient temp for 28 days	189-192
4,4'-azopyridine:suberic acid	4,4'-azpy:SuA	1:1	Ethanol-slow evaporation	Ambient temp for 25 days	160-163
4,4'-azopyridine:sebacic acid	4,4'-azpy:SeA	1:1	Methanol-slow evaporation	Ambient temp for 12 days	144-147

4.3 Results

We have structurally characterized five co-crystals, *i.e.* **3,3'-azpy:SA, 3,3'-azpy:AA, 3,3'-azpy:SuA, 3,3'-azpy:SeA** and **4,4'-azpy:SuA**. Crystal structures of **4,4'-azpy:SA**[5b], **4,4'-**

azpy:AA[5a] and **4,4'-azpy:SeA**[5a] were previously reported and their single crystal structures were characterized using XRD. Table 4.2 lists the IR stretches for O-H···N hydrogen bonds and the C=O stretch in the acid and corresponding co-crystal. Detailed hydrogen bond geometries for **3,3'-azpy** and **4,4'-azpy** co-crystals are listed in table 4.3.

Table 4.2 IR spectroscopy C=O stretch and O-H···N stretches in co-crystals of 3,3'-and 4,4'-azopyridine

Compound	O-H···N stretches (cm-1)	Co-crystal C=O stretch (cm^{-1})	Acid C=O stretch (cm^{-1})
3,3'-azpy-SA	2480;1894	1704	1686
3,3'-azpy-AA	2489;1876	1693	1683
3,3'-azpy-SuA	2492;1888	1692	1684
3,3'-azpy-SeA	2504;1887	1691	1682
4,4'-azpy-SuA	2447;1894	1700	1684

Table 4.3 Hydrogen bond geometries in co-crystals of 3,3'-and 4,4'-azopyridine

Structure	D-H···A/Å	D-H/Å	H···A/Å	D···A/Å	D-H···N/°
3,3'-azpy:SA	O(21)-H(21)...N(11)	0.946(15)	1.748(15)	2.6924(12)	176.5(13)
3,3'azp:AA	O(21)-H(21)...N(11)	0.913(17)	1.778(17)	2.6893(11)	176.5(15)
3,3'-azpy:SuA	O(21)-H(21)...N(11)	0.925(16)	1.756(16)	2.6798(11)	177.0(13)
3,3'-azpy:SeA	O(31)-H(31)...N(11)	1.04(3)	1.65(3)	2.682(3)	175(2)
	O(40)-H(40)...N(21)_#1	1.08(3)	1.61(3)	2.683(3)	171(2)
4,4'-azpy:SuA	O(21)-H(21)...N(11)	0.885(17)	1.809(18)	2.6633(13)	161.6(15)

Symmetry code: #1 1+x, 1+y, 1+z

4.3.1 Structural characterization of co-crystals

4.3.1.1 Crystal structure of 3,3'-azpy:SA

In the crystal structure of **3,3'-azpy:SA**, the molecular recognition occurs at the expected acid-pyridine interface. Azopyridine interacts with succinic acid via O-H···N hydrogen bonds forming 1-D chains (Fig 4.6). The1-D chains run perpendicular to each other in the crystal lattice forming an interlocked network (Fig 4.7). These chains are connected via secondary C-$H_{(phenyl)}\cdots O_{(carbonyl)}$ interactions between neighboring 1-D chains (Fig 4.8)

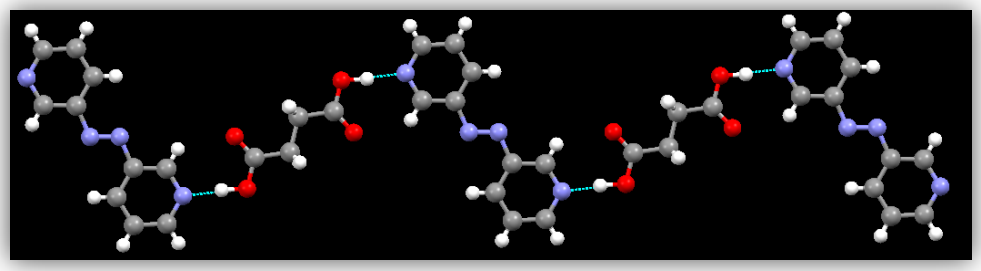

Figure 4.6 1-D chain formed via O-H…N hydrogen bonds in 3,3'-azpy:SA co-crystal

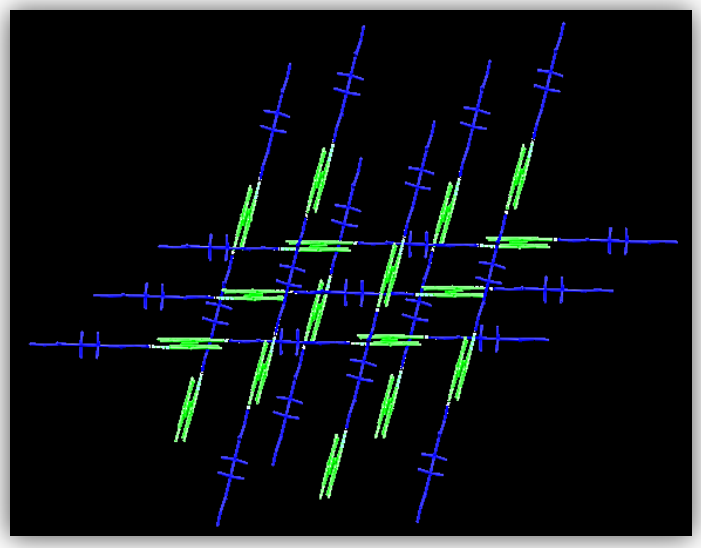

Figure 4.7 1-D chains running perpendicular to each other, green (azopyridine) and blue (succinic acid)

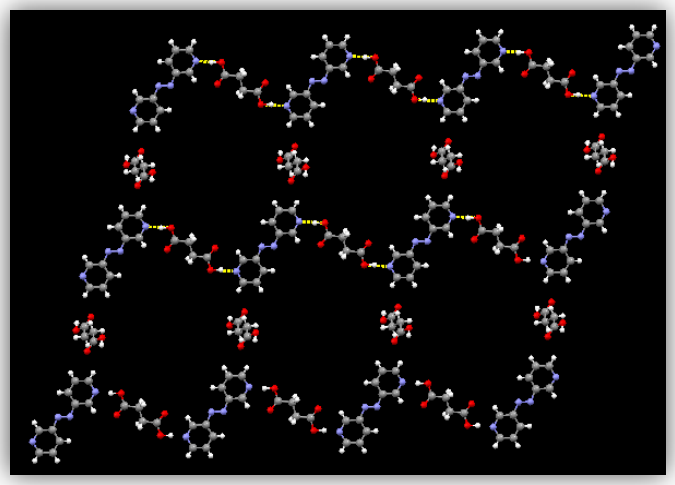

Figure 4.8 A top view of the weaker C-H···O (between phenyl and acid) interactions connecting neighboring perpendicular chains

4.3.1.2 Crystal structure of *3,3'-azpy:AA, 3,3'-azpy:SuA and 3,3'-azpy:SeA*

In the crystal structures of **3,3'-azpy:AA**, **3,3'-azpy:SuA** and **3,3'-azpy:SeA** the primary mode of interaction between the acid and base is via O-H···N hydrogen bonds on either side of the diacid resulting in infinite 1-D chains. The chains then connect into 2-D planar sheets through auxiliary $C\text{-}H_{(phenyl)}\cdots O_{(carbonyl)}$ hydrogen bonds in neighboring chains and close contacts between azopyridine units (Fig 4.9). All three co-crystals show similar structure and arrangement in two dimensions.

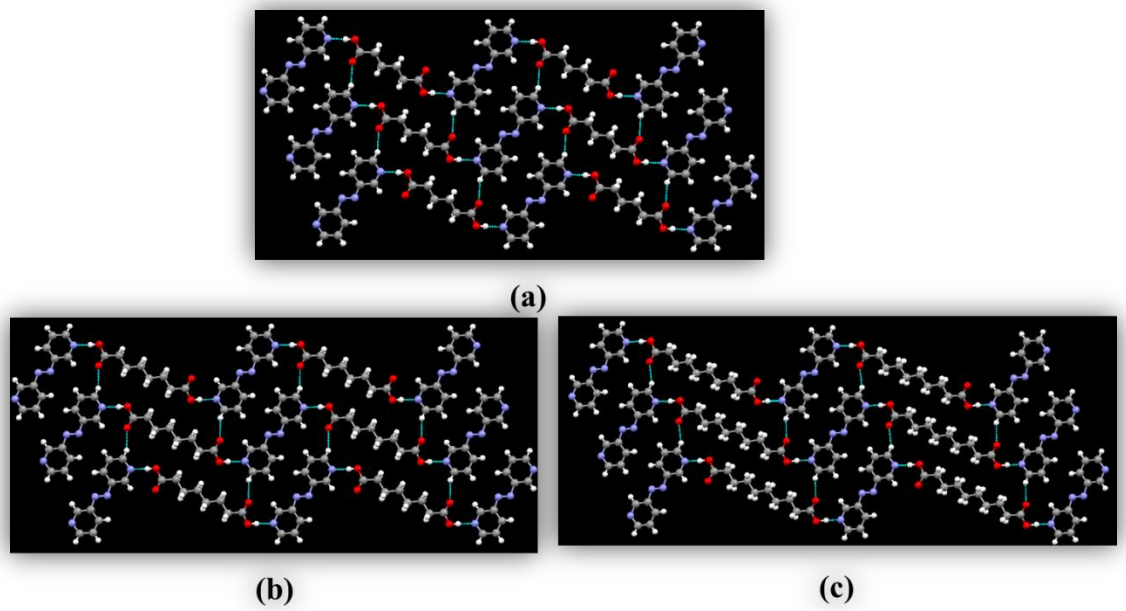

Figure 4.9 2-D planar sheets in co-crystals of a) 3,3'-azpy:AA **b)** 3,3'-azpy:SuA **and c)** 3,3'-azpy:SeA

4.3.1.3 Crystal structure of 4,4'-azpy:SuA

In the crystal structures of **4,4'-azpy:SuA**, O-H···N interactions lead to infinite 1-D chains that are further organized into 2-D planar sheets via secondary C-H···O interactions (Fig 4.10). Two types of auxiliary C-H···O interactions, *i.e.* $C\text{-}H_{(phenyl)}\cdots O_{(carbonyl)}$ and $C\text{-}H_{(phenyl)}\cdots O_{(hydroxyl)}$ connect the 1-D chains. Unlike in **3,3'-azpy** co-crystals, there are no close contacts between neighboring azopyridine moieties.

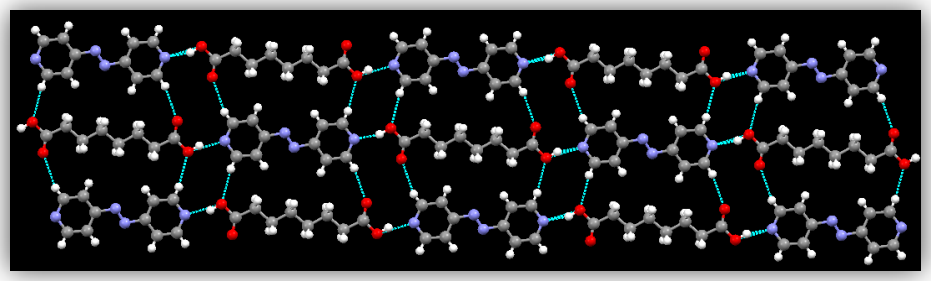

Figure 4.10 2-D planar sheet in 4.4'-azpy:SuA co-crystal

4.3.2 Unit cell parameters of co-crystals

The unit cell parameters of the co-crystals are listed in Table 4.4.

Table 4.4 Unit cell parameters of 3,3'-**and** 4,4'-azpy **co-crystals**

Co-crystal	**3,3'-azpy:SA**	**3,3'-azpy:AA**	**3,3'-azpy:SuA**	**3,3'-azpy:SeA**	**4,4'-azpy:SuA**
Crystal system	Monoclinic	Triclinic	Triclinic	Triclinic	Triclinic
Space group, Z	P21/c, 2	P-1, 1	P-1, 1	P-1, 2	P-1, 1
a, Å	11.9092(7)	5.2025(4)	5.4680(6)	7.0388(14)	5.8269(6)
b, Å	5.2342(3)	7.0703(6)	7.0381(7)	8.2451(18)	8.6817(8)
c, Å	11.3589(7)	11.4579(10)	11.9358(12)	17.490(4)	9.0827(9)
α, °	90.00	99.247(5)	98.867(6)	77.525(14)	76.314(6)
β, °	91.198(3)	102.957(6)	93.592(6)	80.368(13)	87.963(6)
γ, °	90.00	101.395(5)	102.392(6)	85.474(14)	77.486(6)
V, Å^3	707.90(7)	393.25(6)	441.09(8)	976.1(3)	435.76(7)

4.4 Discussion

4.4.1 Co-crystal vs salts

In the pharmaceutical industry a pK_a thumb rule is often used to predict the formation of a salt in acid-base reactions.[8] It is generally accepted that a Δ pK_a (pK_a base- pK_a acid) value > 2 or 3 will result in a salt formation between the acid and base.[9] An extension to this rule was recently proposed by Nangia et al.[10] for co-crystal systems with a series of carboxylic acids and pyridine based bases. According to their analysis, a negative pK_a difference between the interacting species will always result in the formation of co-crystals, as opposed to salts. Another highlight of the study was the observation that when the Δ pK_a is between 0-3, the accurate prediction of neutral or ionic synthons in the solid state is not possible.[11]

A pK_a analysis of our acid-base system gives us a negative Δ pK_a value for all five combinations of azopyridine and the diacids (Table 4.5)[12]. Thus one can reliably predict a neutral acid-pyridine heterosynthon to be formed between azopyridine and corresponding diacids as opposed to an ionic one (Fig 4.11). As previously discussed in Chapter 2, we can distinguish between neutral O-H···N and ionic $O^-\cdots H\text{-}N^+$ charge assisted interactions by analyzing structural parameters such as the acid C-O bond distances in the resulting single crystal structure and the endocyclic C-N-C bond angle which is sensitive to protonation.

Table 4.5 pK_a values of components in 3,3'-**and** 4,4'-azpy **cocrystals**[12]

Co-crystal	pK_a (acid)	pK_a (base)	Δ pK_a
3,3'-azpy:SA	4.24	3.76	-0.48
3,3'-azpy:AA	4.39	3.76	-0.57
3,3'-azpy:SuA	4.46	3.76	-0.7
3,3'-azpy:SeA	4.48	3.76	-0.72
4,4'-azpy:SuA	4.46	1.93	-2.53

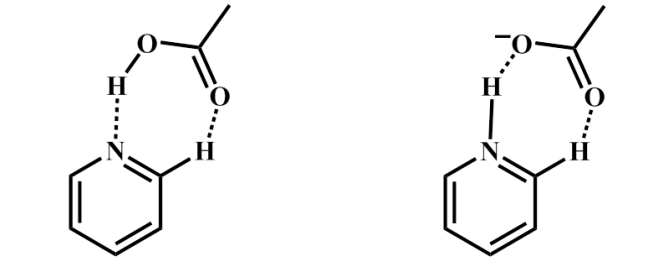

Figure 4.11 Neutral and charged assisted heterosynthons between acid-pyridine pair

4.4.1.1 Characterization using IR spectroscopy

In our set of experiments we have obtained 5/5 co-crystals, *i.e.* 100% co-crystallization success. The co-crystals were first screened using IR spectroscopy. Co-crystal formation was confirmed by i) two broad stretches in the 1800-2500 cm^{-1} region, representing the intermolecular O-H···N hydrogen bond and ii) C=O stretch, which in all cases was above 1670 cm^{-1} (Table 4.2) indicating the presence of neutral carboxylic acid moiety, (Figure 4.12).

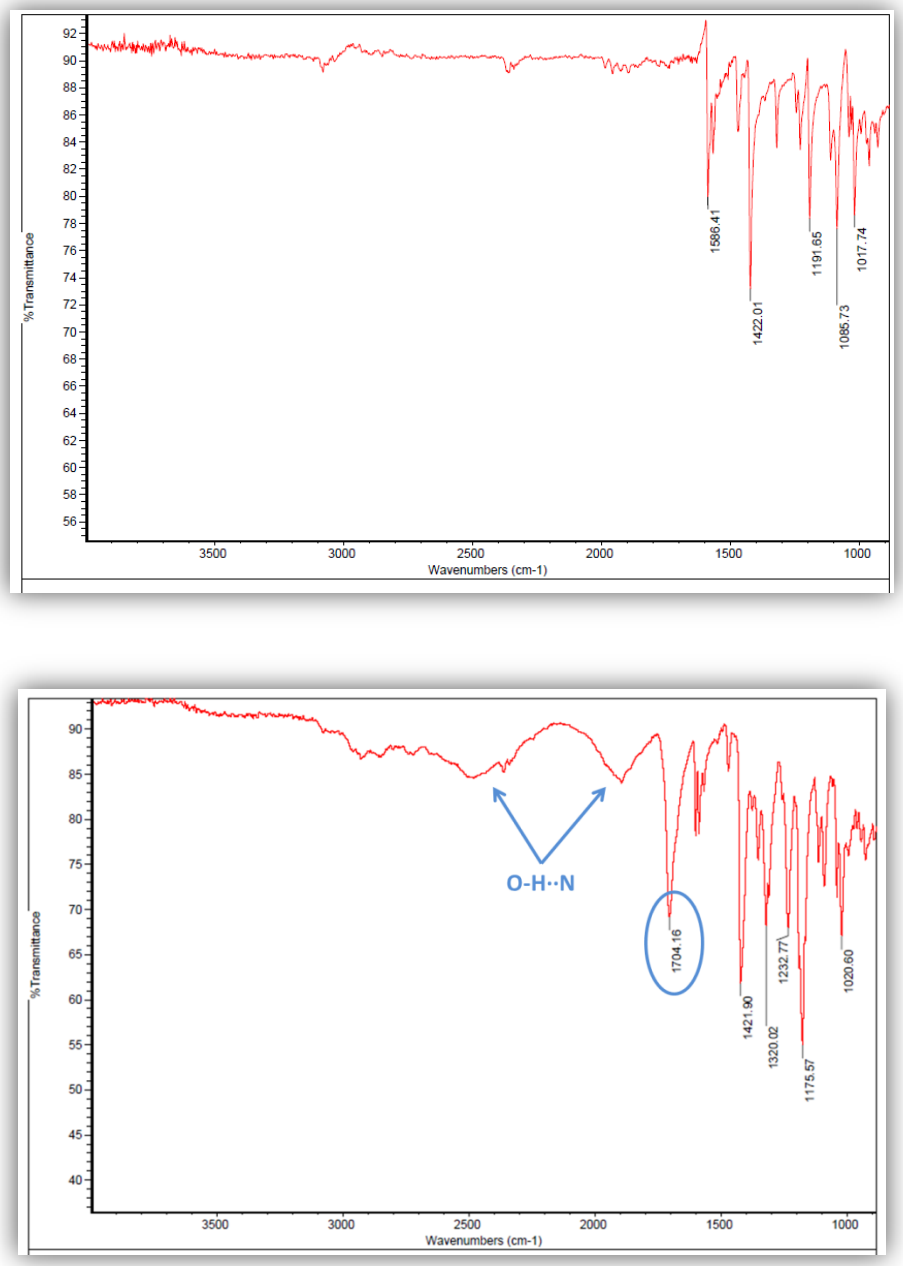

Figure 4.12 IR spectra of 3,3'-azpy **(above) and** 3,3'-azpy:SA **(below)**

4.4.1.2 Characterization using structural parameters

Structural parameters of the ancillary groups like C-N-C endocyclic bond angle and C-O bond distances in the carboxylic acid can be used to interpret the neutral or ionic nature of an acid-pyridine heterosynthon. The C-O (short) bond distances in our crystal structures range from 1. 204- 1.218 Å and C-O (long) bond distances range from 1.313-1.339 Å, while the C-N-C bond

angles range between 117.4°- 118.7°. With reference to Fig 2.21, our bond distance and angle values indicate that a neutral heterosynthon is formed in all five crystal structures.

4.4.2 Examination of the motifs and packing pattern in the crystal structures

In all five crystal structures, the primary synthon formed is the acid-pyridine heterosynthon via neutral O-H···N hydrogen bonds. The resulting architecture is 1-D chain, which extends into 2-D layered structure via weaker $_{(py)}$C-H···O$_{(acid)}$ intra-layer interactions. Although the final outcome in all crystal structures is 2-D sheets, there is however a basic difference in the way 1-D chains are arranged with respect to each other to form the extended 2-D architecture.

4.4.2.1 3,3'-Azopyridine co-crystal structures

In **3,3'-azpy:AA, 3,3'-azpy:SuA** and **3,3'-azpy:SeA** individual 1-D chains are organized into 2-D planar sheets in an in-phase arrangement, ***motif 4*** (Fig 4.5 and 4.9). The chains are connected via C-H$_{(phenyl)}$···O$_{(carbonyl)}$ interactions. Short contacts between the azopyridine moieties are also observed in all three crystal structures within the plane of each layer.

In **3,3'-azpy:AA** (Fig 4.13a), the packing between individual sheets result in inter-layer short contacts between $_{(acid)}$C-H···C$_{(py)}$ and $_{(acid)}$C-H···O$_{(acid)}$. In **3,3'-azpy:SuA** (Fig 4.13b), the layers are stacked one above the other using not only $_{(acid)}$C-H···O$_{(acid)}$ interactions but also Π-Π interactions between azopyridine molecules. In **3,3'-azpy: SeA** (Fig 4.13c)**,** there are alternating interlayer $_{(acid)}$C-H···O$_{(acid)}$ and Π-Π interactions.

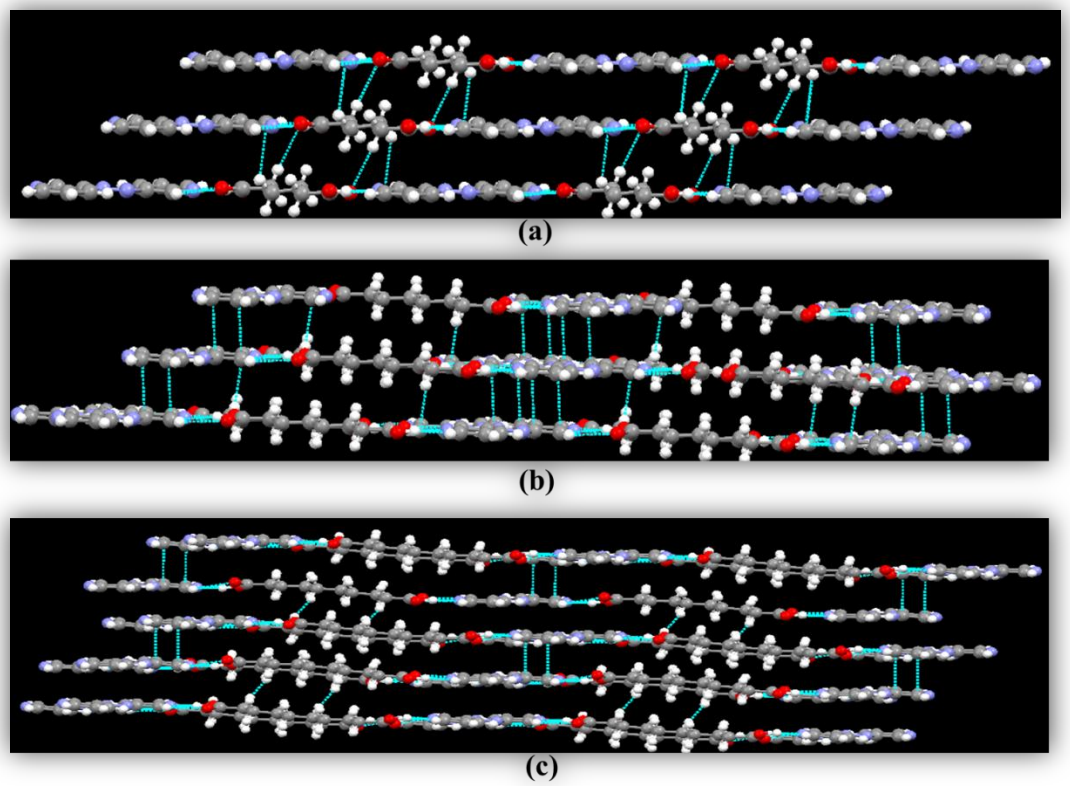

Figure 4.13 Packing of 2-D sheets in a) 3,3'-azpy: AA **b)** 3,3'-azpy:SuA **and c)** 3,3'-azpy:SeA

In **3,3'-azpy:SA**, the packing is very different. An *unexpected motif* is observed with two types of 1-D chains that run perpendicular to each other and result in a 3-D interlocked network. The crystal structure lacks close packing between individual chains as observed in other three co-crystals of **3,3'-azpy** (Fig 4.7 and 4.8).

4.4.2.2 4,4'-azopyridine co-crystal structures

In the crystal structures of **4,4'-azpy:SA**[5b], **4,4'- AA**[5a] and **4,4'-azpy:SuA,** ***motif 1*** exists with the 1-D chains arranged in an out of phase pattern with respect to each other forming 2-D sheets (Fig 4.5, 4.10 and 4.14).

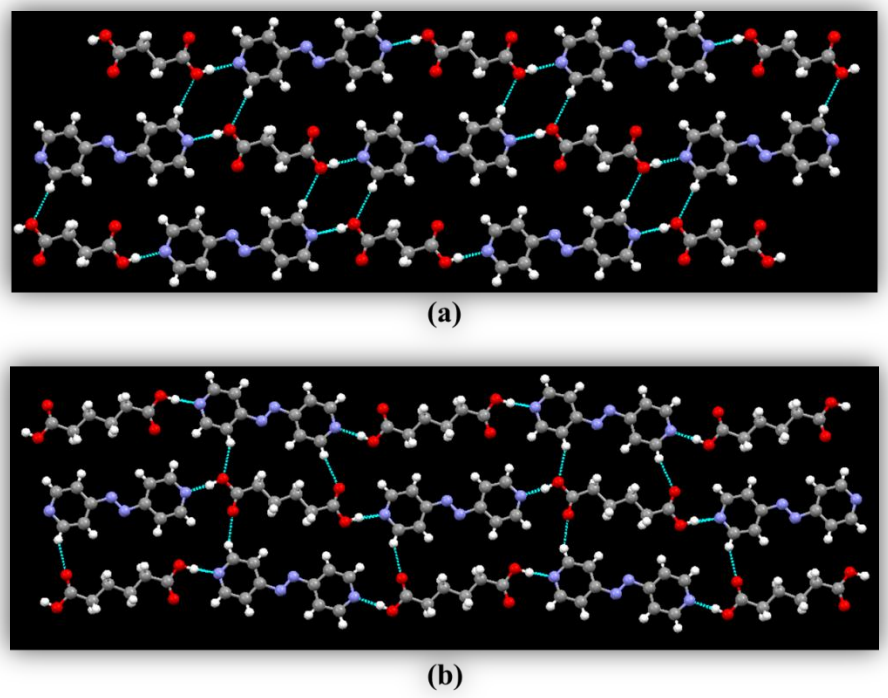

Figure 4.14 2-D sheets in a) 4,4'-azpy:SA **and b)** 4,4'-azpy:AA **co-crystals**[5]

In **4,4'-azpy:SA** the 2-D layers are stacked via interlayer $_{(py)}$C-H···O$_{(acid)}$ and Π-Π interactions between neighboring layers. In **4,4'-azpy:AA** and **4,4'-azpy:SuA** only $_{(acid)}$C-H···C$_{(py)}$ contacts are used to connect the layers (Fig 4.15).

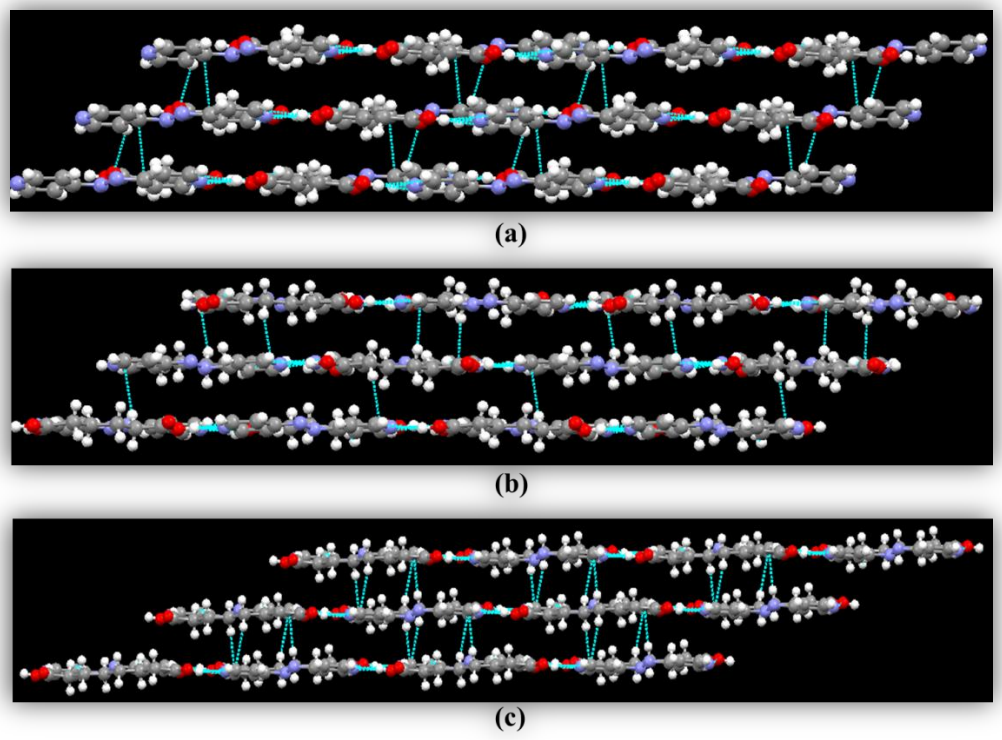

Figure 4.15 Packing of 2-D sheets in a) 44,'-azpy:SA**; b)** 4,4'-azpy:AA **and c)** 4,4'-azpy:SuA

The crystal structure of **4,4'-azpy:SeA** displays ***motif 2***, where chains are organized in an in-phase arrangement to form planar 2-D layers (Figs 4.5 and 4.16). The 2-D layers are then packed via $_{(acid)}$C-H···C$_{(py)}$ interactions (Fig 4.17).

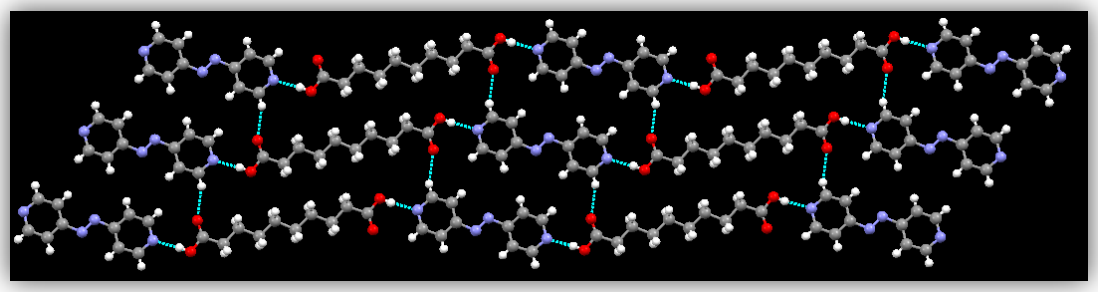

Figure 4.16 2-D sheet in 4,4'-azpy:SeA co-crystal

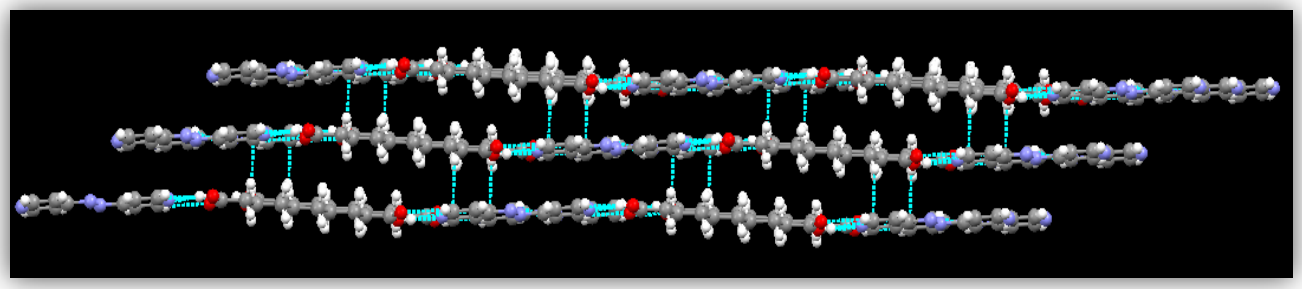

Figure 4.17 Packing pattern of 2-D sheets in 4,4'-azpy:SeA **co-crystal**

Thus an analysis of all eight crystal structures of 3,3'-and 4,4'-azopyridine co-crystals gives the following distribution of motifs (Fig 4.18);

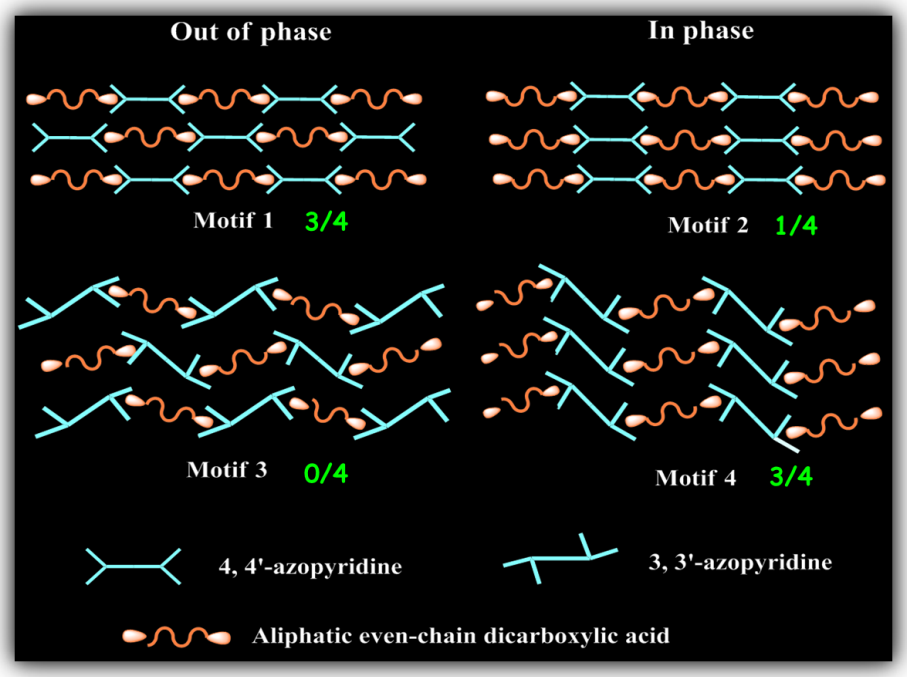

Figure 4.18 Distribution of motifs observed in our crystal structures

4.4.3 Analysis of thermal behavior of co-crystals

Melting point of solids is an important physical property that can have implications for different applications and most importantly for processing, shelf-life and storage purposes.[13] The physical properties of bulk solids depend by and large on the solid-state structure and packing arrangement in the crystal lattice. If we can successfully prove that thermal behavior and

molecular structure are interrelated, then simple co-crystallization techniques can be used as a means of modulating the thermal behavior of bulk solids in a reliable manner.

4.4.3.1 Correlating thermal behavior as a function of acid chain length

In **4,4'-azpy** co-crystals with succinic (C4), adipic (C6), suberic (C8) and sebacic (C10) acid, structural consistency is maintained as we systematically increase the carbon chain length in the diacids from C4 to C10. Although in **4,4'-azpy:SeA**, ***motif 2*** is observed instead of ***motif 1*** (observed in all other cases), the packing pattern is similar in all four cases, *i.e.* the 1-D chains are closely arranged into 2-D layers using weaker intra-layer interactions (Fig 4.10, 4.14 and 4.15) followed by 2-D layers via weaker inter-layer interactions (Figs 4.16 and 4.17). This consistency in the crystal structure is reflected in their melting points (Table 4.1). In a plot of **4,4'-azpy** co-crystal melting points against the carbon chain length in the corresponding diacids, a near-linear correlation is observed which indicates reliable structure-property interdependence (Figure 4.19).

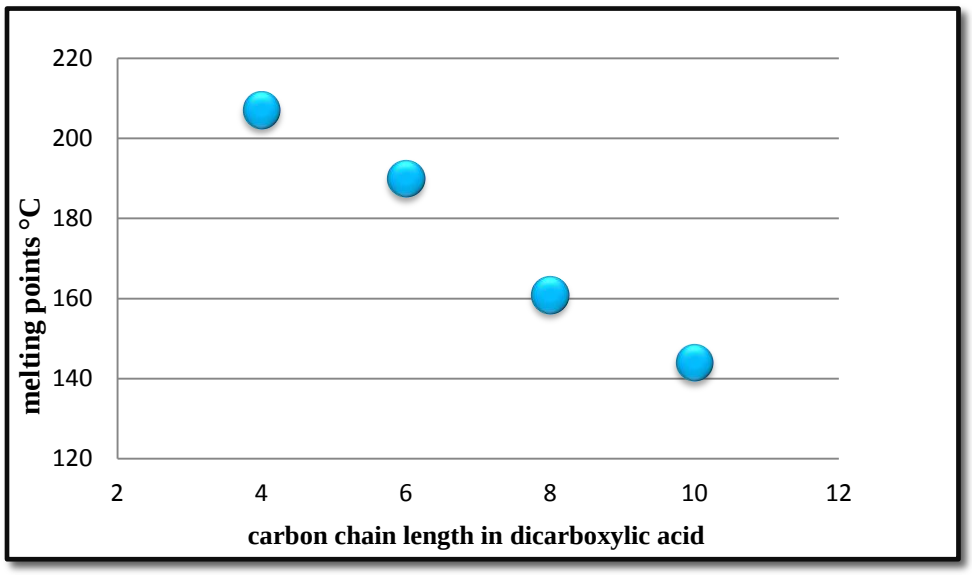

Figure 4.19 Melting point of 4,4'-azpy **co-crystals as a function of carbon chain length**

In **3,3'-azpy** co-crystals ***motif 4*** was observed in 3/4 cases, where 1-D chains were arranged into 2-D layers via intra-layers interactions (Fig 4.9), followed by their close packing (Fig 4.13), thus maintaining structural consistency in **3,3'-azpy:AA, SuA** and **SeA** co-crystals. The outlier **3,3'-azpy:SA** displays an unexpected motif with a very different packing of 1-D

chains (Fig 4.7 and 4.8). This discrepancy in the crystal structure is also reflected in its melting point which is lower than in the other solids (Fig 4.20).

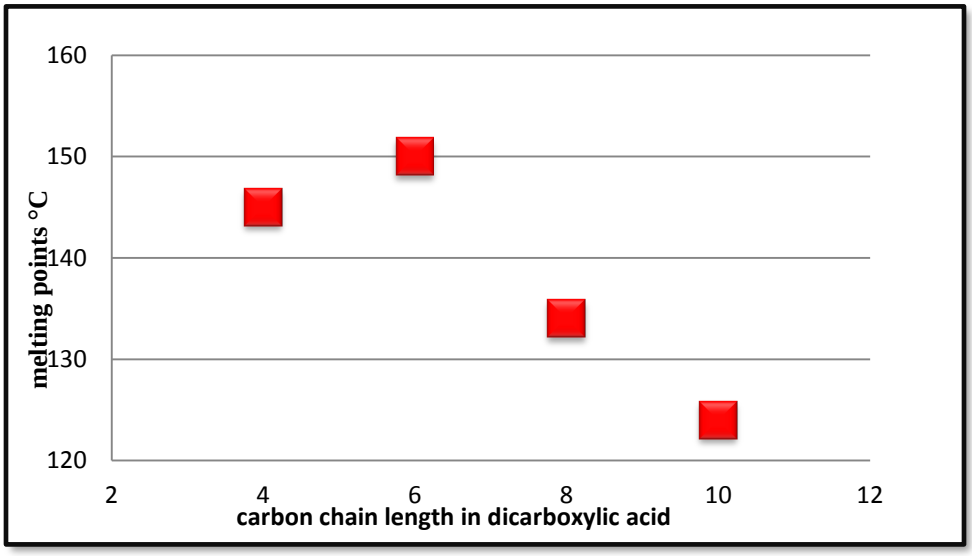

Figure 4.20 Melting point of 3,3'-azpy **co-crystals as a function of carbon chain length**

4.4.3.2 Effect of binding site geometrical bias on melting point

The position of the binding site on the co-crystallizing agent plays an important role in arranging the building blocks during the assembly process. Any alteration in the relative orientation is reflected in differences in packing and overall assembly in solid-state. Changes in the solid-state structure will also bring about variations in the bulk physical properties.

In our experiments, the two acceptors have their binding sites oriented at different angles with respect to each to other. Although this does not affect the primary molecular recognition event forming 1-D chains, the packing pattern of the resulting 1-D chains is very different across the group. The two classes of co-crystals display very different melting points with respect to the diacids themselves. **3,3'-azpy** co-crystals have melting points lower than the diacids, whereas **4,4'-azpy** co-crystals have melting points higher than those of the diacids (Fig 4.21).

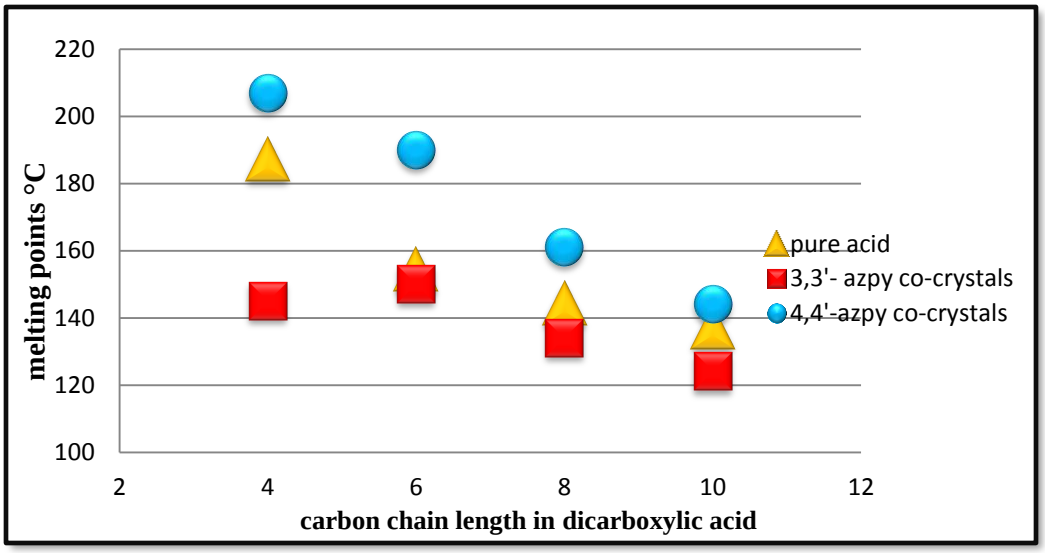

Figure 4.21 Melting point correlation between 3,3'-**and** 4,4'-azopy **co-crystals and molecular structure of diacids**

In order to provide a reasonable explanation for the observed trend in melting points between the two classes of co-crystals, we tried to examine their packing co-efficient values using Olex v 2.1 (Table 4.6). However, the packing co-efficients of the two classes of co-crystals fall within the range of 61-69% and do not display any correlation to the observed melting point behavior.

Table 4.6 Packing co-efficients of 3,3'-and 4,4'-azpy co-crystals

	SA	AA	SuA	SeA
3,3'azpy	64%	66%	65%	65%
4,4'-azpy	64%	66%	69%	61%

The observed differences in the melting point of 3,3'-and 4,4'-azopyridine co-crystals can be attributed to the variation in packing arrangement due to the differences in the orientation of binding sites on the acceptor molecules. This argument can be supported by the work done by Braga et al. where the co-crystals of dicarboxylic acids (adipic, suberic and sebacic acid) with 1,2-bis- (4-pyridyl)ethane (**BPA**) displayed higher melting points than the corresponding diacids whereas co-crystals with 1,2-bis(4-pyridyl)propane (**BPP**) displayed lower melting points than the corresponding diacids. Since the same set of diacids was used, the difference observed can be

attributed to the difference in packing arrangements caused as a result of the binding site biased in **BPA** and **BPP** (Fig 4.22)**.**[2]

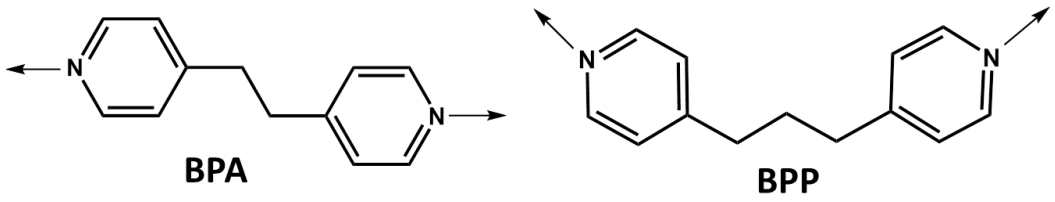

Figure 4.22 Schematic of BPA **and** BPP

4.5 Conclusion

We have synthesized two isomeric pyridine based acceptors 3,3'-and 4,4'-azopyridine with even chain diacids and demonstrated the following;

1) Reliable and consistent assemblies can be produced in both groups of azopyridine co-crystals of dicarboxylic acid.
2) Based on our crystal structure and thermal behavior analysis, a reliable structure-property correlation is established within a given series as long as structural consistency is maintained. Any deviation from this is reflected in the thermal behavior.
3) The position of the binding site plays a key role in directing the overall assembly formation and hence the bulk physical property like melting point.[14]

---

[1] Aakeröy, C.B.; Panikkattu, S.; DeHaven, B.; Desper, J., *Cryst. Growth Des*., **2012**, 12, 2579–2587

2 Aakeröy, C. B.; Forbes, S.; Desper, J.; *J. Am. Chem. Soc*., **2009**, 12, 17048-17049; Braga, D.; Dichiarante, E.; Palladino, G.; Grepioni, F.; Chierotti, M. R.; Gobetto, R and Pellegrino, L. *CrystEngComm*, **2010**, 12, 3534-3536.

3 (a) Leviel, J, L.; Auvert, G.; Savariault, J, M.; *Acta Cryst.* **1981**, B**37**, 2185-2189; (b) Housty, J.; Hospital, M., *Acta Crystallogr.* **1965**, 18, 693; (c) Housty, J.; Hospital, M., *Acta Crystallogr.* **1965**, 18, 753; (d) Housty, J.; Hospital, M., *Acta Crystallogr.* **1966**, 20, 325

4 Desiraju, G. R.; *Crystal Engineering: The design of organic solids,* Elsevier, **1989**, ISBN 0-444-87457-7; Du, M.; You, Y. P.; Zhang, Z, H.; *Acta Crystallographica Section C*, **2006**, C62, 33- 35

5 Zhang, J.; Wu, L.; Fan, Y. *J. Mol. Struct.,* **2003**, 660, 119-129; Zhang, J.; Ye, L.; Wu, L. *Acta Crystallogr.Section C*, **2005**, 61, 38-40

6 Spaleniak, G. P.; Daszkiewicz, Z. and . Kyzio, J. B. *Chemical papers*, **2009,** 3, 312-322.

7 Iranpoor, N.; Firouzabadi, H.; Khalili, D.and Motevalli, S. *J. Org. Chem*. **2008**, 73, 4882–4887.

8 Stahl, P. H.; Wermuth, C. G. *Handbook of pharmaceutical salts; properties, selection and use*, Wiley-vch, **2002**

9 Johnson, S. L and Rumon, K. A, *J. Phys. Chem*., **1965,** 69, 74–86; Tong, W. Q. T and Whitesell, G. *Pharm. Dev. Technol*., **1998**, 3, 215–223

10 Bhogala, B. R.; Basavoju, S and Nangia, A., *CrystEngComm*, **2005**, 7, 551–562

11 Childs, S. L.; Stahly, G. P and Park, A., *Mol. Pharmaceutics*, **2011**, 4, 323–338

12 Calculated using Advanced Chemistry Development (ACD/Labs) Software V11.02 (© 1994-2013 ACD/Labs)

13 Eddleston, M. D.; Lloyd, G. O and Jones, W., *Chem. Commun*. **2012**, 48, 8075–8077

14 Aakeröy, C. B.; Panikkattu, S.; DeHaven, B.; Desper, J., *CrystEngComm,* **2013**,15, 463-470

Chapter-5 Competing hydrogen-bond and halogen-bond donors in crystal engineering

5.1 Introduction

The hydrogen bond is by far the most commonly used synthetic tool for engineering molecular solids.[1] Hydrogen-bonded synthons such as acid···pyridine[2], phenol···pyridine[2], oxime···$N_{(heterocycle)}$[3] have been explored and are considered as reliable and robust synthons in crystal engineering (Fig 5.1).

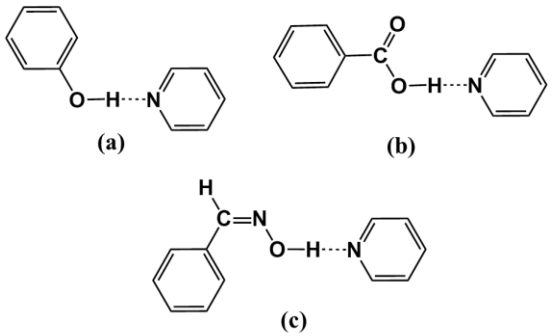

Figure 5.1 Hydrogen bonded heterosynthons a) acid-pyridine b) phenol-pyridine and c) oxime-pyridine

Recently halogen bonds[4] have been explored extensively for its use as 'supramolecular glue' in crystal engineering. Halogen bonding is a non-covalent interaction between a covalently bonded halogen atom (X) and Lewis base (A). The halogen bonding interaction is linear (D-X···A) and parallels the behavior observed in hydrogen bonds.[5] Halogen-bond distances are markedly shorter than the sum of their van der Waals radii, and the shorter the X···A distance, stronger the interaction.[6] The interaction energies of halogen bonds are in the range of 5-180 kJ mol^{-1} (the strong interaction $I_2 \cdots I^-$ in I_3^- is the extreme)[7,8], while the energy for hydrogen-bond interactions falls in the range of 10-65 kJ mol^{-1}.[9] The halogen bonds thus show energetic and geometric trends that are comparable to hydrogen bonds. A halogen bond is typically a single point interaction and is less sensitive to the pka of a given system. For example, many hydrogen-bond donors can undergo a proton transfer if the donor molecule has strong electron withdrawing groups[10] thus resulting in a salt formation instead of a co-crystal. A halogen atom (I or Br) is typically "activated" by introducing a fluorinated backbone[11] or used in its acetylated form[12],

both of which increase the positive charge at the tip of the halogen atom making them more powerful electron acceptors. As an example, Fig 5.2 shows an increasing positive charge on iodine atom in activated tetrafluoroiodo benzene (+220kJ/mol) and iodoethynyl benzene (+250kJ/mol) as compared to non-activated iodobenzene (+111kJ/mol).[13]

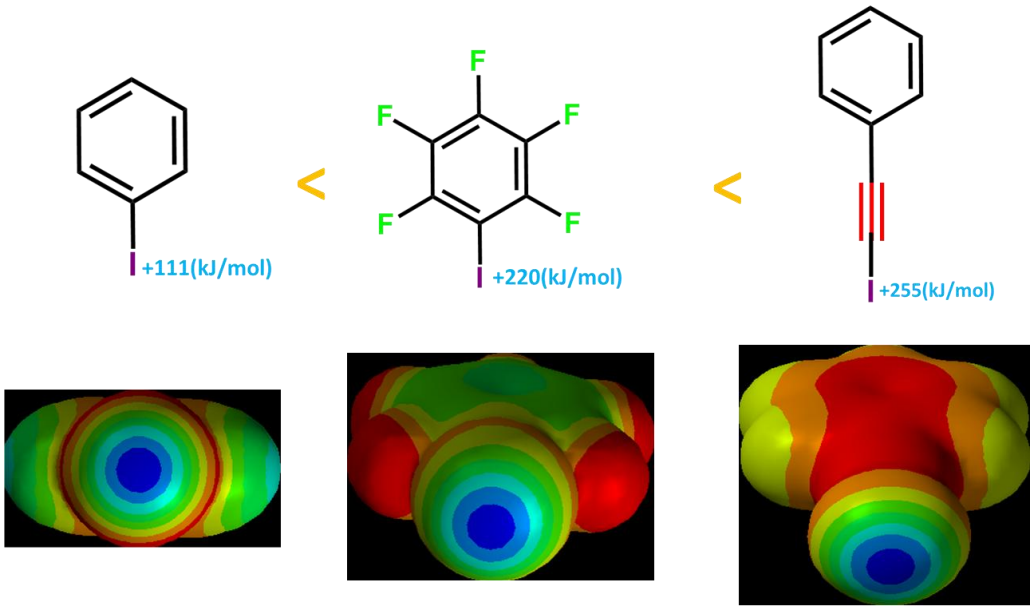

Figure 5.2 Charges on iodine atoms in activated and non-activated halogen-bond donors (generated using molecular surface potential calculations)

Since hydrogen bonds and halogen bonds have comparable features, it is very likely that they can compete in a supramolecular synthesis. Several studies have demonstrated the potential of pyridine based molecules to interact with hydrogen bond donors like acid, phenol and oxime as well as halogen bond donors like iodine and bromine. A CSD search was conducted on co-crystals by limiting the search parameters to aromatic acid, phenol, oxime, iodo and bromo benzenes (as donors) with pyridine type compounds (as acceptors). We found several examples in the CSD that have explored the interaction of pyridine type heterocycles with hydrogen bond donors (HB) (823 hits) and halogen bond donors (XB) (132 hits) individually (Fig 5.3). In our experiments we will combine the two donors on one single backbone and thus investigate the competition and structure directing balance between HBs and XBs.

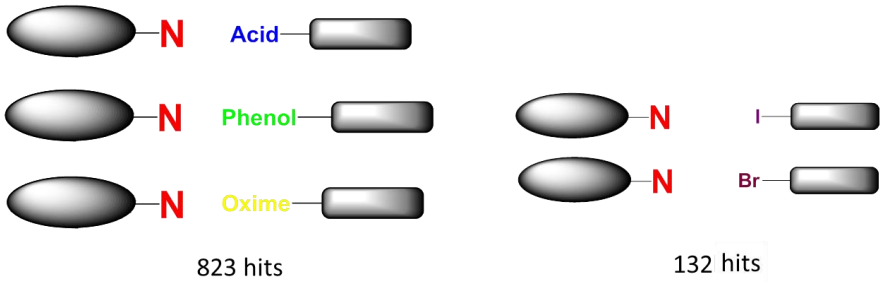

Figure 5.3 Number of hits in the CSD of pyridine based co-crystals with HB and XB donors

In our study we wish to investigate the following;

1. Competition between HB and XB donors for the pyridine nitrogen atom.
2. Influence of geometric bias of the acceptors on the competition and final assembly.
3. Participation of auxiliary acceptors like carbonyl 'O', hydroxyl 'O' and azo 'N' in interacting with the donors.

We have employed six bi-functional donor molecules equipped with one HB and one XB on the same backbone; 4-iodotetrafluorobenzoic acid (**COOH-I**), 4-bromotetrafluorobenzoic acid (**COOH-Br**), 4-iodotetrafluoro phenol (**OH-I**), 4-bromotetrafluoro phenol (**OH-Br**), 4-iodotetrafluoro oxime (**Ox-I**) and 4-bromotetrafluoro oxime (**Ox-Br**) (Fig 5.4). These molecules were co-crystallized with two symmetric acceptors 3,3'-azopyridine (**3,3'-azpy**) and 4,4'-azopyridine (**4,4'-azpy**) (Fig 5.4).

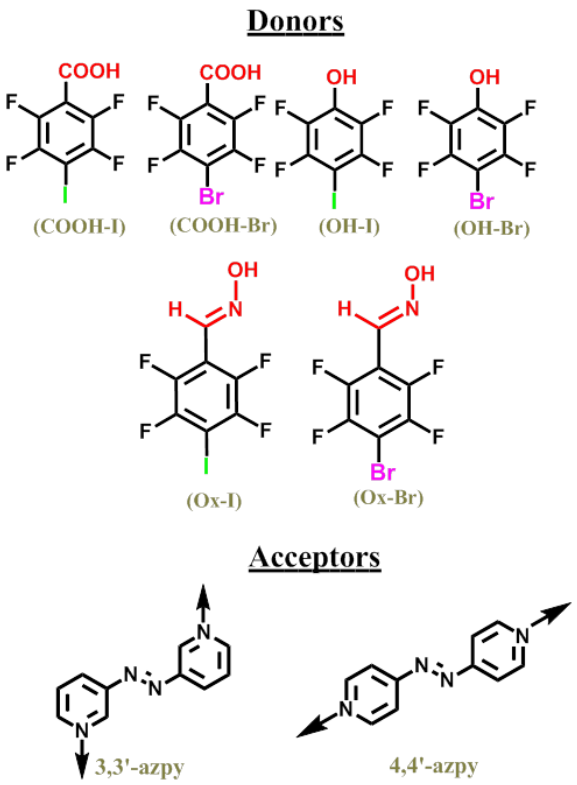

Figure 5.4 Bi-functional donors and symmetric acceptors

Electrostatic charges play an important role in directing the molecular recognition event between interacting building blocks. The best electron donor (highest negative potential) will preferentially pick up the best electron acceptor (highest positive potential) in the given supramolecular system.[14] However in our study, the target acceptors are symmetrical and thus are electrostatically unbiased but geometrically biased as seen previously in Chapter 4, Fig 4.4. In **3,3'-azpy** the binding sites are oriented anti-parallel with respect to each other, while in **4,4'-azpy** they are co-linear (Fig 5.4). With two types of donor atoms (**HB** and **XB**) and one most basic acceptor atom ('N') in our system, there are three different possible outcomes of a 1:1 combination of the azopyridines and the bi-functional donors (Fig 5.5).

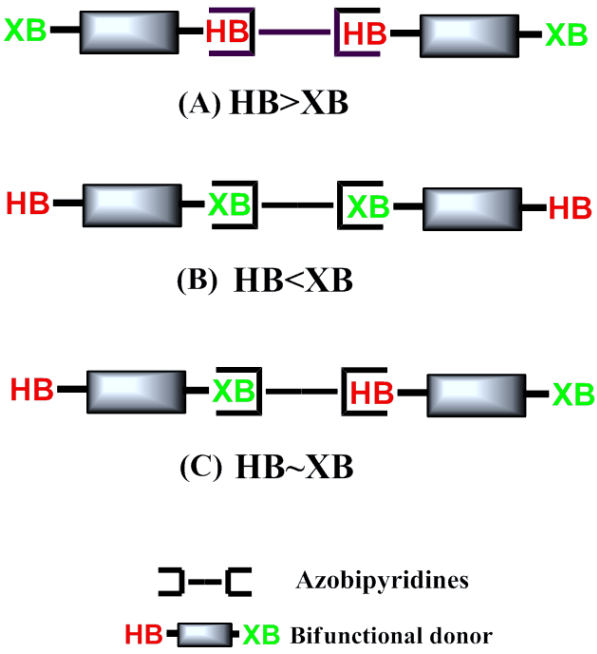

Figure 5.5 Postulated outcomes

5.2 Experimental

5.2.1 Synthesis of ligands

All chemicals, unless noted, were purchased from Sigma Aldrich and used without further purification. Melting points were determined on a Fisher- Johns melting point apparatus. ^{1}H and ^{13}C NMR spectra were recorded on a Varian Unity plus 400 MHz or 200 MHz spectrometer in $CDCl_3$ or D_6-DMSO.

5.2.1.1 Synthesis of 3,3'-and 4,4'-azopyridine[6,7]

See Chapter 4, section 4.2.1.

5.2.1.2 Synthesis of bi-functional donors[15]

The bi-functional donors were synthesized by Prashant Chopade.[15]

5.2.2 Synthesis of co-crystals

Stoichiometric amounts of the donor and acceptor were dissolved in suitable organic solvents and co-crystals were grown using slow evaporation, Table 5.1

Table 5.1 Synthesis of 3,3'-and 4,4'-azopyridine co-crystals

Acceptors	Donors	Co-crystal abbreviation	Mole ratio	Solvent	Melting points °C
3,3'-azopyridine	4-iodotetrafluorobenzoic acid	3,3'-azpy:COOH-I	1:1	Ethanol	182-185
	4-bromotetrafluorobenzoic acid	3,3'-azpy:COOH-Br	1:1	Ethanol	155-157
	4-iodotetrafluorophenol	3,3'-azpy:OH-I	1:1	Ethanol	125-127
	4-bromotetrafluorophenol	3,3'-azpy:OH-Br	1:1	Ethanol	170-173
	4-iodotetrafluoroaldoxime	3,3'-azpy:Ox-I	1:1	Ethanol	145-148
	4-bromotetrafluoroaldoxime	3,3'-azpy:Ox-Br	1:1	Ethanol	105-108
4,4'-azopyridine	4-iodotetrafluorobenzoic acid	4,4'-azpy:COOH-I	1:1	Ethanol	220-222
	4-bromotetrafluorobenzoic acid	4,4'-azpy:COOH-Br	1:1	Ethanol	190-191
	4-iodotetrafluorophenol	4,4'-azpy:OH-I	1:1	Ethanol	163-165
	4-bromotetrafluorophenol	4,4'-azpy:OH-Br	1:1	Ethanol	133-136
	4-iodotetrafluoroaldoxime	4,4'-azpy:Ox-I	1:1	Ethanol	115-116
	4-bromotetrafluoroaldoxime	4,4'-azpy:Ox-Br	1:1	Ethanol	125-126

5.3 Results

We have obtained crystal structures of twelve co-crystals of 3,3'-and 4,4'-azopyridine with six bi-functional donors each. The hydrogen-bond and halogen-bond geometries of all 12 structures are listed in Tables 5.2 and 5.3, respectively.

Table 5.2 Hydrogen-bond geometries in co-crystals of 3,3'-and 4,4'-azopyridine

Structure	D–H…A/Å	D–H/Å	H···A/Å	D···A/Å	D–H···N/°
3,3'-azpy:COOH-I	N(11)-H(11)···O(21A)_#1	1.22(2)	1.32(2)	2.536(2)	174(2)
3,3'-azpy:COOH-Br	O(21)-H(21)···N(11)_#1	1.14(3)	1.41(3)	2.549(2)	177(3)
3,3'-azpy:OH-I	O(21)-H(21)···N(11)_#1	0.90(2)	1.75(2)	2.6162(15)	159(2)
3,3'-azpy:OH-Br	O(31)-H(31)···N(11) O(41)-H(41)···N(21)	0.88(2) 0.88(2)	1.77(2) 1.73(2)	2.6224(16) 2.5963(15)	163.2(18) 166.8(18)
3,3'-azpy:Ox-I	O(27)-H(27)···N(27)_#1_#2	0.72(2)	2.18(2)	2.8460(17)	153(2)
3,3'-azpy:Ox-Br	O(17)-H(17)···N(21)_#1	0.76(4)	1.95(4)	2.708(3)	178(4)
4,4'-azpy:COOH-I	N(11)-H(11)···O(31B)_#1	0.88 0.88	1.75 1.73	2.605(9) 2.598(6)	164.3 167.5

4,4'-azpy:COOH-Br	O31A1-H31A1···N11A1	0.84	1.76	2.566(10)	158.8
	O31B1-H31B1···N21B1_#1	0.84	1.84	2.67(3)	167.6
	O31A2-H31A2···N11A2	0.84	1.75	2.587(9)	170.0
	O31B2-H31B2···N21B2_#2	0.84	1.83	2.67(4)	175.3
4,4'-azpy:OH-I	O(31)-H(31)···N(11)	0.84	1.84	2.614(4)	152.3
4,4'-azpy:OH-Br	O(31)-H(31)···N(11)	0.83(2)	1.86(2)	2.6342(16)	155(2)
4,4'-azpy:Ox-I	O(37)-H(37)···N(11)	0.82(2)	1.90(2)	2.7052(19)	169(2)
4,4'-azpy:Ox-Br	O(27)-H(27)···N(11)_#1	0.94(6)	1.79(6)	2.704(6)	162(6)

Symmetry codes: 3,3'-azpy:COOH-I #1 -x-1,-y,-z+2. 3,3'-azpy:COOH-Br #1 -x+2,-y+1,-z. 3,3'-azpy:OH-I #1 -x+1,-y+1,-z+1. 3,3'-azpy:Ox-I #1 -x,-y,-z+2 #2 -x+3,-y+1,-z. 3,3'-azpy:Ox-Br #1 -x,-y,-z-1. 4,4'-azpy:COOH-I #1 x+2,y-2,z+1. 4,4'-azpy:COOH-Br #1 x-1,y+1,z+1 #2 x+2,y+1,z+1. 4,4'-azpy:Ox-Br #1 -x+2,-y+3,-z+1

Table 5.3 Halogen-bond geometries in co-crystals of 3,3'-and 4,4'-azopyridine

Structure	C-X···A	X···A/Å	C-X···A/°
3,3'-azpy:COOH-I	C-(24A)-I(1)···O(22A)_#2	2.8694(13)	170.66(6)
3,3'-azpy:COOH-Br	C-(24)-Br(1)···O(22)_#2	2.8792(17)	172.23(7)
3,3'-azpy:OH-I	C(24)-I(1)···O(21)_#2	3.0913(10)	156.81(4)
3,3'-azpy:OH-Br	C(34)-Br(1)···O(31)_#1	3.1138(11)	156.32(5)
	C(44)-Br(2) ···O(41)_#2	3.0750(10)	158.68(5)
3,3'-azpy:Ox-I	C(24)-I(1)···N(11)	2.8279(12)	174.75(4)
3,3'-azpy:Ox-Br	C(14)-Br(1)···O(17)_#1	3.0557(19)	158.49(9)
4,4'-azpy:COOH-I	C(34A)-I(1A) ···N(21)_#1	2.796(5)	173.4(3)
4,4'-azpy:COOH-Br	C(34A1)-Br(1A1)···N(21A1)_#1	2.802(7)	176.9(4)
4,4'-azpy:OH-I	C(34)-I(1)···N(21)_#1	2.960(3)	165.98(11)
4,4'-azpy:OH-Br	C(34)-Br(1)···N(21)_#1	2.9717(12)	165.95(5)
4,4'-azpy:Ox-I	C(34)-I(1)···N(21)_#1	2.8200(15)	178.38(5)
4,4'-azpy:Ox-Br	C(24)-Br(1)···N(14)_#1	3.395(4)	171.94(17)

Symmetry codes 3,3'-azpy:COOH-I #2 x+1,-y+1/2,z-1/2. 3,3'-azpy:COOH-Br #2 x-1,-y+1/2,z+1/2. 3,3'-azpy:OH-I #2 -x+1/2,y-1/2,-z+3/2. 3,3'-azpy:OH-Br #1 -x+1,y-1/2,-z+1/2 #2 -x,y+1/2,-z+3/2. 3,3'-azpy:Ox-Br #1 x,y+1,z+1. 4,4'-azpy:COOH-I #1 x-2,y+2,z-1. 4,4'-azpy:COOH-Br #1 x-1,y+1,z+1. 4,4'-azpy:OH-I #1 x-2,y+1,z+1. 4,4'-azpy:OH-Br #1 x+2,y-1,z-1. 4,4'-azpy:Ox-I #1 x-1/2,-y-1/2,z+1/2. 4,4'-azpy:Ox-Br #1 x-1/2,-y+3/2,z-1/2.

5.3.1 Description of the crystal structures

5.3.1.1 Co-crystals of 3,3'-azopyridine

5.3.1.1.1 3,3'-Azopyridine:4-iodotetrafluorobenzoic acid; 3,3'-azpy:COOH-I

In a reaction between **3,3'-azpy** and 4-iodotetrafluorobenzoic acid, the primary recognition occurs between the acid and pyridine moiety via O-H···N hydrogen bonds forming a trimer (Fig 5.6). The positive tip of the iodine atom interacts with a lone pair on a carbonyl oxygen atom with I···O halogen bonds, thus connecting individual trimers and extending the architecture along two dimensions (Fig 5.7).

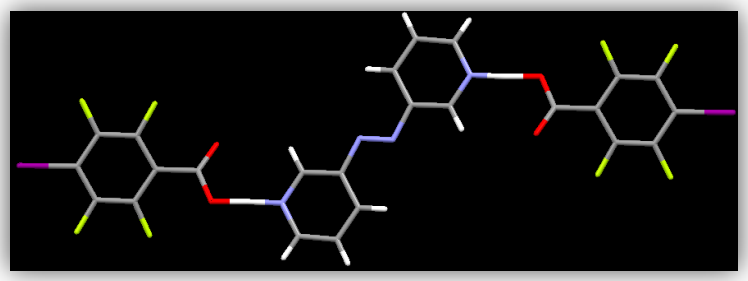

Figure 5.6 Trimer formed via acid...pyridine heterosynthon in 3,3'-azpy:COOH-I **(*The apparent 'covalent' bond between COOH and py is due to a disorder over two positions of the haloacid).***

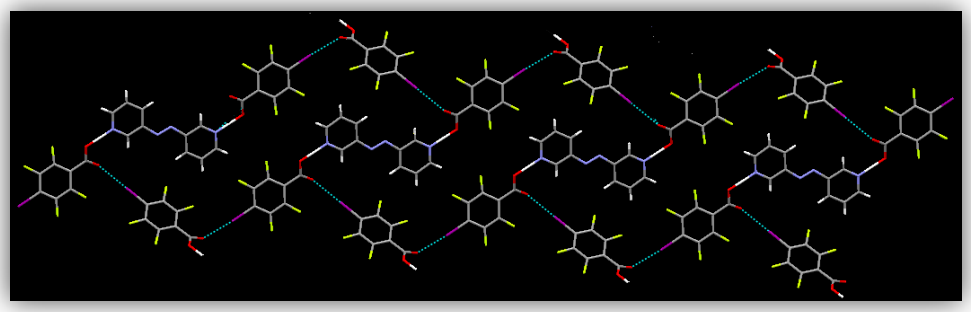

Figure 5.7 2-D network formed via O-H…N(py) and C-I…O interactions in 3,3'-azpy:COOH-I **co-crystal.**

5.3.1.1.2 3,3'-Azopyridine:4-bromotetrafluorobenzoic acid; *3,3'-azpy:COOH-Br*

Similar to the previous crystal structure, in **3,3'-azpy:COOH-Br** acid-pyridine interactions produce the primary trimers followed by their extension into 2-D sheets via weaker C-Br···O interactions (Fig 5.8).

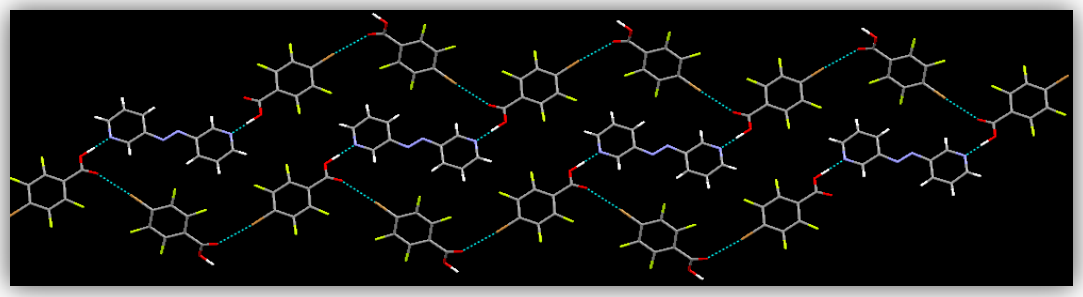

Figure 5.8 3,3'-azpy:COOH-Br **co-crystal showing primary O-H…N(py) and secondary C-Br…O interactions**

5.3.1.1.3 3,3'-Azopyridine:4-iodotetrafluorophenol; *3,3'-azpy:OH-I*

Of the two potential single point donor atoms ('OH' and 'I') in 4-iodotetrafluorophenol, both pyridine site on the acceptor picks up the hydroxyl hydrogen atom forming an O-H···N heterosynthon. The trimers are then connected into 2-D layers via intra-layer C-I···O interactions (Fig 5.9).

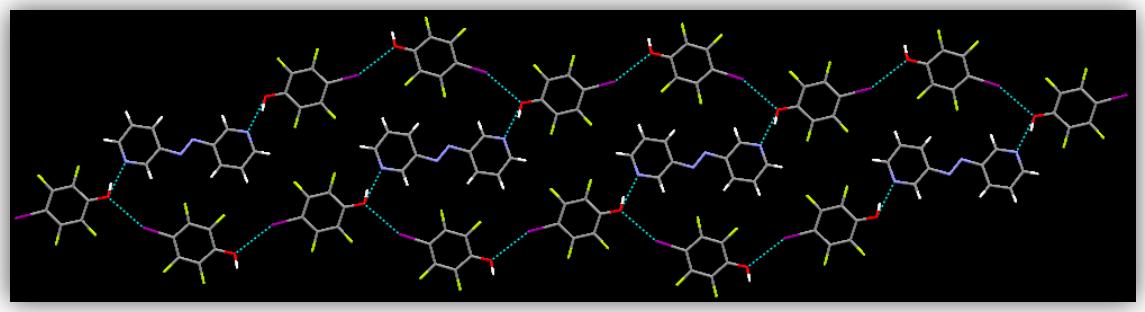

Figure 5.9 3,3'-azpy:OH-I **crystal structure showing primary O-H…N(py) and secondary C-I…O interactions forming 2-D layer.**

5.3.1.1.4 3,3'-Azopyridine:4-bromotetrafluorophenol; *3,3'-azpy:OH-Br*

In the **3,3'-azpy:OH-Br** co-crystal, intermolecular O-H···N hydrogen bonds produce trimeric supermolecules. These individual supermolecules then assemble into 2-D layers via C-Br···O interactions (Fig 5.10).

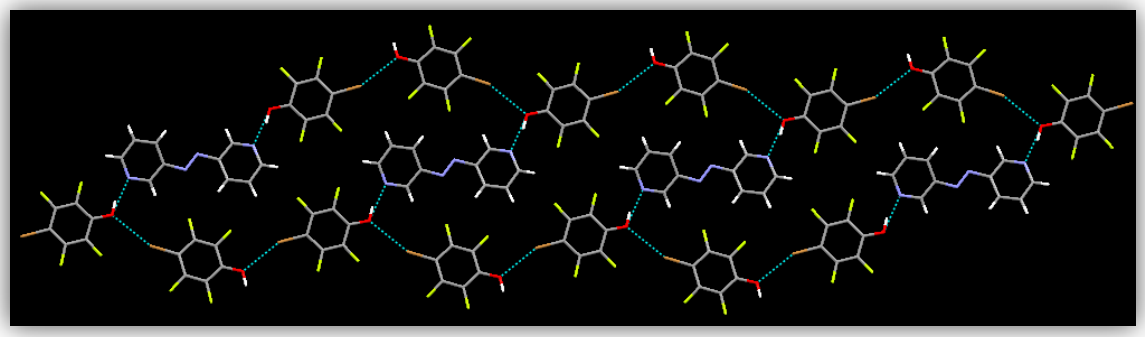

Figure 5.10 3,3'-azpy:OH-Br **crystal structure showing intermolecular O-H…N(py) and C-Br…O interactions.**

5.3.1.1.5 3,3'-Azopyridine:4-iodotetrafluorooxime; *3,3'-azpy:Ox-I*

The crystal structure of **3,3'-azpy:Ox-I** is different from the other co-crystals of 3,3'-azpy in this study. In **3,3'-azpy:Ox-I,** the two pyridine nitrogen atoms on azopyridine picks up a iodine atom to form C-I···N halogen bonds. The oxime group engages in a homomeric dimer, thus resulting in a 1-D infinite chain like assembly (Fig 5.11).

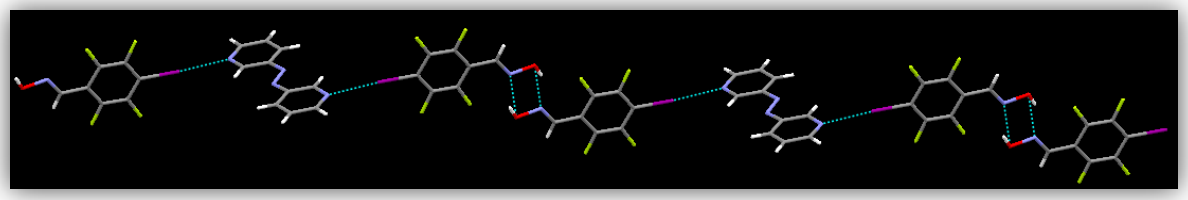

Figure 5.11 3,3'-azpy:Ox-I co-crystal with oxime-oxime dimer and C-I…N(py) halogen bonds forming 1-D corrugated chain

5.3.1.1.6 3,3'-Azopyridine:4-bromotetrafluorooxime; *3,3'-azpy:Ox-Br*

In **3,3'-azpy:Ox-Br** crystal structure, a trimer is produced via O-H···N hydrogen bonds, followed by their assembly into 2-D layers via secondary C-Br···O interactions (Fig 5.12).

Unlike in the case of **3,3'-azpy:Ox-I**, where the oxime engages in a homomeric dimer, in this case the oxime is a part of the primary structure directing force.

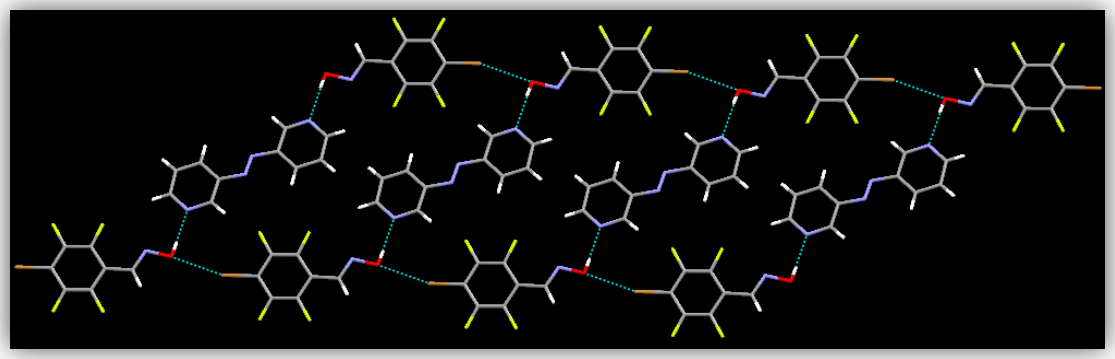

Figure 5.12 3,3'-azpy:Ox-Br **crystal structure showing O-H…N(py) primary hydrogen bonds and secondary C-Br…O interactions**

5.3.1.2 Co-crystals of 4,4'-azopyridine

5.3.1.2.1 4,4'-Azopyridine:4-iodotetrafluorobenzoic acid; 4,4'-azpy:COOH-I

In the crystal structure of **4,4'-azpy:COOH-I**, the primary recognition event occurs between acid-pyridine (O-H···N hydrogen bonds) and I-pyridine (C-I···N halogen bonds) in parallel. The resulting assembly is an infinite 1-D chain (Fig 5.13).

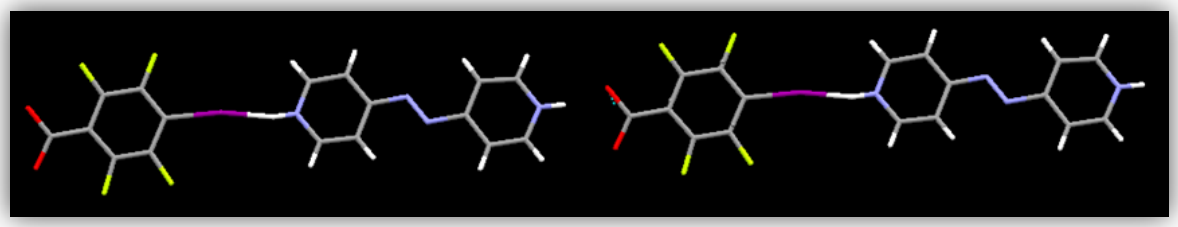

Figure 5.13 1-D infinite chain in 4,4'-azpy:COOH-I **co-crystal formed via O-H…N(py) and C-I…N(py) hydrogen and halogen bond, respectively.**

5.3.1.2.2 4,4'-Azopyridine:4-bromotetrafluorobenzoic acid; 4,4'-azpy:COOH-Br

Similar to the previous structure, **4,4'-azpy:COOH-Br** displays a 1-D chain architecture formed via both hydrogen bond (O-H···N) as well as halogen bonds (C-Br···N), (Fig 5.14).

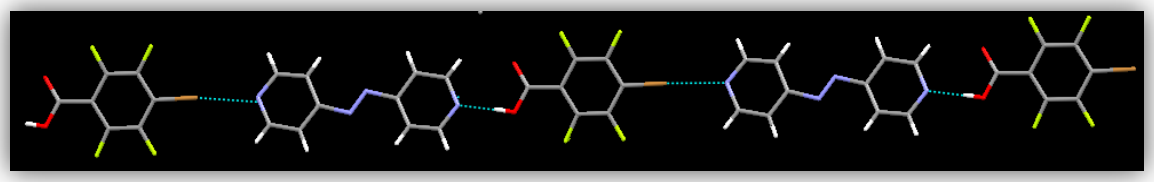

Figure 5.14 4,4’-azpy:COOH-Br **co-crystal showing O-H…N(py) hydrogen bonds and C-Br…N(py) halogen bond interactions**

5.3.1.2.3 4,4’-Azopyridine:4-iodotetrafluorophenol; *4,4’-azpy:OH-I*

The crystal structure of **4,4’-azpy:OH-I** displays a 1-D chain formed from O-H···N hydrogen bonds as well as C-I···N halogen bonds on either sides of the azopyridine (Fig 5.15).

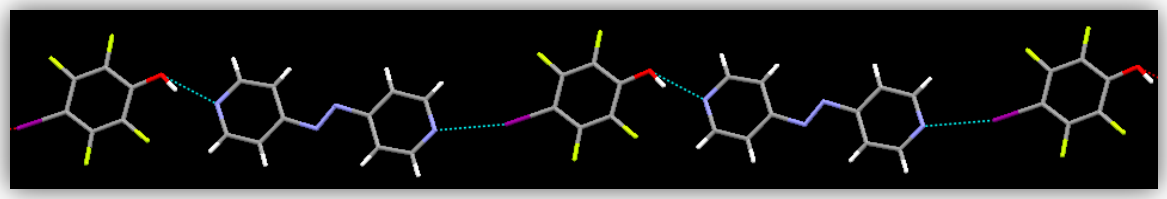

Figure 5.15 4,4’-azpy:OH-I **crystal structure indicating 1-D chains formed via both O-H…N(py) and C-I…N(py) primary interactions**

5.3.1.2.4 4,4’-Azopyridine:4-iodotetrafluorophenol; *4,4’-azpy:OH-Br*

4,4’-azpy:OH-Br co-crystal displays a 1-D chain formed via hydrogen bonds (O-H···N) and halogen bonds (C-Br··· N)(Fig 5.16).

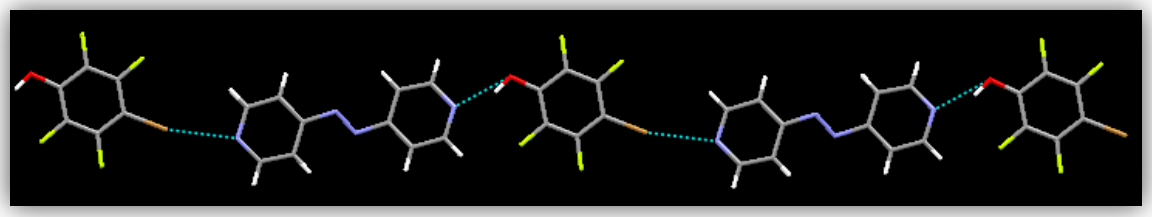

Figure 5.16 4,4’-azpy:OH-Br **co-crystal structure showing 1-D chain formed via both hydrogen (O-H…N(py)) and halogen (C-Br…N(py)) bonds**

5.3.1.2.5 4,4'-Azopyridine:4-iodotetrafluorophenol; 4,4'-azpy:Ox-I

In the crystal structure of **4,4'-azpy:Ox-I**, the primary recognition events occur between oxime-pyridine (O-H···N hydrogen bonds) and I-pyridine (C-I···N halogen bonds) in parallel. The resulting assembly is an infinite 1-D chain (Fig 5.17). No oxime-oxime dimers are observed in this case.

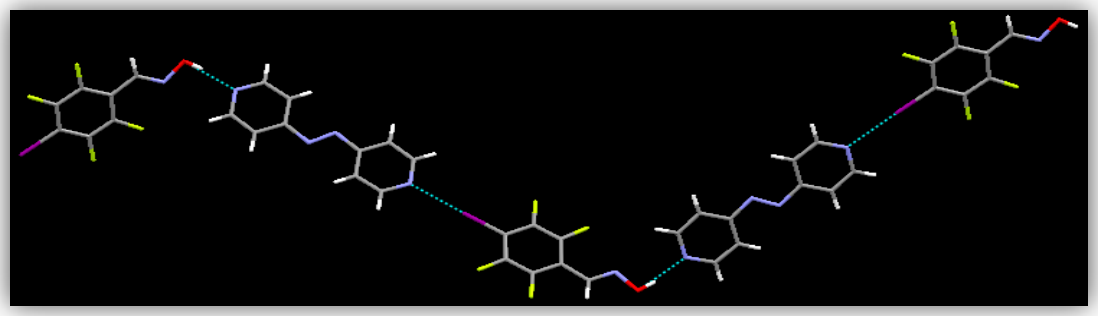

Figure 5.17 4,4'-Azpy:Ox-I **crystal structure with primary C-I…N(py) and O-H…N(py) interactions forming 1-D chain**

5.3.1.2.6 4,4'-Azopyridine:4-iodotetrafluorophenol; 4,4'-azpy:Ox-Br

When iodine is replaced by bromine in **4,4'-azpy:Ox-Br**, the resulting assembly is very different. The primary recognition occurs at the oxime-pyridine interface forming 1-D assembly. Interestingly the free bromine atom interacts with an azo nitrogen atom (despite the presence of other secondary, and better, acceptors like oxygen or nitrogen atoms of the oxime in the system) (Fig 5.18). This interaction runs perpendicular to the 1-D chain resulting in an interlocked 3-D network (Fig 5.19).

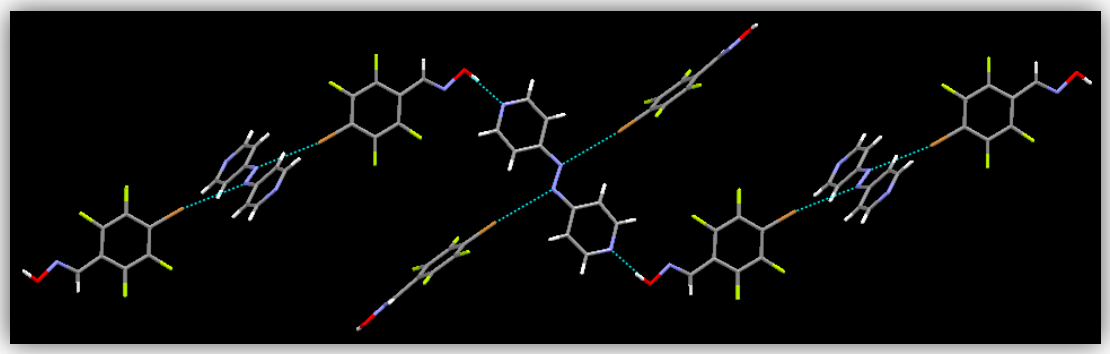

Figure 5.18 4,4'-azpy:Ox-Br **crystal structure with primary O-H…N(py) hydrogen bonds and secondary C-Br…N(azo) interactions**

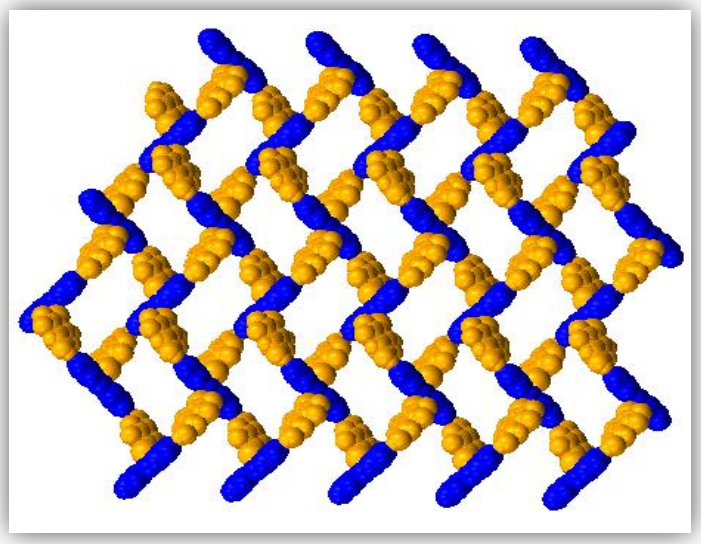

Figure 5.19 3D-architecture in 4,4'azpy:OxBr **co-crystal**

5.4 Discussion

In order to study the structure-directing influence and the competition between hydrogen bond (acid, phenol, oxime) and halogen bond (I, Br) donors with an electrostatically unbiased but geometrically biased system, we set up a total of twelve co-crystallization experiments. We obtained 100% supramolecular yield, each combination produced a co-crystal and analysis of all twelve crystal structures showed that both hydrogen and halogen bond donors actively participated in the assembly process either via primary or secondary interactions. A map of the structural landscape is displayed in Table 5.4 and Fig 5.20.

Table 5.4 Summary of the structural outcome in 3,3'-and 4,4'-azobipyridine co-crystals of bi-functional donors.

	COOH-I (acid-H)	COOH-Br (acid-H)	OH-I (phenol-H)	OH-Br (phenol-H)	Ox-I (oxime-H)	Ox-Br (oxime-H)
3,3'- azpy	OH > I **A**	OH > Br **A**	OH > I **A**	OH > Br **A**	OH_{ox} < I **C**	OH_{ox} > Br **A**
4,4'- azpy	OH = I **B**	OH = Br **B**	OH = I **B**	OH = Br **B**	OH_{ox} = I **B**	OH_{ox} > Br **A**

A: HB>XB, B: HB=XB, C: HB<XB

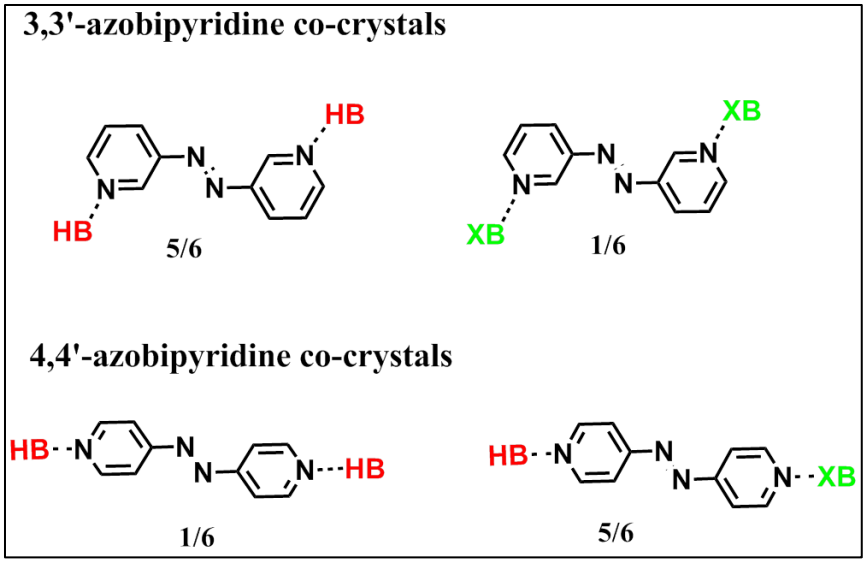

Figure 5.20 Summary of the outcome in 3,3'-and 4,4'-azobipyridine co-crystals

5.4.1 Structural comparison with the CSD

The Cambridge Structural Database (CSD) was used to compare the bond distances, *i.e.* O···N and X···N (X=I, Br) obtained in our crystal structures with those found in the literature. We did a CSD search on O···N and X···N intermolecular bond distances between pyridine type compounds and aromatic hydrogen bond donors and halogen bond donors respectively (Fig 5.21 and 5.22). The comparison of bond distances is listed in Table 5.5.

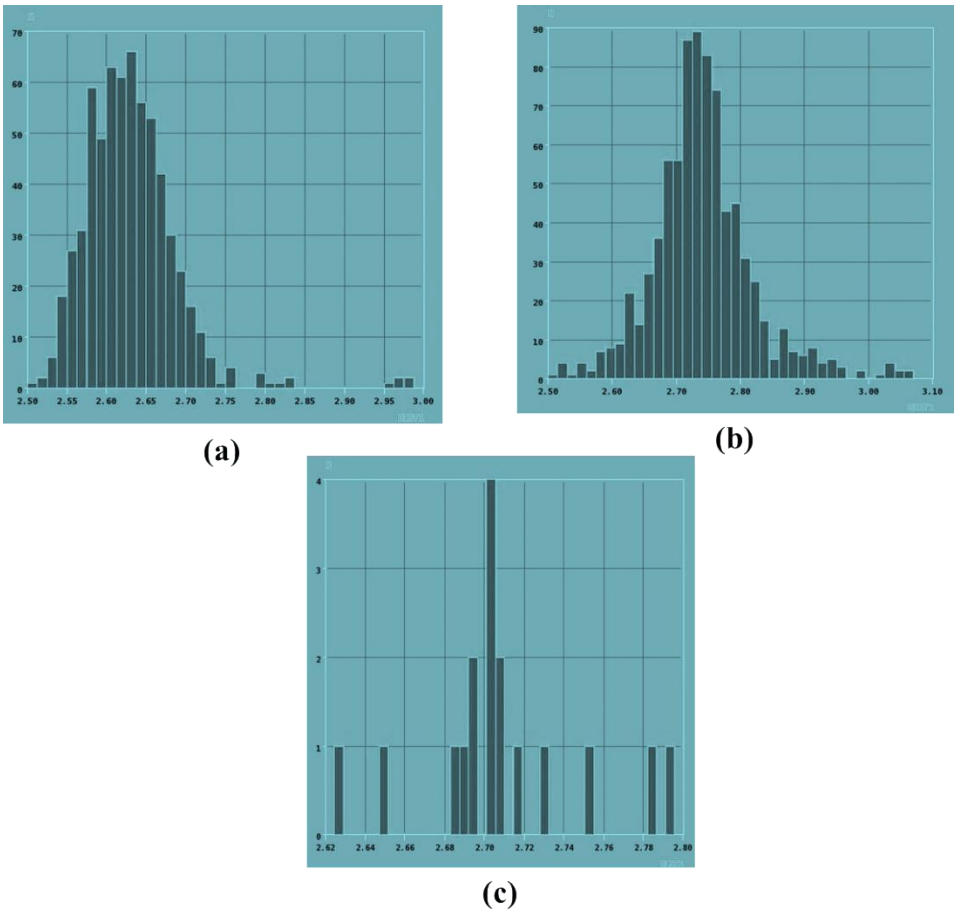

Figure 5.21 Histogram displaying a) acid-pyridine b) phenol-pyridine and c) oxime-pyridine O...N intermolecular bond distances from the CSD

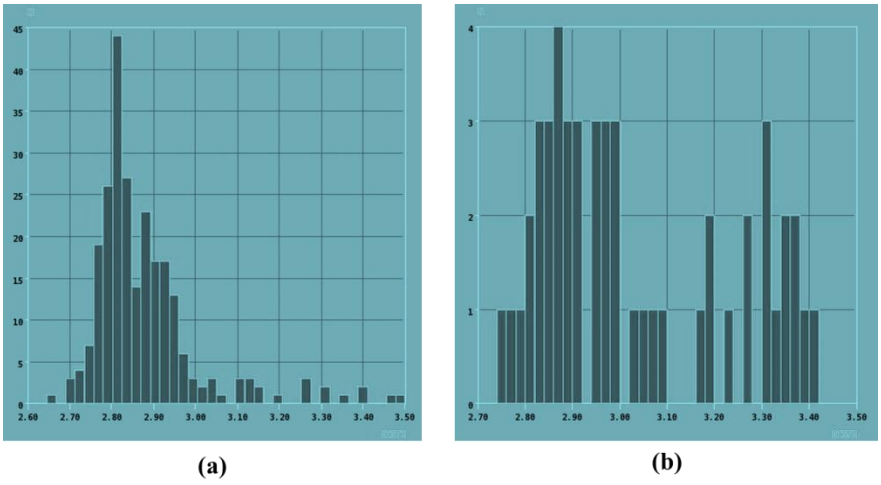

Figure 5.22 Histogram displaying X...N bond distances a) I...N and b) Br...N from the CSD

Table 5.5 Bond distance comparison

Intermolecular bond	Number of hits in CSD	Distance(Å) (CSD)	Distance(Å) (Experimental)
O···N (acid-py)	456	2.63(6)	2.60
O···N (phenol-py)	482	2.74(8)	2.62
O···N (oxime-py)	10	2.70(4)	2.71
I···N	157	2.880 (130)	2.86
Br···N	41	3.031 (20)	2.90

Based on data from the CSD and from our experiments, it is clear that the O···N bond distance in acid-py interaction is much shorter than in phenol-py and oxime-py (Table 5.5). The average O···N bond distance in phenol-py and oxime-py interactions are very similar. However, it may not be possible to make inferences about the 'strengths' of the different interactions and rank them purely based on the D···A bond distances due to other extraneous factors that contribute to the arrangement of molecules in the crystal lattice.

The I···N bond distance is shorter than the Br···N bond distance and is consistent in both the literature as well as our crystal structures (Table 5.5). From the experimental values, the X···N bond distances correspond to a contraction of 18.3% and 10.6% in I···N and Br···N compared to the van der Waals radii of I···N and Br···N, respectively. An increased contraction is indicative of a stronger halogen bond (I···N).[6] Iodine is thus a better halogen bond donor than bromine, which is also in good agreement with the electrostatic argument which shows that iodine with a more positive σ hole is a better donor than bromine. To support this further, iodine engages in a primary halogen bonded interaction with the most basic nitrogen atom in 4/6 cases, while bromine does so only in 2/6 instances. Bromine is involved in secondary interactions with auxiliary acceptors like 'O' or azo 'N' 4/6 times, while iodine interacts only 2/6 times. All these factors suggest that iodine is a more potent donor than bromine.

5.4.2 Structural consistency

5.4.2.1 Co-crystals of 3,3'-azopyridine

The crystal structures of **3,3'-azpy** with six bi-functional donors indicate that in 5/6 structures the primary interaction occurs between a hydrogen bond donor and pyridine nitrogen (Table 5.4 and Fig 5.20). The halogen atoms acts as XB donors and serve to link primary motifs into two dimensions via secondary interactions with other potential acceptors. The resulting architecture is 2-D planar sheets. In all five cases hydrogen bond "wins" over the halogen bond,

i.e. HB > XB. The only outlier is **3,3'-azpy:Ox-I**, where the iodine atom "wins" over the oxime hydrogen, *i.e.* XB > HB.

5.4.2.2 Co-crystals of 4,4'-azopyridine

In **4,4'-azpy** co-crystals, very different structural assemblies are observed. Both types of donors equally contribute in the structure directing assembly process forming 1-D chains (5/6) (HB = XB) (Table 5.4 and Figure 5.20). The only outlier in this series is **4,4'-azpy:Ox-Br**, where hydrogen atom wins over bromine, while bromine interacts with azo nitrogen atoms (1/6) (HB > XB).

In all the co-crystal combinations there were several potential donors (acid, phenol, oxime, iodine and bromine) and acceptors ('N'$_{py}$, 'N'$_{azo}$, 'O'$_{carbonyl}$ and 'O'$_{hydroxyl}$). In such a complex system, it was perfectly reasonable to expect some degree of structural 'chaos'. However, we note a high degree of structural fidelity in the binding pattern within two classes of acceptors (Table 5.4 and Figure 5.20).

5.4.3 Plausible explanations for the observed trend

There is a clear binding preference observed in the two classes of azopyridine with the same donor probe. In **3,3'-azpy** co-crystals, hydrogen bonding dominates over halogen bonding, whereas in **4,4'-azpy** both interactions occur concomitantly. This binding preference cannot be explained purely based on an electrostatic argument of the acceptors, since the charges on the pyridine nitrogen in the two acceptors differ only by a couple of kJ mol^{-1} (Ch 4, Fig 4.4). This difference is not significant enough to have an influence on the binding preference between the two types of donor atoms. In order to seek an explanation for the observed binding pattern, we have explored the electrostatic potentials on donor molecules as well as examined the packing co-efficient values and melting point trends in the two classes of azopyridine co-crystals.

5.4.3.1 Electrostatic surface potential calculations of donor probes

Geometry optimizations were carried out followed by molecular electrostatic potential surface (MEPS) calculations on the six bi-functional donors using Spartan, 2010 (Wavefunction, Inc. Irvine, CA). Both semi-empirical and DFT (B3LYP, 6-31G++G** basis set) methods were used (Table 5.6).

Table 5.6 Electrostatic surface potentials expressed as charges in kJ mol^{-1}

	COOH-I		COOH-Br		OH-I		OH-Br		Ox-I		Ox-Br	
	H	I	H	Br	H	I	H	Br	H	I	H	Br
PM3	144	222	144	160	156	202	163	152	134	204	135	147
DFT	296	166	305	142	305	155	314	121	283	153	276	129

Although the numbers obtained for the surface potentials using PM3 and DFT methods were different, the trend observed was the same, *i.e.* the positive potentials on the donors decreased in the following order; phenol-H > acid-H > ox-H. This trend is also consistent with the previously reported hydrogen-bond parameters for common functional groups.[16] Another inference that can be made based on the surface calculations is that iodine has a more positive σ potential than bromine, which makes it a better halogen bond donor. The MEPS however fail to provide an additional insight into why hydrogen bonds are formed primarily in **3,3'-azpy** co-crystals while hydrogen and halogen bonds are preferred in **4,4'-azpy** class of co-crystals.

5.4.3.2 Packing co-efficients and melting points of co-crystals

The packing co-efficient values and melting points of co-crystals are listed in Tables 5.7 and 5.8 respectively. Packing co-efficients were calculated using Olex2 v1.2 software.

Table 5.7 Packing co-efficient and melting points in 3,3'-azpy **co-crystals**

	COOH-I	COOH-Br	OH-I	OH-Br	Ox-I	Ox-Br
Packing co-efficient %	74	69	68	71	69	69
Melting points °C	182-183	155-157	125-127	170-173	145-148	105-108

Table 5.8 Packing co-efficient and melting points in 4,4'-azpy **co-crystals**

	COOH-I	COOH-Br	OH-I	OH-Br	Ox-I	Ox-Br
Packing co-efficient %	74	76	67	69	66	67
Melting points °C	220-222	190-191	163-165	133-136	115-116	125-126

The packing co-efficient values in all 12 co-crystals range from 66-74%. The values across the two classes with the same donors are very similar. There is no observable deviation in the packing co-efficient values of the outliers in each series when compared to the other five co-

crystals in the same series. Thus packing co-efficient values are ineffective in providing a plausible reason for the observed structural behavior.

Along similar lines, melting points of the co-crystals also show no trend within each series. The melting points of the outliers (**3,3'-azpy:Ox-I and 4,4'-azpy:Ox-Br**) do not display noticeable difference from the other co-crystal in each series. Thus melting points do not provide an insight into the observed binding preference within each class of co-crystals.

5.4.3.3 Geometric bias on the acceptor molecule

An investigation of the electrostatic potentials, packing co-efficients and melting point trends did not provide any plausible explanation for the observed structural behavior in the two classes of co-crystals. We therefore propose to rationalize the observed 'synthon crossover' event based on the differences in the binding site orientation of the two acceptor molecules (Fig 5.4).

In 3,3'-azopyridine the binding sites have an anti-parallel orientation with respect to each other (Fig 5.4). The six donor molecules under consideration also have their two donor sites at a 1-4 position, *i.e.* linear (Fig 5.4). Considering the geometric non-complementarity between the two interacting species, it is conceivable that for 1-D chain formation, molecules need to be forcefully brought into close proximity at suitable angles. This would increase the energy of the system thus compromising on its stability. On the other hand, the molecules complement themselves well enough to form discrete trimer which is less challenging and easy on the system. The trimers can then be connected into 2-D sheets via secondary interactions. Under such conditions, a hydrogen atom (which is considered to be slightly more competitive than a halogen atom as a donor) binds to the best acceptor forming stable trimers. The halogen atoms are then used to connect individual trimers via interactions with secondary acceptors into extended architectures.

4,4'-azopyridine has the binding sites oriented linear with respect to each other (Fig 5.4). The geometries of the acceptors and donors complement each other very well to favor easy formation of linear 1-D chains without any energy expense. Under such conditions, there is a 50:50 chance that the pyridine nitrogen will pick up both, hydrogen as well as halogen atom on either side to form 1-D chains which is what we observe in five out of six co-crystals.

5.5 Conclusion

We have synthesized twelve co-crystals of 3,3'-and 4,4'-azopyridine with six bi-functional donors each and demonstrated the following;

1) Structural consistency is obtained in the crystal structures within each class, *i.e.* in **3,3'-azpy** co-crystals trimers are formed by hydrogen bonds followed by their extension into 2-D sheets via secondary halogen bond interactions (5/6 HB > XB) and in **4,4'-azpy** co-crystals 1-D chains are formed via both hydrogen as well as halogen bonds (5/6 HB = XB).
2) Both halogen bond and hydrogen bond donors participate in primary interactions and the choice of the acceptor for either of them is governed by the geometric bias on acceptor sites.
3) Auxillary acceptors such as carbonyl 'O', hydroxyl 'O' and azo 'N' all participate in secondary interactions in extending the lattice.

Since hydrogen and halogen bond donors are comparable and competitive in a given system, a larger number of data needs to be generated and analyzed in order to establish a reliable ranking between the two. A deeper investigation of similar experiments carried out using 3,3'-and 4,4'-stilbene derivatives (analogous to 3,3'-and 4,4'- azopyridines) along with the six bifunctional donors will provide us with a larger dataset and further evidences to support our findings. Since the stilbenes are analogous to azobenzenes, we expect similar structural outcomes in the two classes of co-crystals as observed in the case of 3,3'-and 4,4'-azopyridines.

---

1 Jeffrey, G.A. An Introduction to Hydrogen Bonding, Oxford University Press, Oxford, 1997; Aakeröy, C.B.; Seddon, K.R. *J. Chem. Soc. Rev*. **1993**, 22, 397

2 Singh, D.; Baruah, J. B., *Cryst.Growth Des.*, **2012,** 12, 3169; Karunatilaka, C.; Bucar, D.K.; Ditzler, L.R.; Friscic, T.; Swenson, D.C., *Angew.Chem.,Int.Ed.* **2011**, 50, 8642 ;Friščić, T.; MacGillivray, L. R., *Chem. Commun*., **2009**, 773-775; Oswald, I. D. H.; Motherwell, W. D. S.; Parsons, S., *Acta Cryst*., **2004**, 60, 1967-1969; Mukherjee, A.; Desiraju, G. R., *Chem. Commun.,* **2011**, 47, 4090-4092

3 Aakeröy, C. B.; Salmon, D.J.; Smith, M. M.; Desper, J., *Cryst. Growth Des*. **2006**, 4, 1033-1042; Aakeröy, C. B.; Salmon, D.J.; Smith, M. M.; Desper, J., *CrystEngComm.* **2009**, 11, 439–443: Aakeröy, C.B.; Fasulo, M.; Schultheiss, N.; Desper, J.; Moore, C., *J.Am.Chem.Soc.* **2007**, 129, 13772

4 Meyer. F and Dubois, P., *CrystEngComm,* **2013**, Advance Article; Metrangolo, P.; Pillati, T.; Resnati, G., *CrystEngComm,* **2006**, 8, 946-947; Raatikainen, K and Rissanen, K *CrystEngComm,* **2011**, 13, 6972–6977; Brammer L.; Espallargas, G. M.; and Libri, S., *CrystEngComm,* **2008**,10, 1712-1727; Wilcken. R.; Zimmermann, M.; Lange, A.; Joerger. A. C. and Boeckler, F. M., *J. Med. Chem*., **2013**, 56, 1363–1388

5 Legon, A. C.; *Phys.Chem.*, **2010,** 12, 7736–774

6 Metrangolo, P.; Meyer, F.; Pilati, T.; Resnati, G.; Terraneo, G., *Angew. Chem. Int. Ed*., **2008**, 47, 6114

7 Metrangolo, P.; Neukirch, H.; Pilati, T.; Resnati, G., *Acc. Chem. Res.* **2005**, 38, 386-395

8 Coradi, E.;Meille, S.V.; Messina, M.T.; Metrangolo, P.; Resnati, G. *Angew. Chem.* **2000**, 112, 1852; Legon, A.C. *Chem. Eur. J.* **1998**, 4, 1890

9 Steed, J. W.; Atwood, J. L., *Supramolecular Chemistry,* 2nd Ed. John Wiley & Sons, Ltd. **2009**

10 Mohamed, S.; Tocher, D. A.; Vickers, M.; Karamertzanis, P. G.; Price, S. L., *Crystal Growth & Design,* 9, **2009**

11 Cinčić , D.; Friščić, T. and Jones, W. *New J. Chem.,* **2008,** 32, 1776-1781

12 Bouchmella, K.; Boury, B.; Dutremez, S. G. van der Lee, A., *Chem-Eur J.,* **2007**, 13, 6130-6138; Perkins,C.; Libri, S.; Adams, H.; Brammer, L., *CrystEngComm* , **2012**, 14, 3033

13 The surface potential energies were calculated using Spartan, 2010 (Wavefunction, Inc. Irvine, CA), semiempirical PM3 method of calculation

14 Etter, M. C., *Acc. Chem. Res.,* **1990**, 23, 120; M. C. Etter, *J. Phys. Chem*., **1991**, 95, 4601; Aakeröy, C. B.; Beatty, A. M.; Helfrich, B. A.; Nieuwenhuyzen, M. *Cryst. Growth Des.* **2003**, 3, 159; Aakeröy, C. B.; Desper, J.; Helfrich, B. A. *CrystEngComm*. **2004**, 6, 19; Bowers, J. R.; Hopkins, G. W.; Yap, G. P. A.; Wheeler, K. A. *Cryst.Growth Des.,* **2005**, 5, 727

15 Aakeröy, C. B.; Panikkattu, S.; Chopade, P. and Desper, J., *CrystEngComm,* **2013,** 15, 3125-3136

16 Abraham, M. H.; Platts, J.A., *J. Org. Chem.,* **2001**, 66, 3484-3491

Chapter-6 Using co-crystallization to alter physical properties of agrochemical pesticides

6.1 Introduction

As the demand for food globally increases with increasing population, the resources needed for meeting the increasing food demand remain limited. Agrochemicals provide a means of increasing the productivity of farming by producing a wide range of chemicals which protect the crops from damage by pests and weeds, thus resulting in better produce.[1] A recent poll about a farmer's perception of pesticides clearly indicates that pesticides play an important role in crop production as they provide us with good quality products in higher yields by killing and controlling the pests that infest the crops (Fig 6.1).[2]

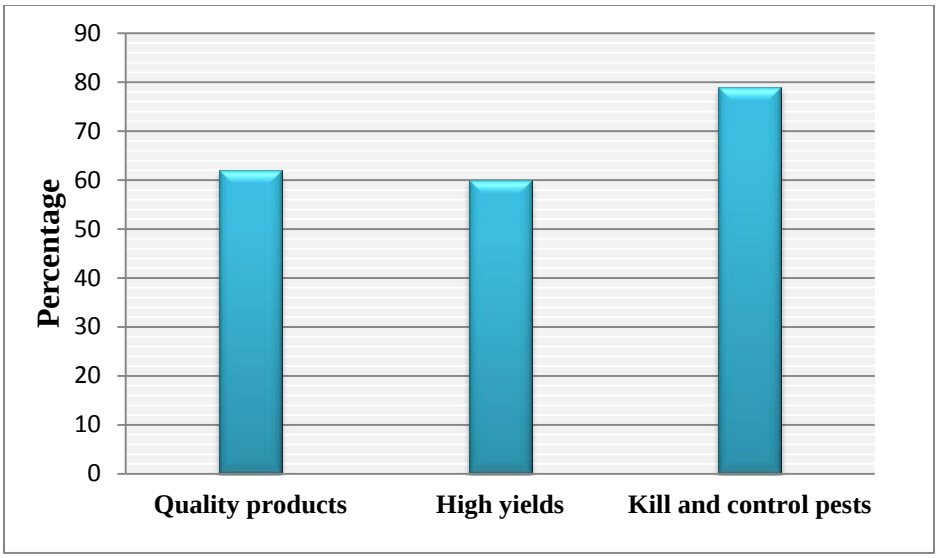

Figure 6.1 Result of a recent poll about farmer's perception of pesticides[2]

Agrochemicals are typically applied to the crops in the form of a solid (dusts, powders or granules) or a liquid (suspension) formulation.[3] For the purpose of effective solid formulation, it is important that certain physical characteristic such as high melting point and crystallinity of the sample is maintained. However, most of the agrochemical actives are amorphous and also have low melting points, resulting in inefficient processing, formulation and application of the active.[4] Likewise, in a liquid formulation, a problem could arise from Ostwald ripening (tendency of crystalline materials to form large crystals due to ageing).[5] In addition, polymorphic

transformation of the active is another area of concern due their potential to switch between different forms under ambient storage conditions resulting in complications during storage, application and formulation.[6] All these issues related with agrochemical actives (Fig 6.2) suggest the need for modification of the physico-chemical properties of the actives that influence the morphology and behavior of the actives, resulting in better end use properties.

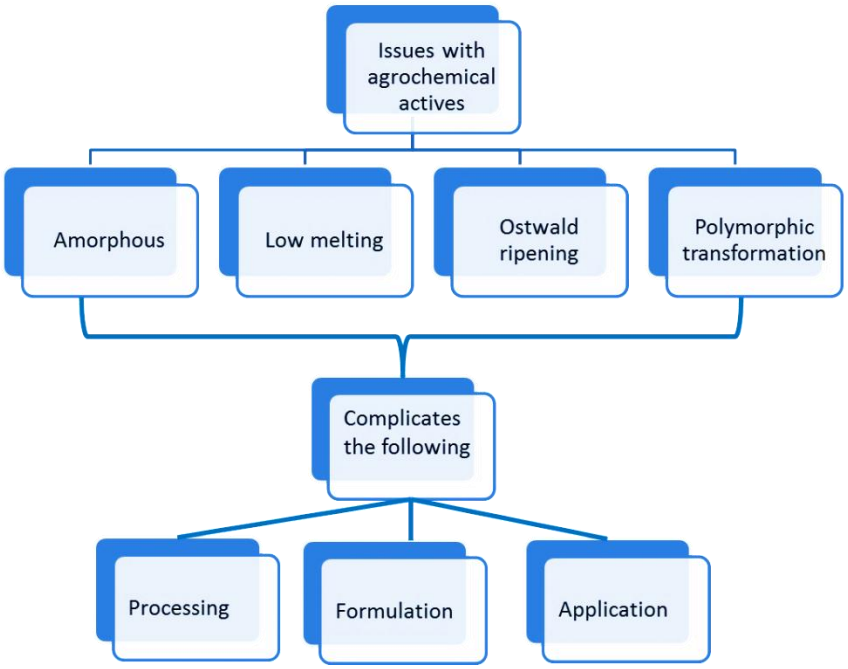

Figure 6.2 Problems with agrochemical actives[3,4,5,6]

Co-crystallization can be used as a reliable technique to form alternative solid forms of agrochemical actives which display,[6]

i) Improved melting points
ii) Increased solubility
iii) Decreased solubility
iv) Improved storage and formulation stability
v) Modified crystal morphology and so on.

In order to demonstrate the effectiveness of co-crystals in generating new crystalline solid forms of the actives with improved physical properties, we have synthesized co-crystals of two

agrochemical pesticides, namely, cyprodinil and terbuthylazine with co-formers such as succinic, adipic, suberic, sebacic and dodecandioic acid (Fig 6.3). Since the actives have amino-pyridine based binding sites, stable supramolecular synthons via hydrogen bonds can be formed with the diacids (as seen previously in section 2.3.1). For the purpose of structural characterization, single crystal structures of all co-crystal combinations were analyzed. Furthermore, changes in solubility, melting point behavior and hygroscopicity as a result of co-crystallization will also be explored for cyprodinil co-crystals.

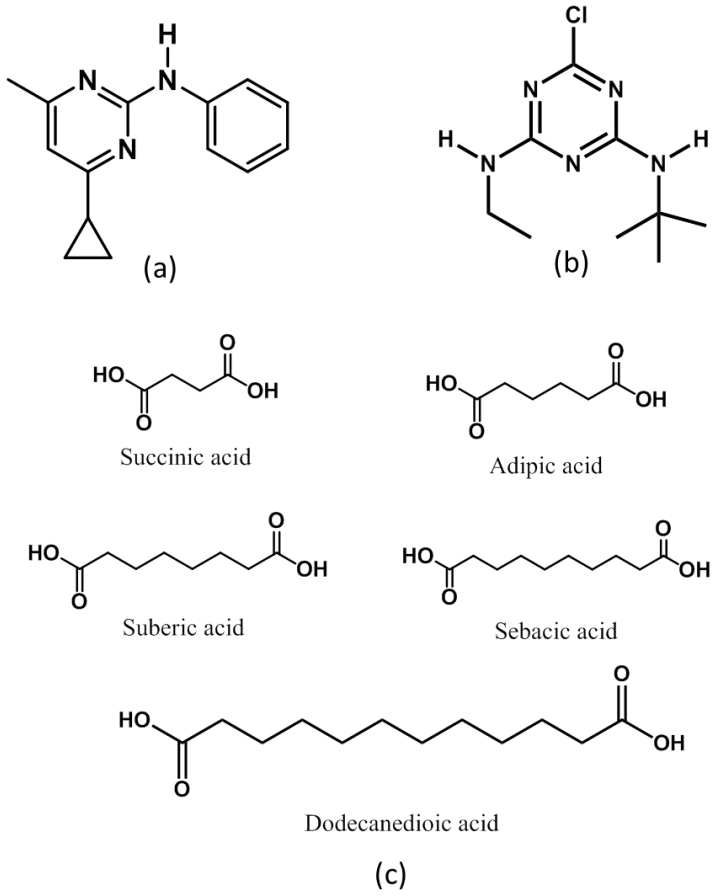

Figure 6.3 a) cyprodinil b) terbuthylazine and c) series of even-chain diacids

The goals of our study are to:

1) Explore the potential of cyprodinil and terbuthylazine in forming co-crystals with diacids.
2) Test the potential of co-crystallization in tuning the solubility and melting point of the agrochemicals.

3) Test the hygroscopicity of the co-crystals and compare them with the parent active.

6.2 Experimental

Cyprodinil and terbuthylazine were acquired from Syngenta and used without further purification. The dicarboxylic acids were purchased from Sigma Aldrich and used without further purification. Melting points were recorded on a Fisher- Johns melting point apparatus and were corrected for using a calibration curve (Fig 6.16). Infrared spectroscopy (IR) was performed on a Nicolet 380 FT-IR. Humidity measurements were carried out in a sealed vessel that was saturated with appropriate salt solutions.

6.2.1 Synthesis of co-crystals

The acid and the active were dissolved in a 1:1 ratio in methanol and the co-crystals were synthesized using slow evaporation method. Good quality crystals were obtained within few days for all combinations with an exception of **Ter:AA** and were submitted for single crystal analysis. The melting points of the co-crystals obtained by solvothermal synthesis are listed in Table 6.1.

Table 6.1 List of co-crystals of Cyprodinil and Terbuthylazine

Actives	Acids (co-formers)	Abbreviation	Melting point (°C)
Cyprodinil	Succinic acid	Cyp:SA	128
	Adipic acid	Cyp:AA	120
	Suberic acid	Cyp:SuA	110
	Sebacic acid	Cyp:SeA	101
	Dodecandioic acid	Cyp:DDDA	119
Terbuthylazine	Succinic acid	Ter:SA	184
	Adipic acid	Ter:AA	143
	Suberic acid	Ter:SuA	153
	Sebacic acid	Ter:SeA	168
	Dodecandioic acid	Ter:DDDA	165

6.2.2 Preparation of co-crystals for solubility measurements

Co-crystals of cyprodinil with the even chain diacids succinic C4, adipic C6, suberic C8. sebacic acid C10 and dodecanedioic acid C12 were prepared via a solvothermal method.[7] Cyprodinil and the acid were combined in a 1:1 ratio and refluxed in 25ml of methanol. After 40 min of heating, the resulting solution was cooled to 5° C. The precipitated solid was filtered, dried and analyzed using IR spectroscopy to confirm co-crystal formation. The PXRD pattern of bulk co-crystal and simulated single crystal pattern was compared to further confirm the homogeneity of the bulk sample, an example of which is shown in Figure 6.4 and the others in appendix B1-B4.

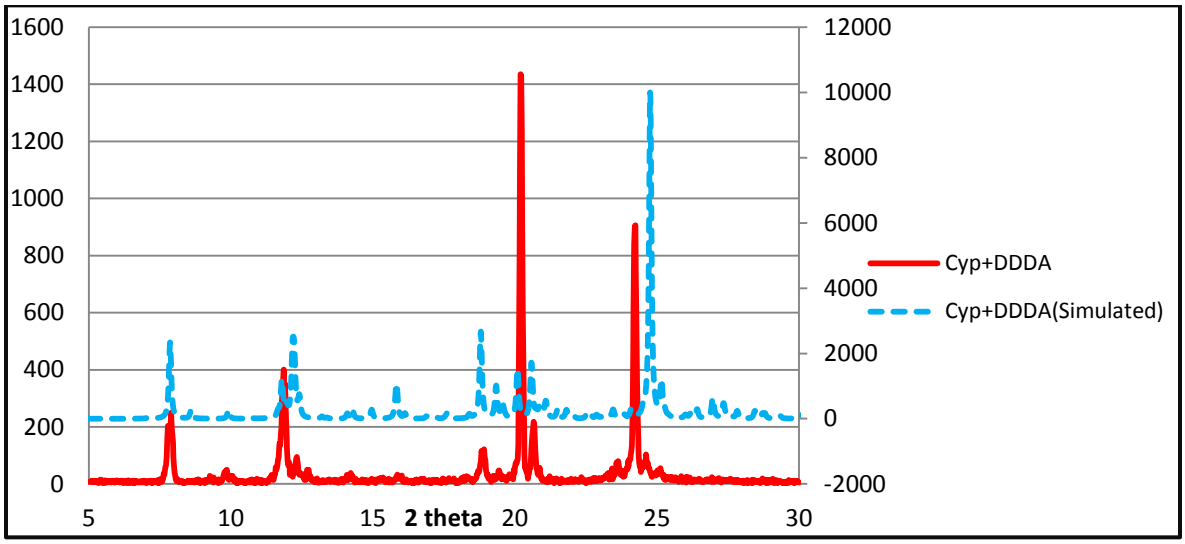

Figure 6.4 PXRD pattern of Cyp+DDDA **bulk (solid red) and simulated pattern (dotted blue)**

6.2.3 Solubility measurements on cyprodinil co-crystals

In order to determine the equilibrium solubility of cyprodinil, first a stock solution of cyprodinil was prepared in distilled water (0.0015g in 100ml) and a calibration curve was constructed by measuring the absorbance of a series of dilutions of known concentrations, made from the stock solution, Fig 6.5. The equation of line obtained from the calibration curve (y = mx) was then used to determine the solution concentrations of the saturated samples at 24, 48 and 72 hour time intervals. The system reached equilibrium within 48hrs (Fig 6.6).

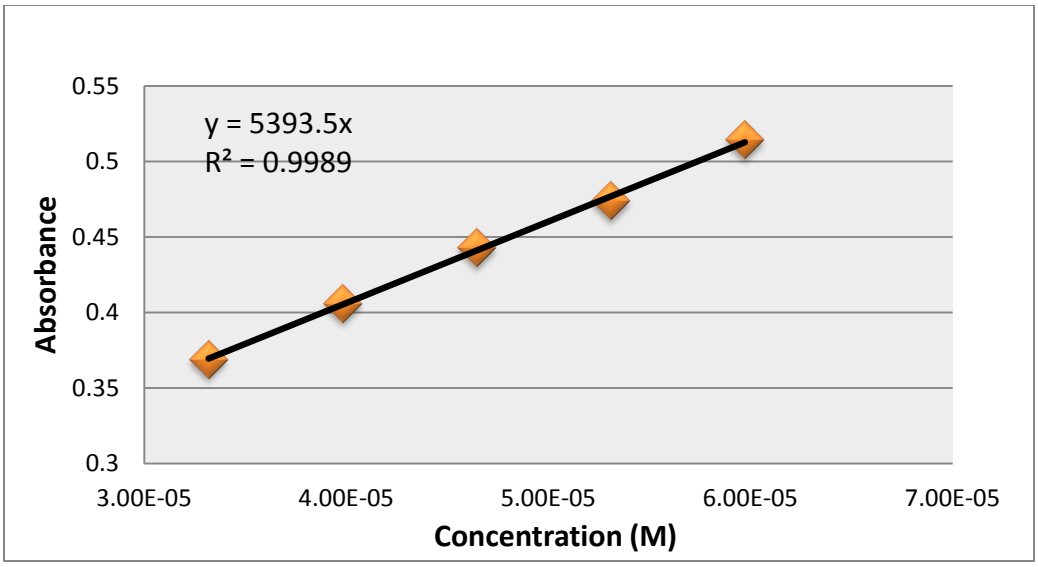

Figure 6.5 Calibration curve for solubility of cyprodinil

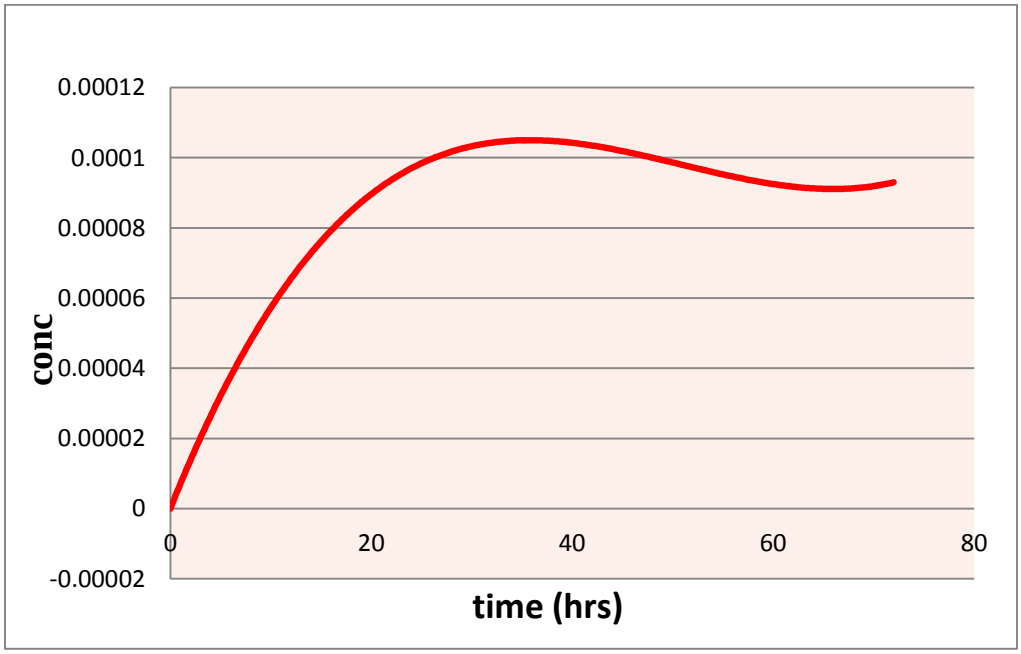

Figure 6.6 Cyprodinil system equilibrium curve

In order to determine the solubility of cyprodinil co-crystals, a suspension of the co-crystal (0.100g) was stirred in 10ml of distilled water in a sealed vial and placed in a water bath to maintain constant temperature. After stirring for 48hrs, the remaining solid was filtered. A 1 ml aliquot of the filtrate was diluted to 10ml using distilled water (dilution factor = 10) and the absorbance of cyprodinil at λ_{max} = 268nm was measured using UV-Vis spectroscopy, Shimadzu

UV-1650-PC. The absorbance (y) values were used to calculate the corresponding concentrations (x) from the equation of line (y=mx) of the calibration curve. The calculated concentration was then multiplied by the dilution factor to get the final concentration and thus the solubility of the active in the co-crystal form.

6.2.4 Hygroscopicity studies on cyprodinil co-crystals

In order to determine the stability of cyprodinil co-crystals in the presence of atmospheric moisture, the co-crystals were subjected to two different humidity conditions, 85% and 43% in a closed chamber. The humidity conditions were generated using saturated salts solutions of potassium chloride (85%) and potassium carbonate (43%) by dissolving 200g of the salt in 90ml of water. The humidity level was tested using a humidity indicator strip. 100mg of co-crystal samples were measured in open glass vials which were placed in a closed chamber. The chambers were filled up to 1/4th its capacity with saturated salt solutions to generate the desired humidity conditions. The water uptake by the samples was measured at different intervals such as 1, 3, 5, 7, 14, 21 and 28 days using the following equation[8],

$$\text{Hygroscopicity} = (Wn - Ws)/(Ws - Wo) \text{ X } 100$$

where Wn : weight of sample + vial (at time t), Ws : weight of sample + vial (t = 0), Wo : weight of empty vial.

X-ray powder diffraction data of the samples were collected at the end of the humidity experiments to get information on the final form.

6.3 Results

There are two known forms of cyprodinil, form A and form B. From the PXRD data, it is clearly evident that the cyprodinil we have used for our experiments is form B (Fig 6.7)[9].

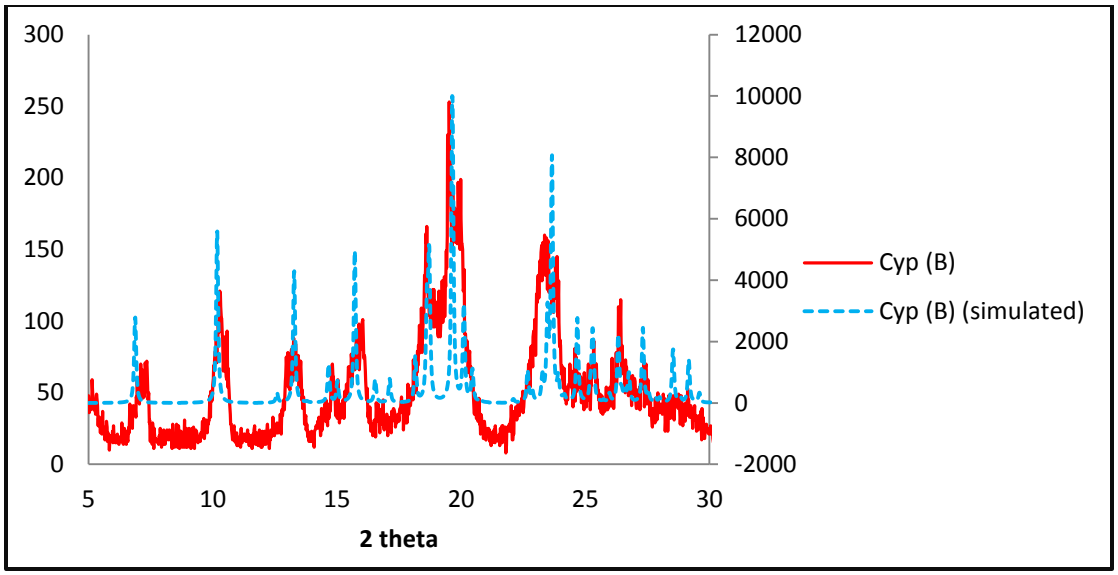

Figure 6.7 PXRD of cyprodinil form B and its simulated pattern

6.3.1 Analysis of the single crystal structures of cyprodinil co-crystals

The crystal structure of cyprodinil displays a dimer formed via hydrogen bond interactions between the amino pyridine sites (Fig 6.8).[9] The second nitrogen atom on the cyprodinil backbone is inactive.

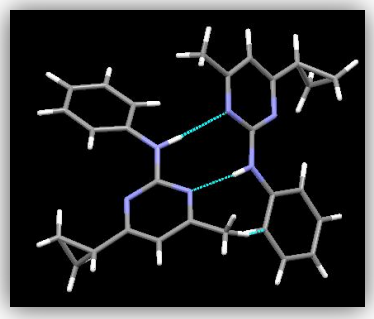

Figure 6.8 Main hydrogen bonds in cyprodinil form B

In the co-crystal of **Cyp:SA, Cyp:AA, Cyp:SuA, Cyp:SeA and Cyp:DDDA** (Fig 6.9), the amino-pyridine dimer interaction between cyprodinil is broken and is replaced by O-H···N hydrogen bonds between the acid and amino-pyridine site resulting in trimers. The second binding site on cyprodinil remains inactive and does not participate in any hydrogen bond. All crystal structures belong to a monoclinic space group, with an exception of **Cyp:SuA** which belongs to triclinic space group.

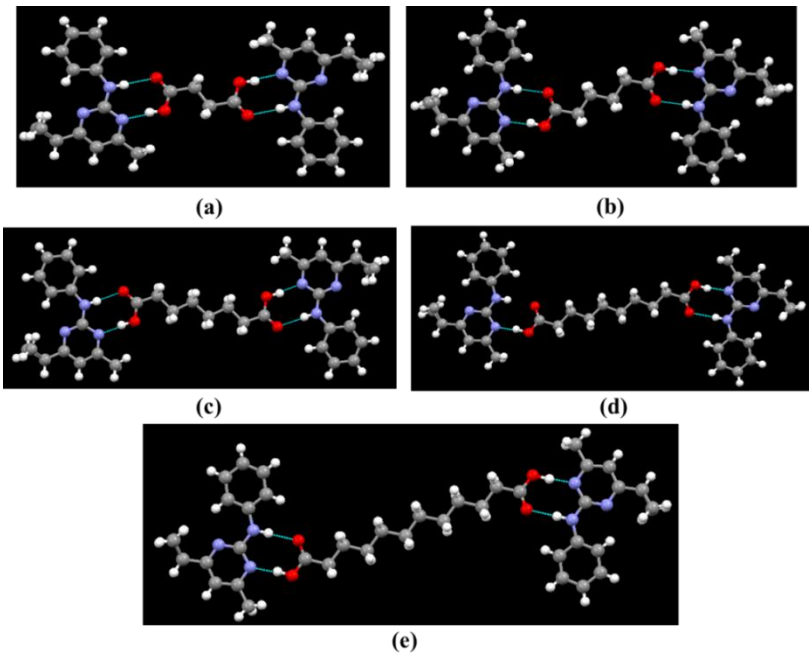

Figure 6.9 Trimers formed in the co-crystals of a) Cyp:SA **b)** Cyp:AA **c)** Cyp:SuA **d)** Cyp:SeA **and e)** Cyp:DDDA **via O-H···N hydrogen bonds between acid and amino-pyridine binding sites**

6.3.2 Analysis of single crystal structures of terbuthylazine co-crystals

The co-crystals of terbuthylazine with succinic, suberic, sebacic and dodecandioic acid display infinite 1-D chains form via two types of interactions, *i.e.* a heteromeric hydrogen bonds between the acid (COOH) and amino-pyridine (N-NH) group and a homomeric interaction between the amino-pyridine groups of two terbuthylazine moieties (Fig 6.10).

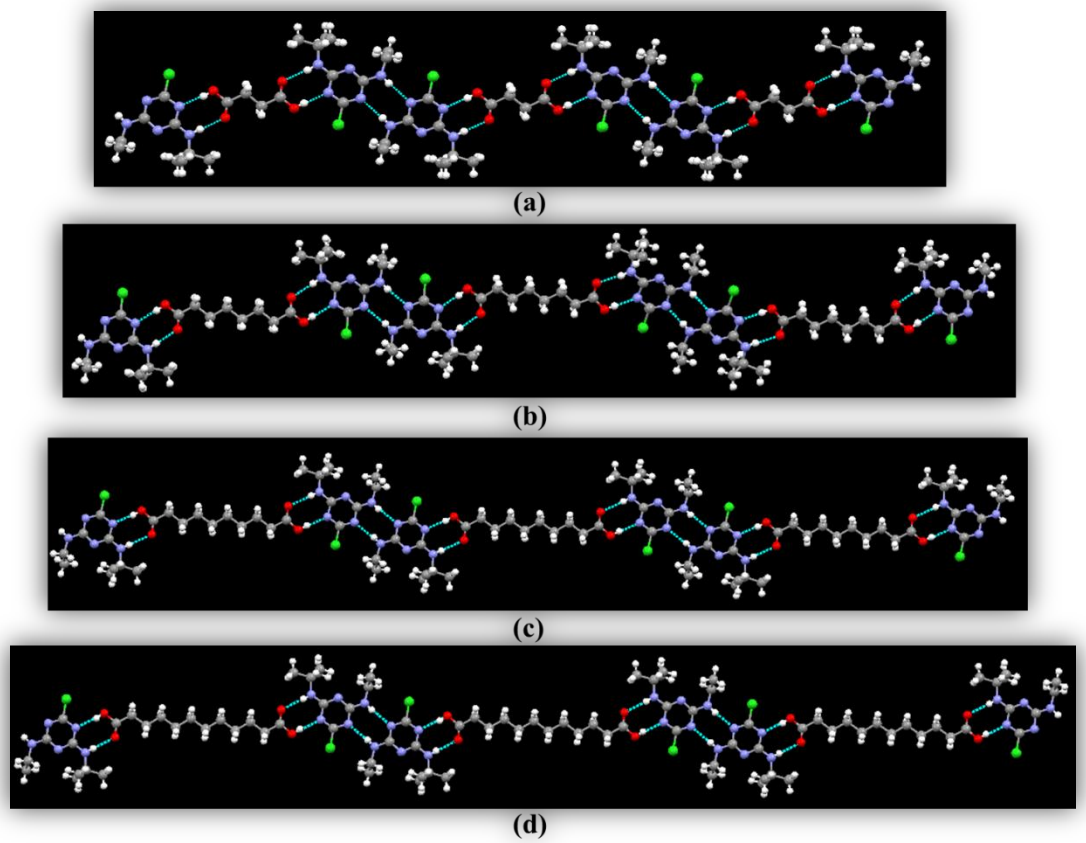

Figure 6.10 1-D chains formed in co-crystals of terbuthylazine with a) succinic acid, b) suberic acid, c) sebacic acid and d) dodecanedioic acid

6.3.3 Tailoring aqueous solubility of cyprodinil

Based on our results, the solubility of cyprodinil is 0.0647(13) g/L. The solubilities of the co-crystals were found to be different from the parent compound, Figure 6.11. In the co-crystal of cyprodinil with succinic acid (C4), a 3.3 fold increase in the solubility is observed. As we move from C4 to longer chain diacids, the solubility decreases along the direction of increasing carbon chain length. The co-crystal of cyprodinil with the longest chain diacid, *i.e.* dodecandioic acid (C12), shows a 0.47 fold decrease in solubility compared to the parent active itself.

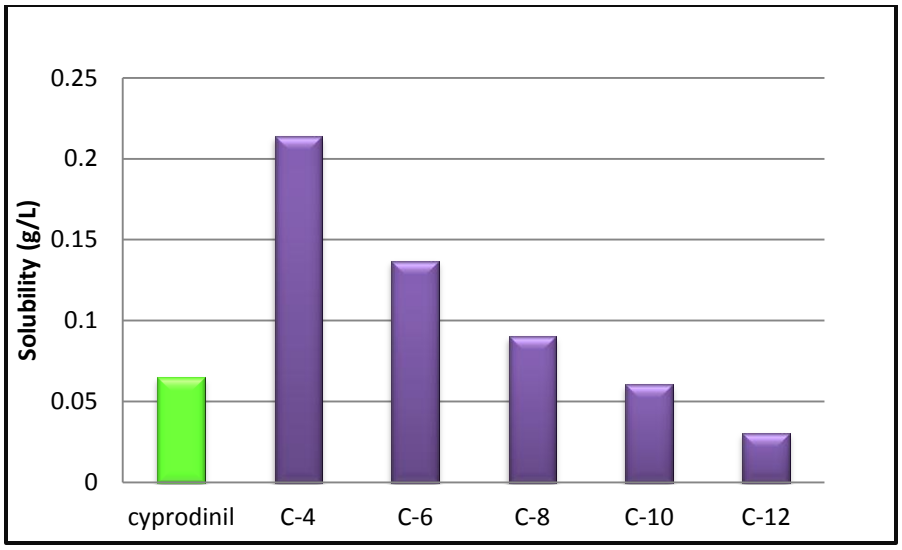

Figure 6.11 Solubility profile of cyprodinil co-crystals

6.3.4 Hygroscopicity studies

In the humidity experiments of cyprodinil co-crystals, there was no significant uptake of water at either 85% or 43% relative humidity conditions, indicating that the co-crystals are relatively stable to humidity stress over a period of 1 month (Fig 6.12 and 6.13). A minimal uptake (< 1.5 % water) at 85% humidity (Fig 6.12) and < 2.5 % water at 43% humidity (Fig 6.13) is observed. The observed differences can be attributed to the physisorption of water on the surface of the solid-samples.

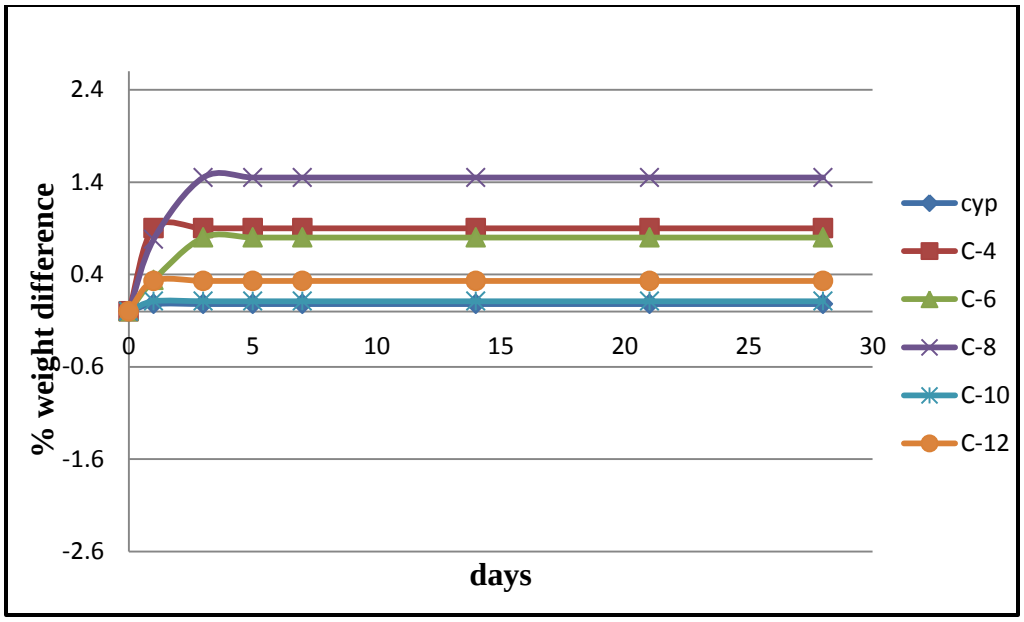

Figure 6.12 Water uptake measured as a function of days in cyprodinil and its co-crystals at 85% relative humidity

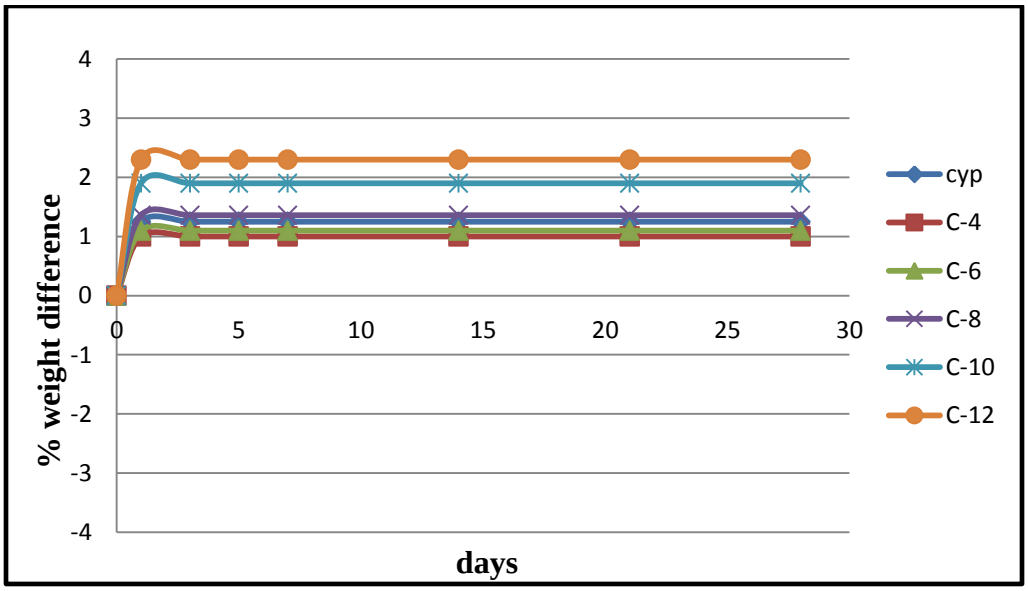

Figure 6.13 Water uptake measured as a function of days in cyprodinil and its co-crystals at 43% relative humidity

PXRD measurements of all co-crystal samples before and after the completion of hygroscopicity studies indicate no change in form of the solid-sample (Fig 6.14-6.15 and appendix B5, B6, B7). This indicates that the co-crystals remain stable under normal processing and storage conditions, which is of significance during a pesticide development process.

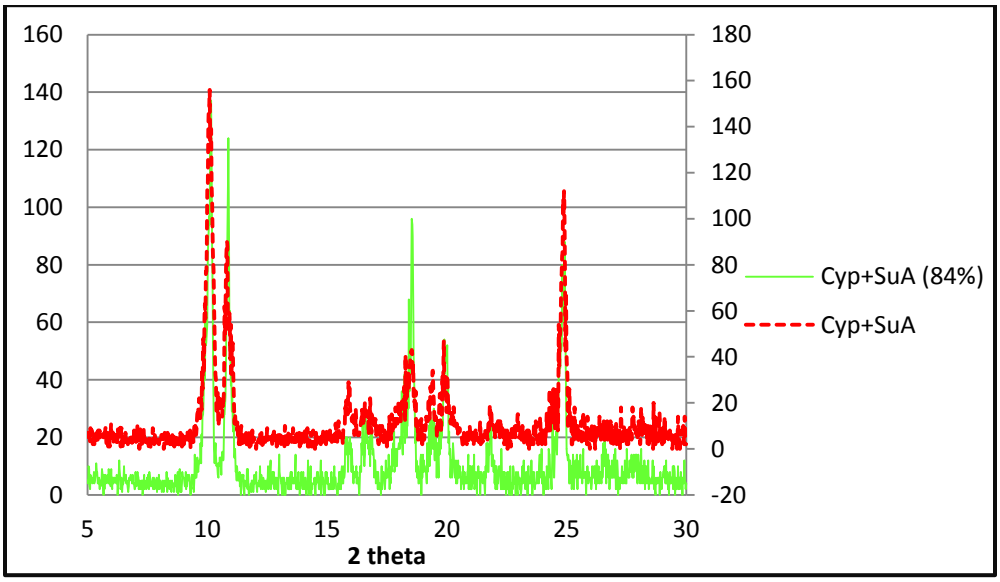

Figure 6.14 PXRD pattern of Cyp:SuA **(red dotted) before hygroscopicity measurements and** Cyp:SuA **84% (green) after 1month of hygroscopicity measurement**

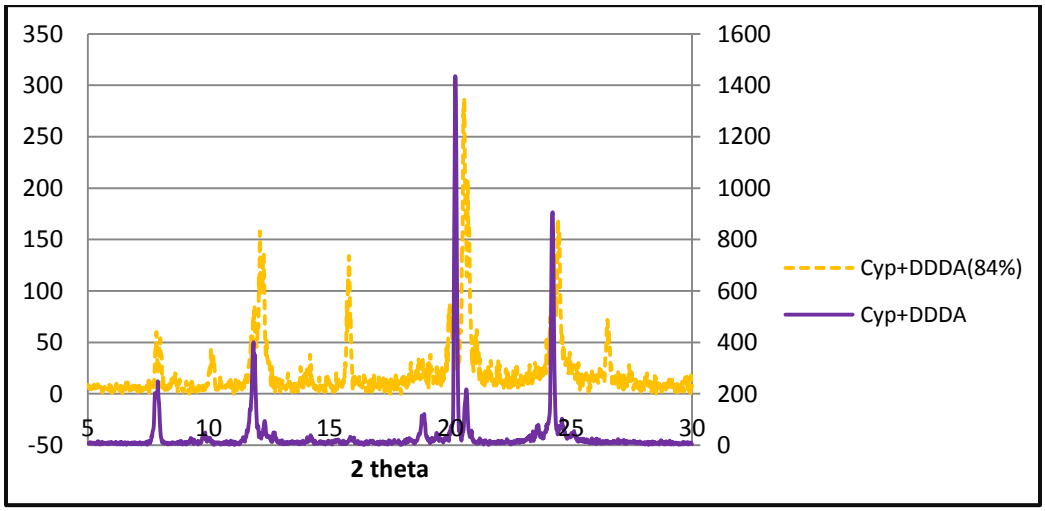

Figure 6.15 PXRD pattern of Cyp:DDDA **(purple solid) before hygroscopicity measurements and** Cyp:SA **84% (orange dotted) after 1month of hygroscopicity measurement**

6.3.5 Melting point variations in cyprodinil and terbuthylazine co-crystals

Melting point is an important physical property for effective handling, processing, formulation and storage of pesticides. From this point of view a higher thermal stability for

compounds is mostly desirable. In order to record the melting points of co-crystals a calibration curve (expected vs. recorded melting points) was constructed for few standard samples whose melting points were accurately known (Fig 6.16).

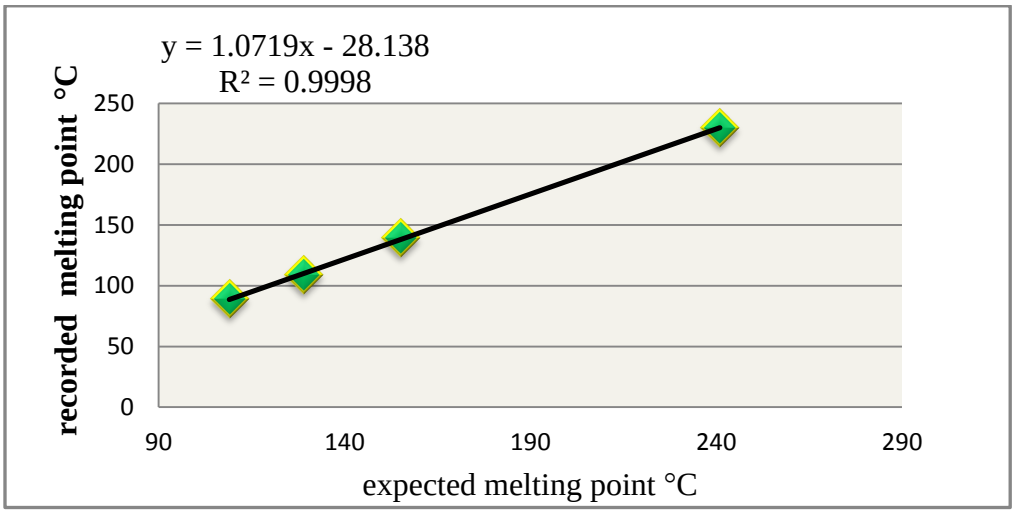

Figure 6.16 Calibration curve for melting point

The calibration curve equation was then used to calculate the expected melting points of co-crystals from their corresponding recorded melting points. It was observed that while cyprodinil had a melting point of 76 °C, the co-crystals of cyprodinil showed an increase in the melting point, Fig 6.17.

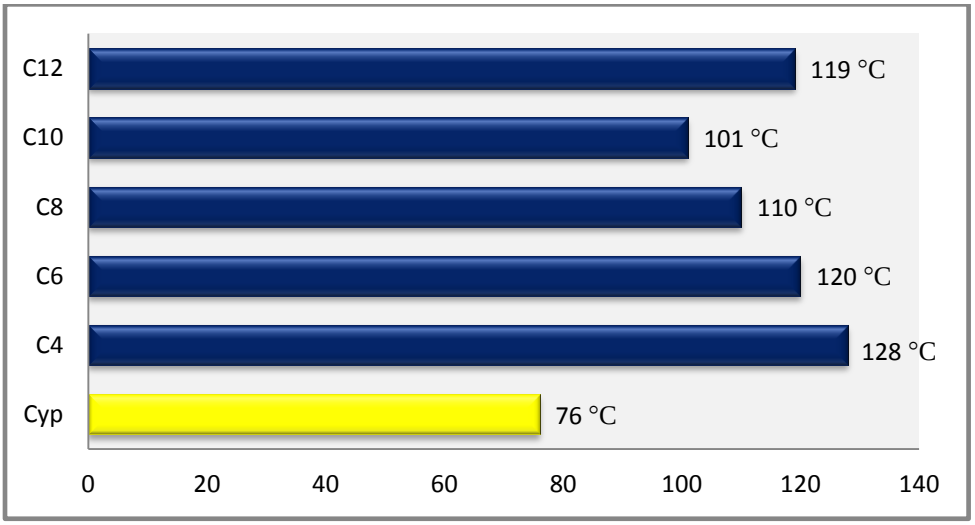

Figure 6.17 Melting point profile of cyprodinil and its co-crystals

Likewise, the melting points of terbuthylazine co-crystals were also calculated using the calibration curve (Fig 6.18)

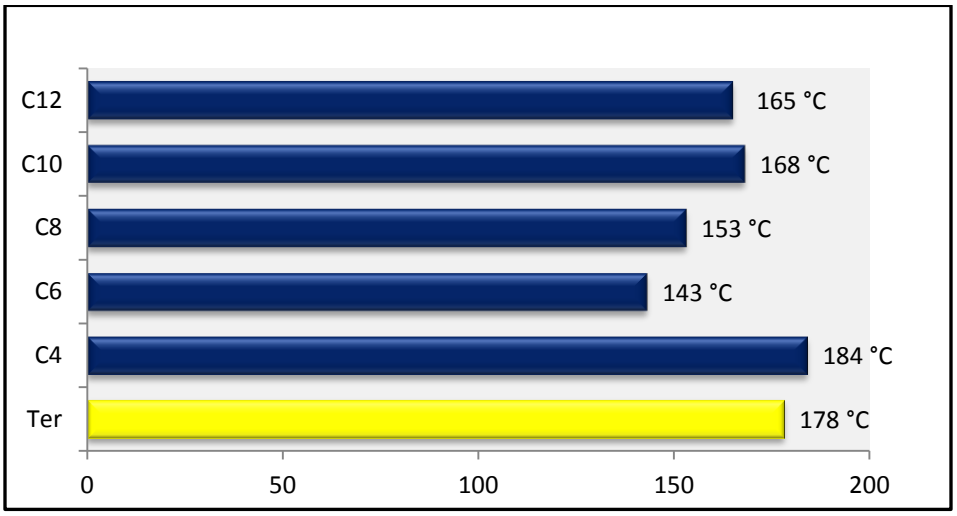

Figure 6.18 Melting point profile of terbuthylazine and its co-crystals

6.4 Discussion

6.4.1 Co-crystals of cyprodinil and terbuthylazine

Molecular electrostatic surface potential calculations performed on cyprodinil and terbuthylazine using semi-empirical PM3 theory suggested the following,

1) In cyprodinil, N(1) has a surface potential charge of -267 kJ/mol and is free from steric hindrance whereas N(2) is sterically hindered by the phenyl group and is not a potential acceptor site (Fig 6.19a).
2) In terbuthylazine, N(1) and N(2) have surface charges of -303 and -294 kJ/mol respectively. The third nitrogen is sterically very hindered by the bulky isopropyl group and thus is not a potential site for hydrogen bonding (Fig 6.19b).

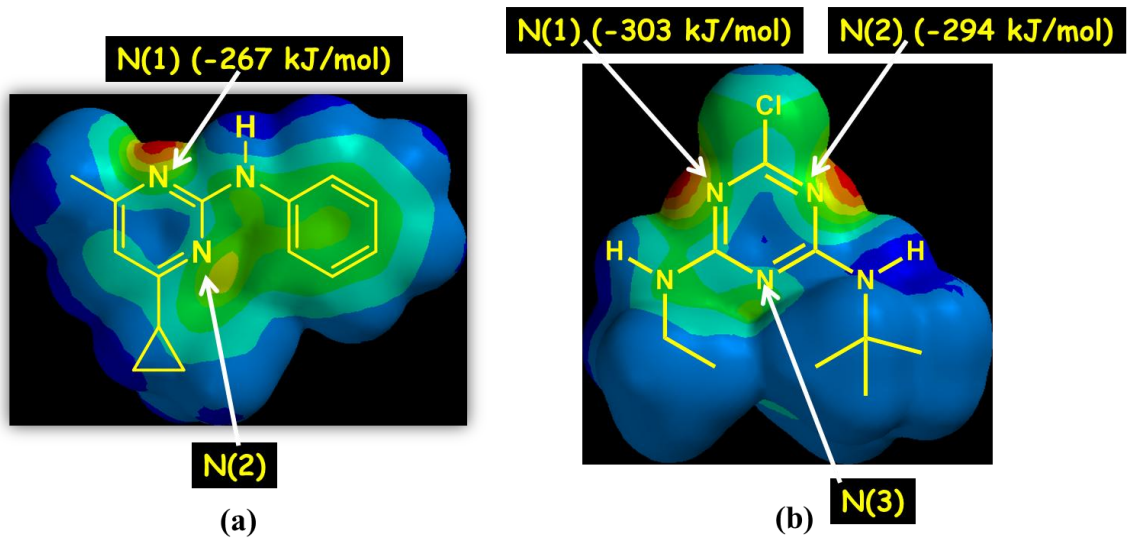

Figure 6.19 Surface potential charges in a) cyprodinil and b) terbuthylazine

Based on the data obtained from our crystal structures (Fig 6.9 and 6.10), the potential of cyprodinil and terbuthylazine in forming co-crystals is clearly evident, *i.e.* 100% co-crystallization. More importantly, all the crystal structures obtained support the theoretical calculations which confirm the inactivity of nitrogen atoms N(2) and N(3) in cyprodinil and terbuthylazine, respectively due to steric hindrance which makes them inaccessible to the approaching hydrogen-bond donors.

6.4.2 Correlating aqueous solubility of co-crystals with co-former solubility

In chapter 3 it was established that the solubility of a given co-crystal is proportional to its corresponding co-former solubility. In parallel to this observation, a very good correlation was also found between cyprodinil co-crystal and their corresponding co-formers (Fig 6.20). As seen before, the solubilities of cyprodinil co-crystals decreased as a function of the increasing hydrophobicity of the co-formers.

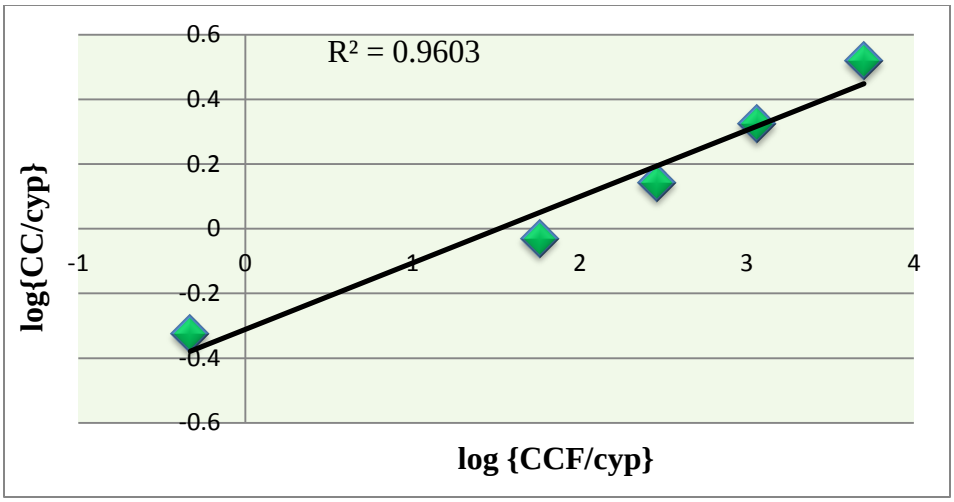

Figure 6.20 Relationship between co-crystal and co-former solubility in cyprodinil co-crystals

6.4.3 Melting point as a function of carbon chain length

In the solid state, diacids form 1-D infinite chains via hydrogen-bond interactions between terminal carboxy groups. This structural consistency is maintained throughout the series from short to long chain diacids. It is well known that the melting point in a series of diacids decreases with an increase in the number of methylene carbon atoms in the diacid backbone.[10] Similar observations were made in multi-component systems, where the observed structural consistency among 1-D infinite chains in a co-crystal (between a diacid and a ditopic acceptor) could be translated into decreasing melting points with increasing carbon atoms of diacid.[11]

In our cyprodinil system, the primary building block in all co-crystals is a trimer between one acid molecule and two cyprodinil moieties on either ends of the diacid. The trimers then pack within the crystal lattice to form the most stable arrangement. The co-crystals of cyprodinil with diacids C4 to C10 display a decreasing trend in melting points with increasing diacid chain length, which is consistent with similar results observed in the literature (Fig 6.21, top). However, the co-crystal with C12 does not follow the trend, but instead displays a higher melting point than the others in the series (Fig 6.21, bottom). This indicates that in the co-crystal of cyprodinil with longer chain diacid (C12), the weaker van der Waal forces play a more significant role, attributed to the longer aliphatic chain of carbon atoms.

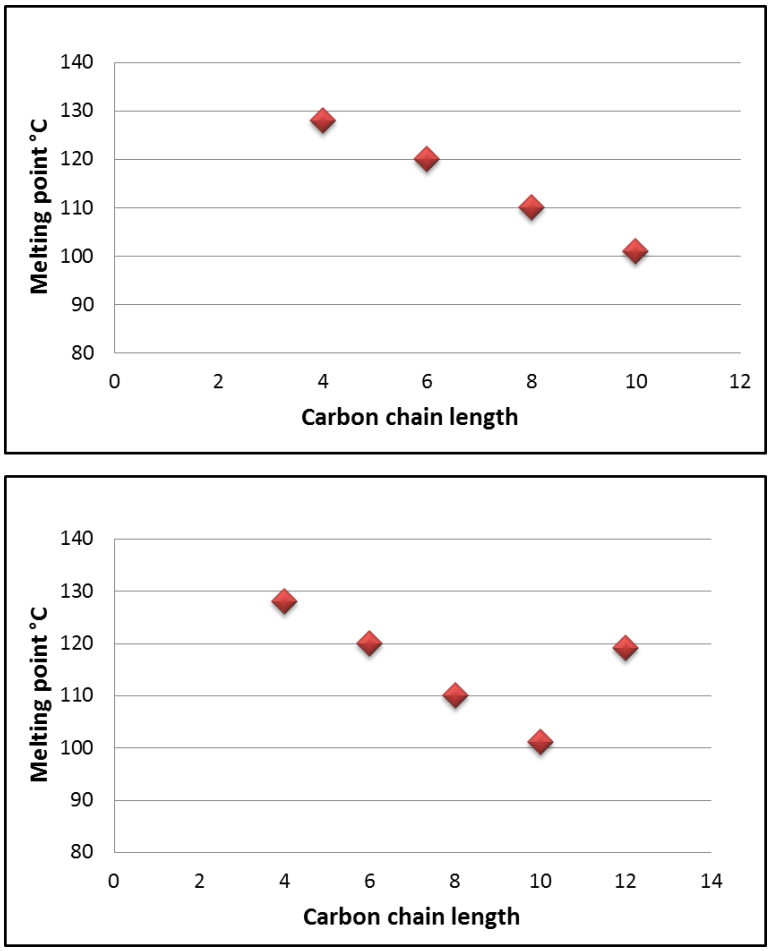

Figure 6.21 Correlation between melting point of co-crystals and carbon chain length C4-C10 (top) and C4-C12 (bottom)

In the crystal structure of terbuthylazine that we obtained via slow evaporation, 1-D chains are formed between neighboring terbuthylazine moieties via two intermolecular N-H···$N_{(amino\text{-}pyridine)}$ homomeric hydrogen bonds. The 1-D chains are further stabilized by weak interactions of chlorine with C-H of the ter-butyl group on neighboring terbuthylazine. The 1-D chains further extend into 2-D network via interchain C-H···Cl halogen bonding interactions between the chlorine atom on one chain and tert-butyl group on the neighboring chain (Fig 6.22). Due to these primary hydrogen bond interactions accompanied by secondary halogen bond interactions, Terbuthylazine displays a higher melting point than its co-crystals, with an exception of **Ter:SA** (Fig 6.18).

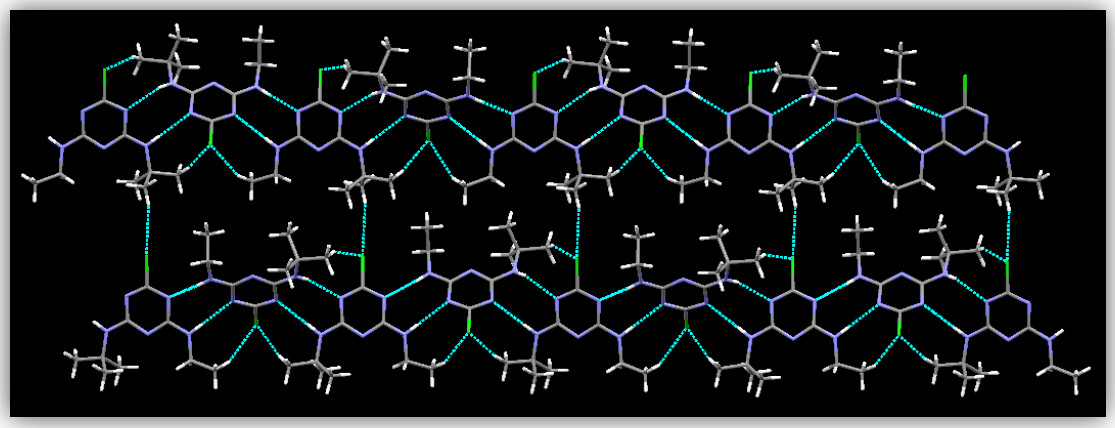

Figure 6.22 Crystal arrangement in terbuthylazine

In the co-crystals, one of the homo-dimer interactions is broken and replaced by an acid-amino-pyridine interaction, while the second homo-dimer interaction is maintained. A notable feature of the co-crystals is the absence of any C-H···Cl halogen bond interactions (Fig 6.10). This could explain why co-crystals of terbuthylazine have lower melting points than the parent active.

Among the co-crystals, **Ter:SA**, **Ter:AA** and **Ter SuA** display a decreasing trend in their melting points with increasing carbon chain length. However, the melting points of **Ter:SeA** and **Ter:DDDA** are higher and do not follow the decreasing trend. Since the primary mode of interactions in all co-crystals is the same (Fig 6.10) forming 1-D chains, the difference in melting point could not be explained purely based on their primary interactions in their crystal structures. A closer investigation of the densities, packing co-efficients and secondary weaker interactions in the crystal structures was performed in order to find a plausible explanation for the observed deviation from the melting point behavior.

6.4.1 Density and packing co-efficients of terbuthylazine co-crystals

Table 6.2 lists the values of densities and packing co-efficients (calculated using Olex2 v1.2 software) of co-crystals of terbuthylazine with succinic, suberic, sebacic and dodecanedioic acid. The values of both density and packing co-efficient of the co-crystals decrease from succinic to dodecanedioic acid. This however does not explain the observed deviation in thermal properties of **Ter:SeA** and **Ter:DDDA** co-crystal.

Table 6.2 Values of density and packing co-efficient in terbuthylazine co-crystals

	Ter	Ter:SA	Ter:SuA	Ter:SeA	Ter:DDDA
Density	1.287	1.288	1.260	1.217	1.195
Packing co-efficient %	59	60	60	59	59

6.4.2 Investigating secondary interactions in terbuthylazine co-crystals

While primary interactions direct the crystal formation, weaker secondary interactions play a very important role in stabilizing the overall crystal structure. We examined the secondary interactions in crystals structures of terbuthylazine co-crystals. The 1-D individual chains extend into two dimensional network via secondary C-$H_{(acid)}\cdots\Pi$ interactions in all four co-crystals (Fig 6.23). In **Ter:SeA** and **Ter:DDDA** co-crystal, the aliphatic backbone of neighboring 1-D chains are aligned in close proximity (Fig 6.23 c and d). Thus there is an additional hydrophobic interaction present between the aliphatic chains of the diacids.

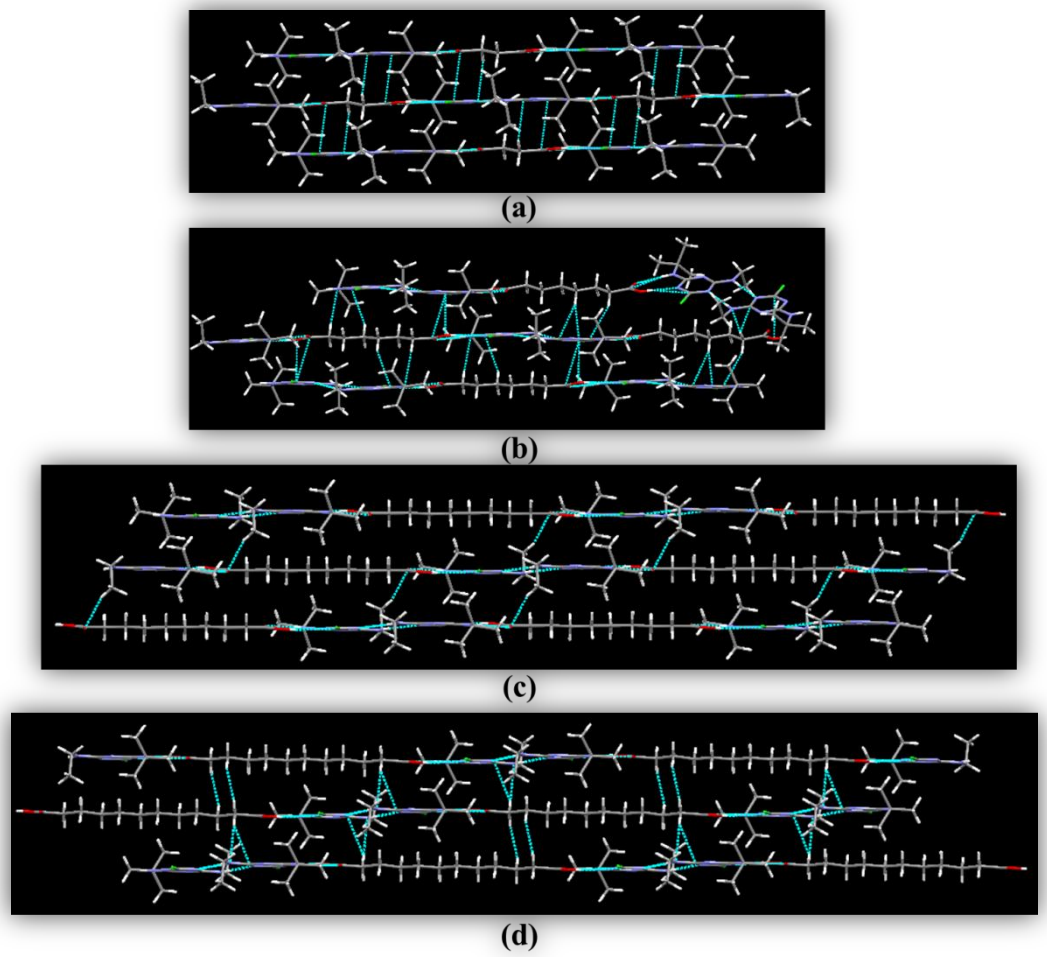

Figure 6.23 Packing of 1-D chains in co-crystals of terbuthylazine with a) succinic acid, b) suberic acid, c) sebacic acid and d) dodecanedioic acid

In addition to the hydrophobic interactions, in **Ter:SeA**, interactions are observed between the tert-butyl groups of terbuthylazine (Fig 6.24), while in **Ter:DDDA**, the tert-butyl group interacts with hydroxyl oxygen atom of the acid (Fig 6.25). All these supplementary interactions provide additional stability to the co-crystals and thus explain the increased melting point observed in **Ter:SeA** and **Ter:DDDA** co-crystals.

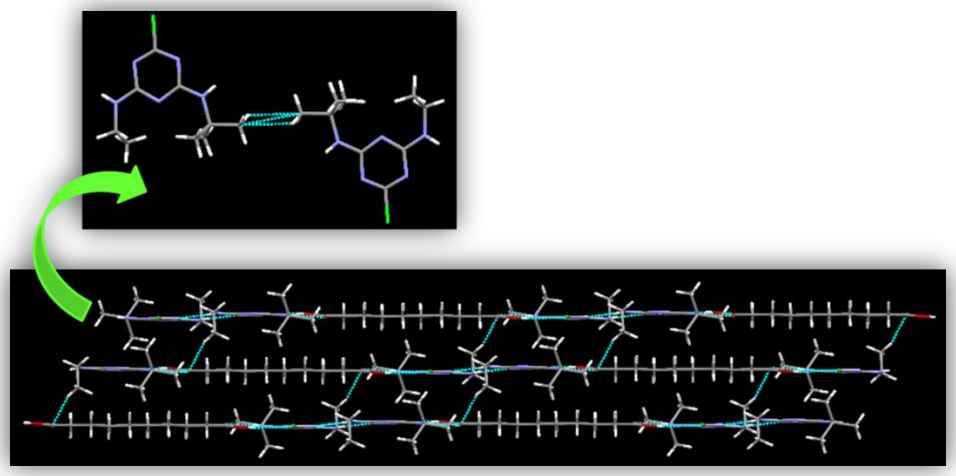

Figure 6.24 Extended architecture in Ter:SeA displaying tert-butyl group interactions

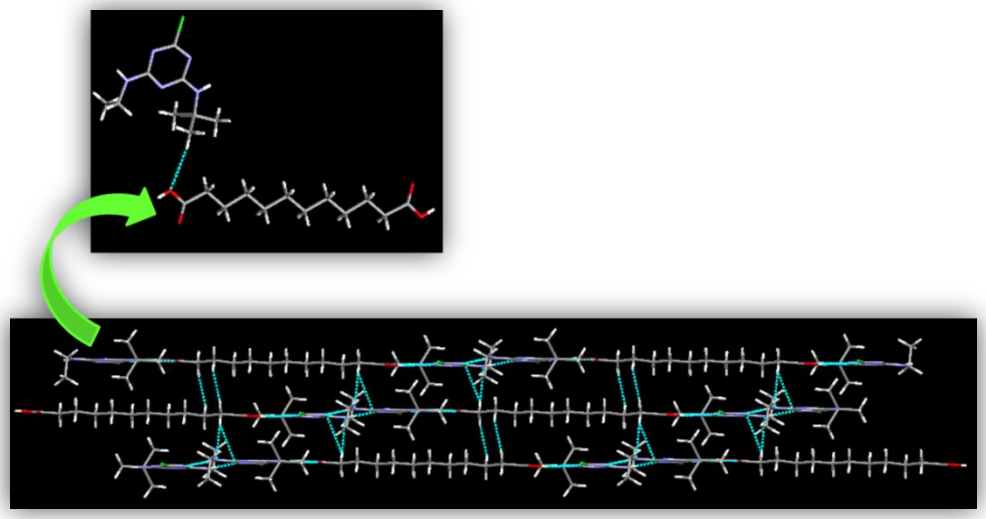

Figure 6.25 Extended architecture in Ter:DDDA with tert-butyl groups interacting with hydroxyl oxygen atoms of the acid

6.5 Conclusion

In conclusion, we have synthesized co-crystals of commercial pesticides, cyprodinil and terbuthylazine with even chain dicarboxylic acids and analyzed their single crystal structures and other physical properties. Bases on our results we can conclude the following;

1) Both cyprodinil and terbuthylazine show the potential to form co-crystals with a series of diacids with 100% supramolecular yield.

2) The co-crystals display melting points different from the parent active.
3) In cyprodinil co-crystals, we could alter the solubility of the active using co-crystallization and a very good correlation between the co-crystal solubility and co-former solubility was observed.
4) No appreciable change in hygroscopicity was observed at 84% and 43% relative humidity conditions for cyprodinil co-crystals. The PXRD patterns collected at the end of humidity experiments indicate no degradation or change in form of the solid samples.

Our experiments thus prove the potential of crystal engineering in altering physical properties of agrochemical actives in a predictable and desirable manner.

---

1 James Tano, *Identity, Physical and Chemical Properties of Pesticides, Pesticides in the Modern World - Trends in Pesticides Analysis*, Dr. Margarita Stoytcheva (Ed.), **2011**, ISBN: 978-953-307-437-5

2 Mokhele, Tholang A.. Potential health effects of pesticide use on farmworkers in Lesotho. *S. Afr. J. Sci*. **2011**, 107, 29-35

3 Kaneko, T.; Akesson, N., Pesticide formulation and application systems, third symposium, issue 828, **1983**

4 Bratz, M.; Brode, I.; Wolfgang H. H.; Israels, R.; Nauha, E.; Nissinen, M.; Saxell, H.E.; Schaefer, A., *European Patent,* **W02011054741(A2)**

5 Collins, H. M.; Hall, F. R.; Hopkinson, M. J., *Pesticide formulation and application system*, **1996**, 15, 1268

6 Neil, G.; Forrest, J.; Gavan, P. T.; Burton, R. C.; Lee, G., Patent, **2008**/117060A3

7 Nehm, S. J.; Rodríguez-Spong, B.; Roderíguez-Hornedo, N. *Cryst. Growth Des*. **2006,** 6, 592

8 Tao, Q.; Chen, J. M.; Ma, L.; Lu, T. B.; *Cryst. Growth Des*., **2012**, 12, 3144-3152

9 Syngenta, private communication

10 Thalladi, V. R.; Nu1sse, M. and Boese, R.*, J. Am. Chem. Soc***. 2000**, 122, 9227-9236

11 Aakeröy, C. B.; Forbes, S.; Desper, J.; *J. Am. Chem. Soc.,* **2009**, 12, 17048-17049

Appendix A – ^{1}H NMR

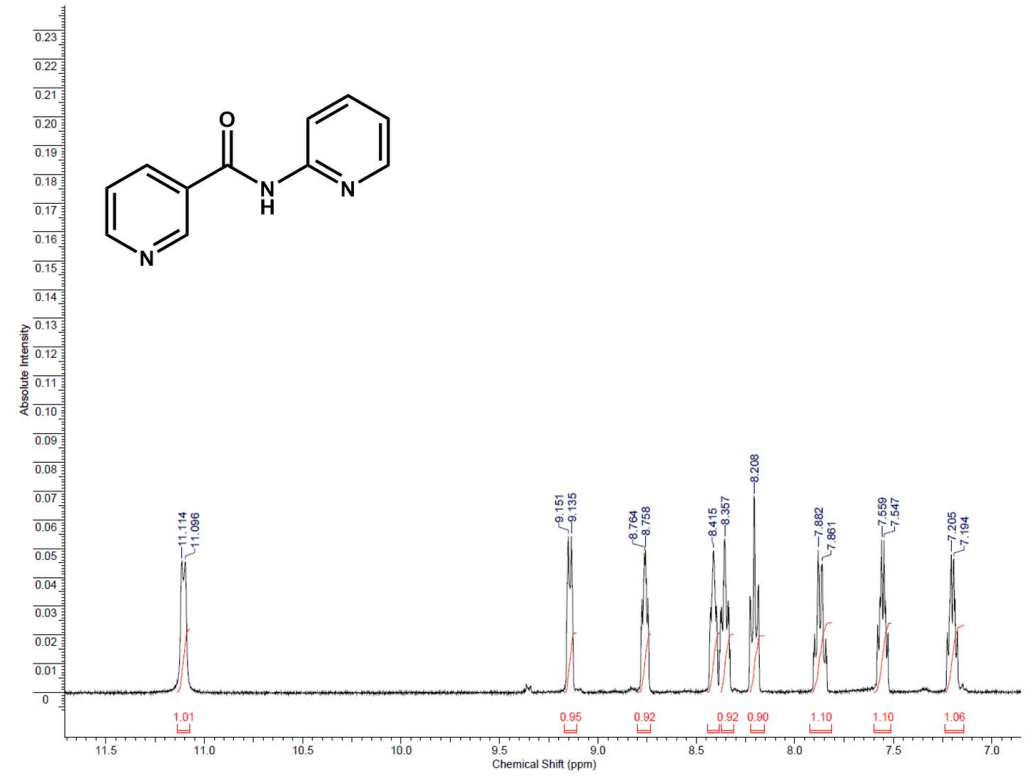

Appendix A 1 ^{1}H NMR of 3N

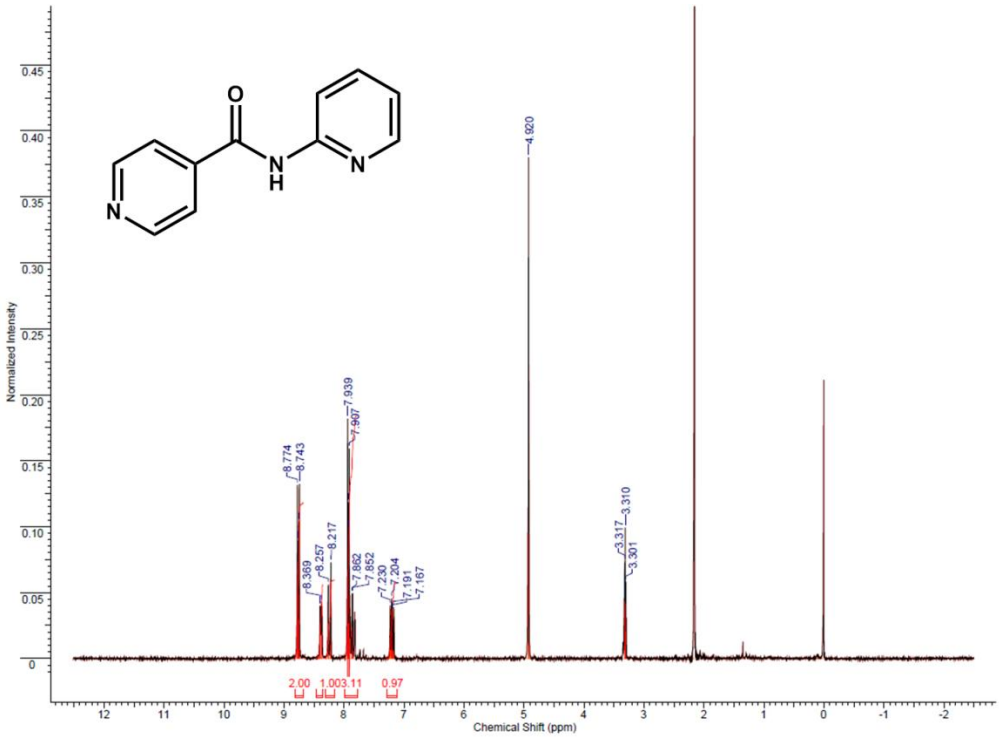

Appendix A 2 ^{1}H NMR of 4N

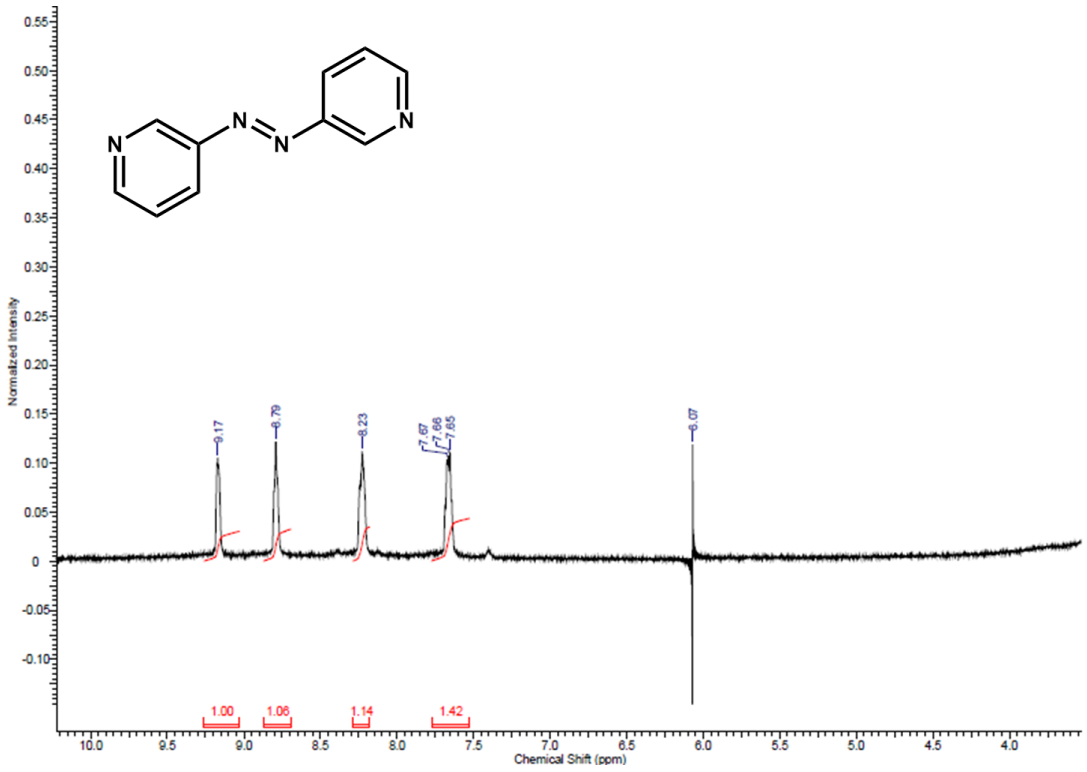

Appendix A 3 ^{1}H NMR of 3,3'-azopyridine

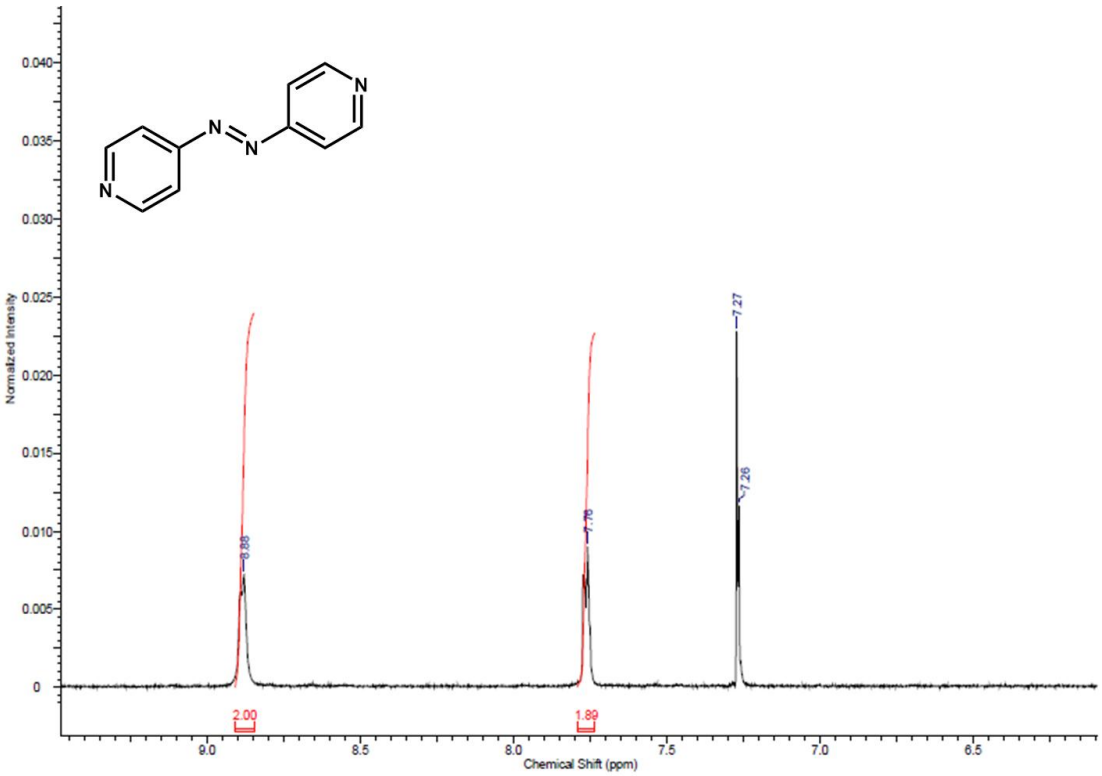

Appendix A 4 ^{1}H NMR of 4,4'-azopyridine

Appendix B - PXRD patterns

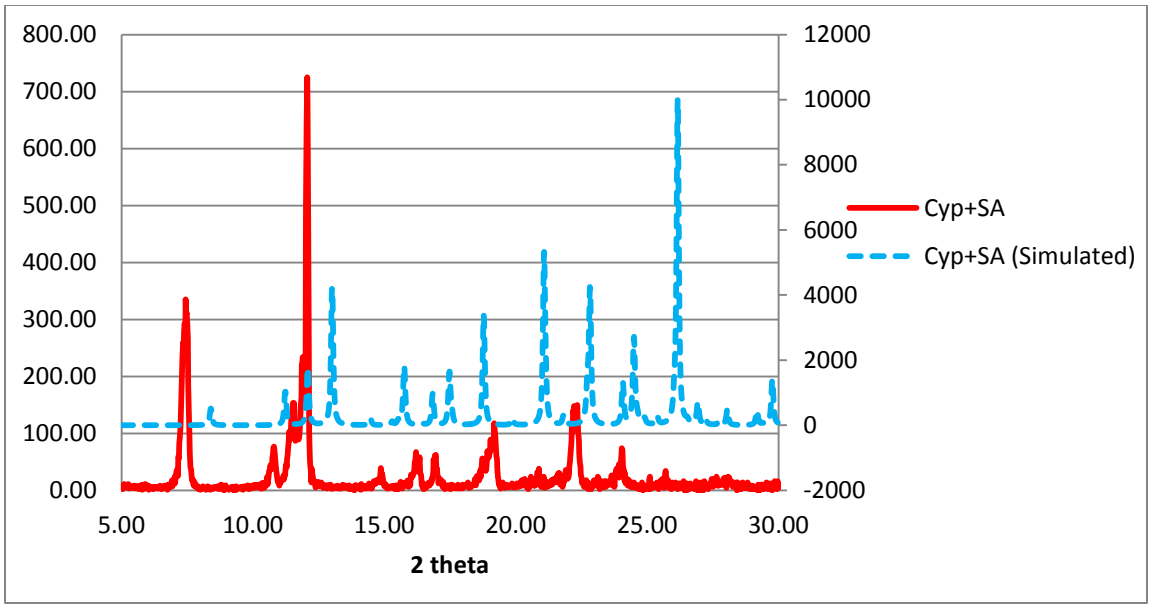

Appendix B 1 PXRD pattern of Cyp:SA **co-crystal**

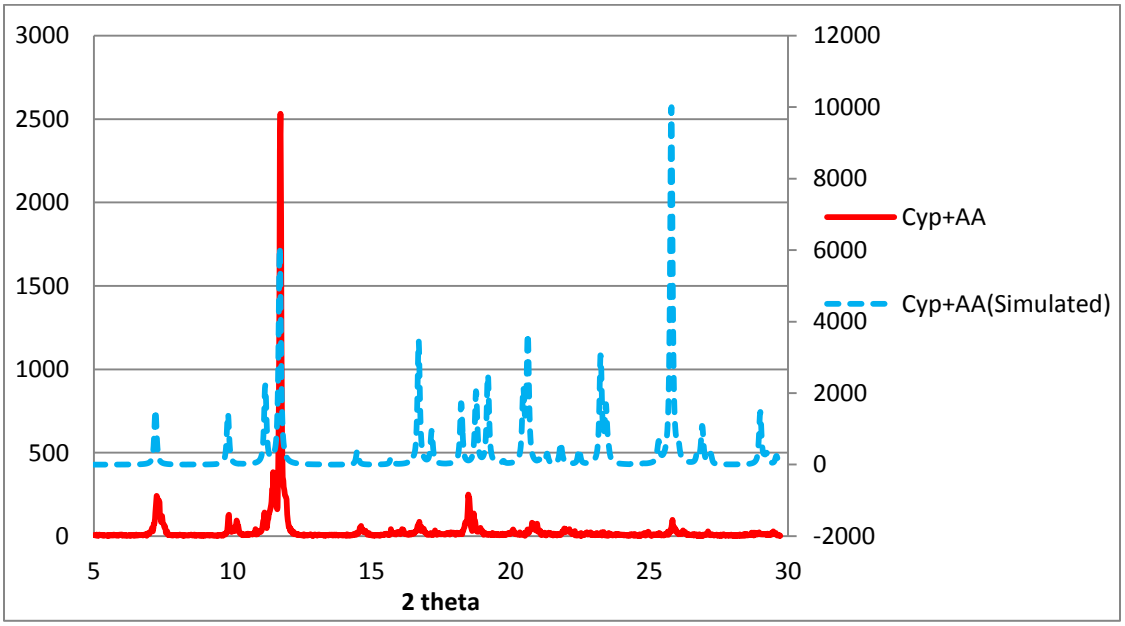

Appendix B 2 PXRD pattern of Cyp:AA **co-crystal**

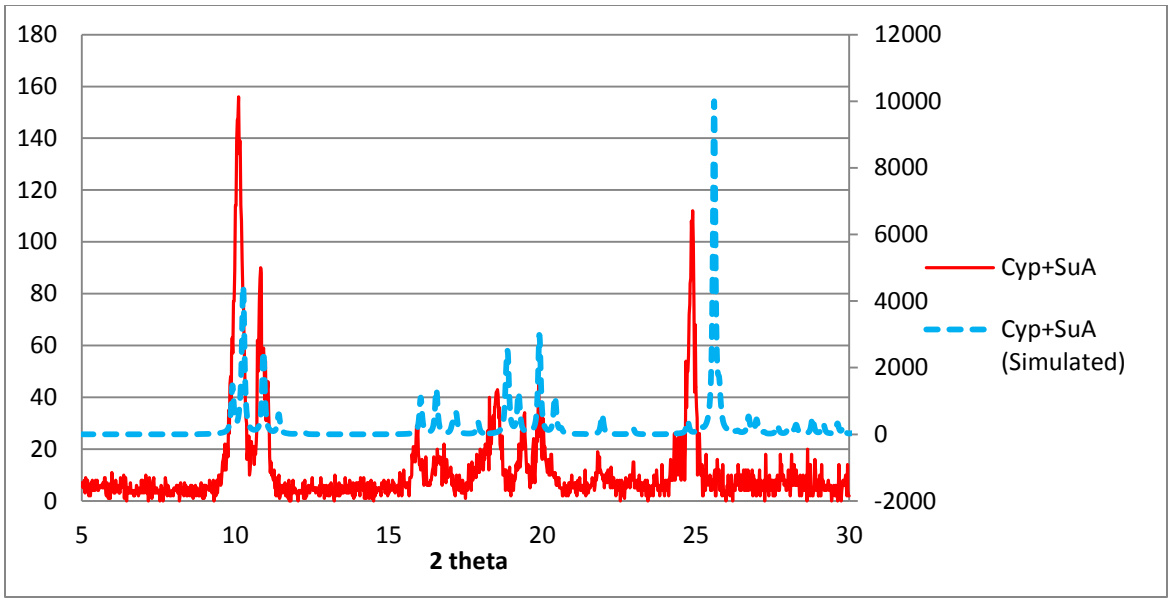

Appendix B 3 PXRD pattern of Cyp:SuA **co-crystal**

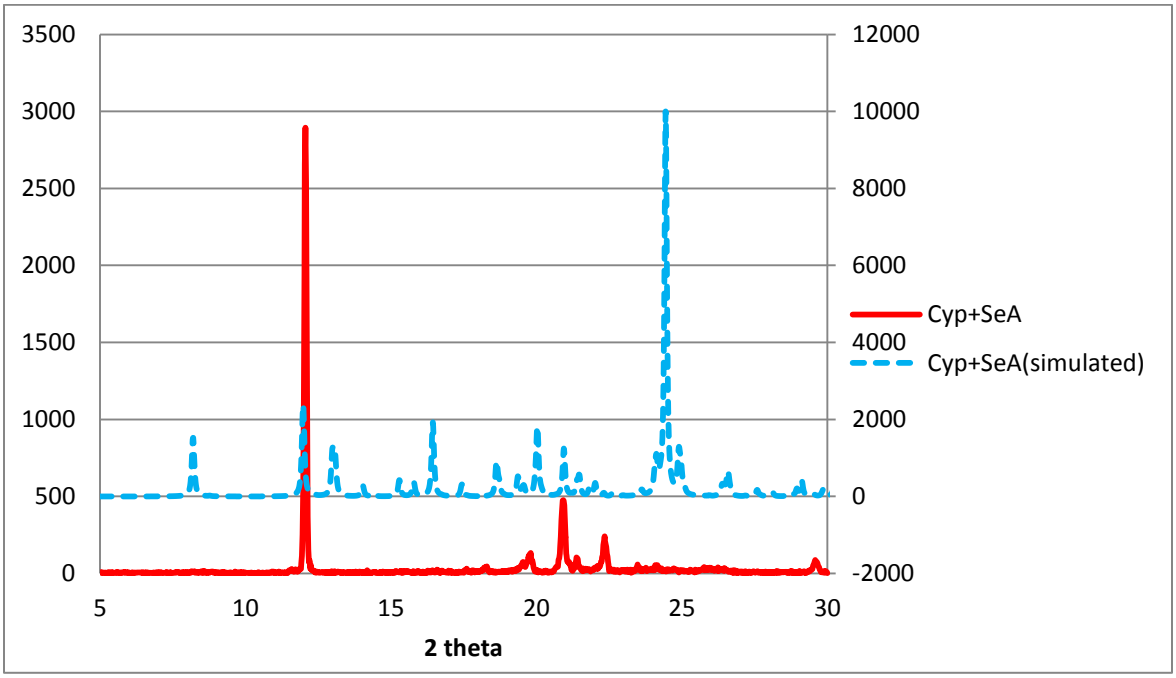

Appendix B 4 PXRD pattern of Cyp:SeA **co-crystal**

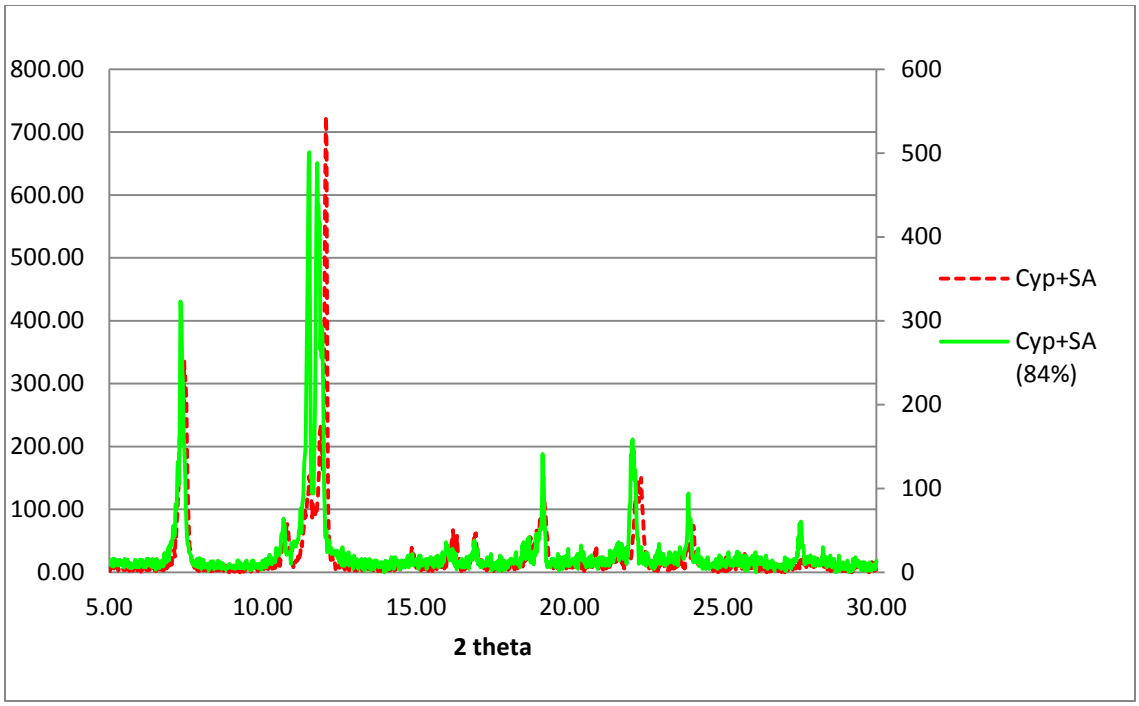

Appendix B 5 PXRD pattern of Cyp:SA **co-crystal after humidity experiment**

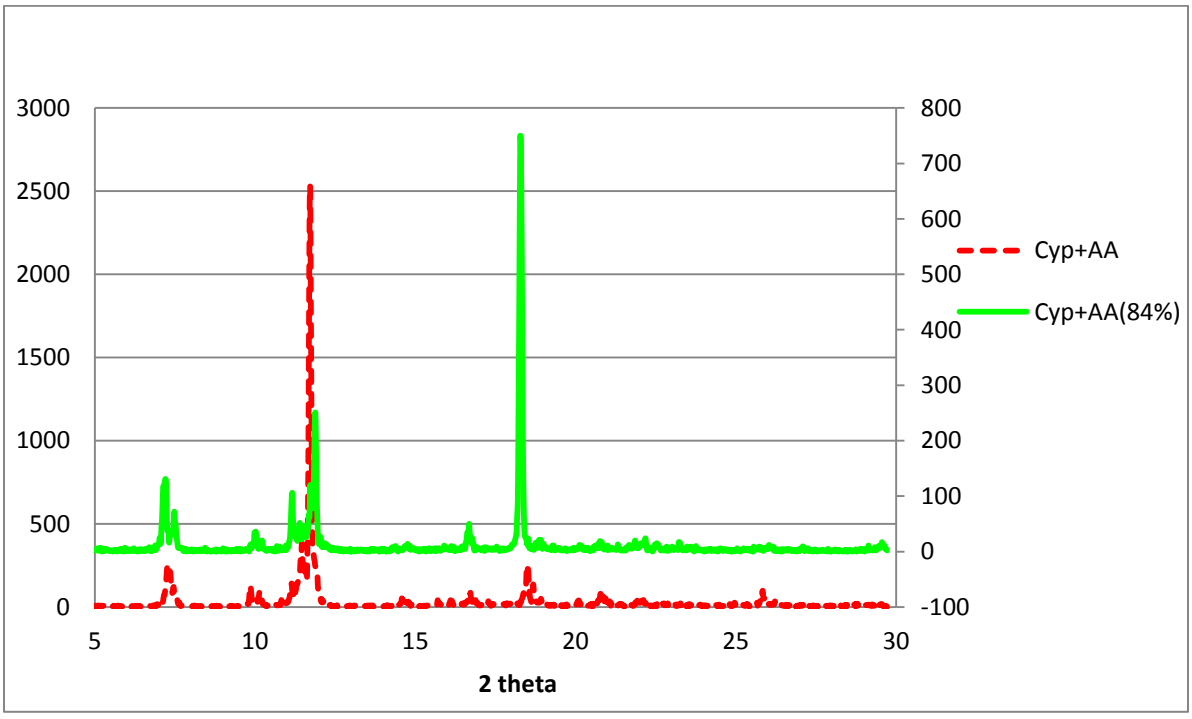

Appendix B 6 PXRD pattern of Cyp:AA **after humidity experiment**

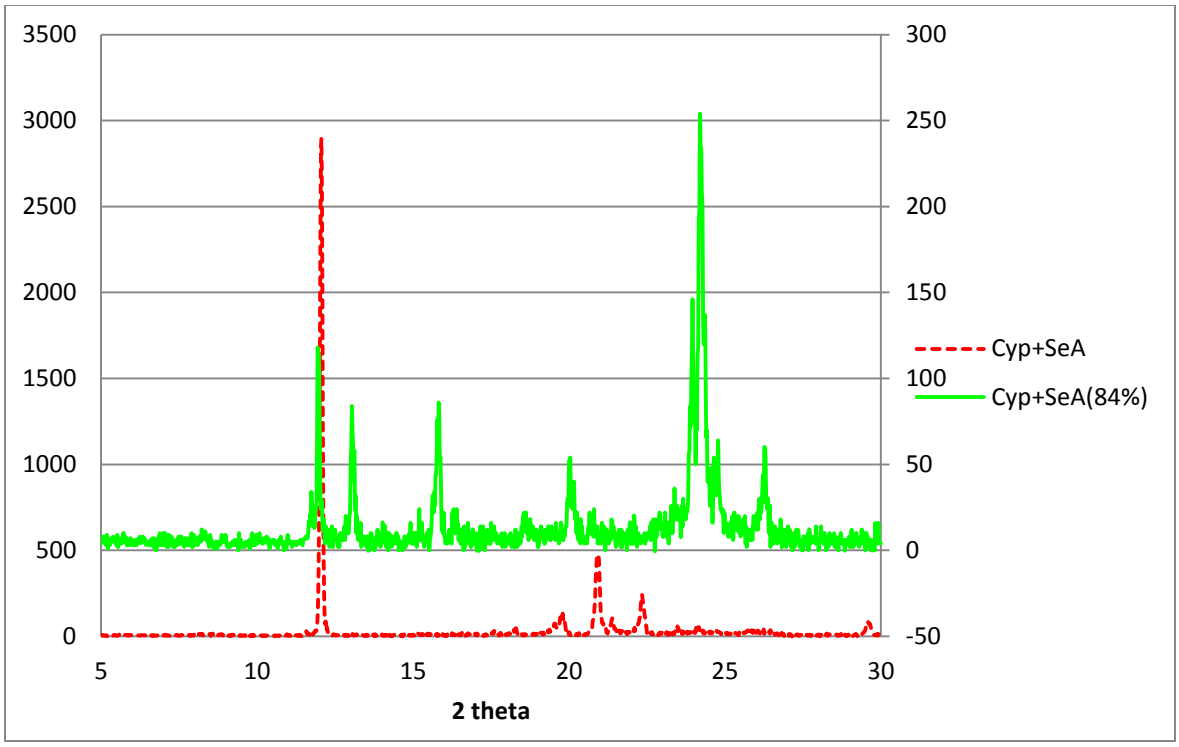

Appendix B 7 PXRD pattern of Cyp:SeA **co-crystal after humidity experiment**